Quarterly Reviews of Biophysics

cambridge.org/qrb

Structures of synthetic helical filaments and tubes based on peptide and peptido-mimetic polymers

Jessalyn G. Miller, Spencer A. Hughes, Charles Modlin and Vincent P. Conticello

Department of Chemistry, Emory University, 1515 Dickey Drive, Atlanta, GA 30322, USA

Review

Cite this article: Miller JG, Hughes SA, Modlin C, Conticello VP (2022). Structures of synthetic helical filaments and tubes based on peptide and peptido-mimetic polymers. *Quarterly Reviews of Biophysics* **55**, e2, 1–39. https://doi.org/10.1017/S0033583522000014

Received: 1 September 2021
Revised: 8 March 2022
Accepted: 9 March 2022

Key words:
Cryo-EM; *de novo* peptide design; filament; helical symmetry; nanotube; near-atomic resolution; peptide self-assembly

Author for correspondence:
Vincent P. Conticello,
E-mail: vcontic@emory.edu

Abstract

Synthetic peptide and peptido-mimetic filaments and tubes represent a diverse class of nanomaterials with a broad range of potential applications, such as drug delivery, vaccine development, synthetic catalyst design, encapsulation, and energy transduction. The structures of these filaments comprise supramolecular polymers based on helical arrangements of subunits that can be derived from self-assembly of monomers based on diverse structural motifs. In recent years, structural analyses of these materials at near-atomic resolution (NAR) have yielded critical insights into the relationship between sequence, local conformation, and higher-order structure and morphology. This structural information offers the opportunity for development of new tools to facilitate the predictable and reproducible *de novo* design of synthetic helical filaments. However, these studies have also revealed several significant impediments to the latter process – most notably, the common occurrence of structural polymorphism due to the lability of helical symmetry in structural space. This article summarizes the current state of knowledge on the structures of designed peptide and peptido-mimetic filamentous assemblies, with a focus on structures that have been solved to NAR for which reliable atomic models are available.

Table of contents

Introduction

Cellular biology provides many examples of filamentous nanomaterials in which control of higher-order structure enables emergent function. Extracellular protein filaments (e.g. pili, flagella, secretory needles and tubes) (Egelman, 2017) and filamentous phage and viruses (Stubbs and Kendall, 2012) represent protein and nucleo-protein assemblies, respectively, in which regulated fabrication from the macromolecular components has led to the evolution of complex function. These extracellular filaments perform a diverse range of functions that would be desirable to emulate in synthetic systems, including chemo-mechanical energy transduction (Poweleit *et al.*, 2016; Wang *et al.*, 2017), controlled delivery (Loquet *et al.*, 2012; Costa *et al.*, 2016), selective and tunable catalysis (Lynch *et al.*, 2017, 2020), and, as recently discovered, electron transfer over multi-micron length scales (Wang *et al.*, 2019). While many synthetic peptide and protein filaments have been proposed as substrates for directed applications in medicine and nanotechnology, the limited availability of structural information at high

CAMBRIDGE UNIVERSITY PRESS

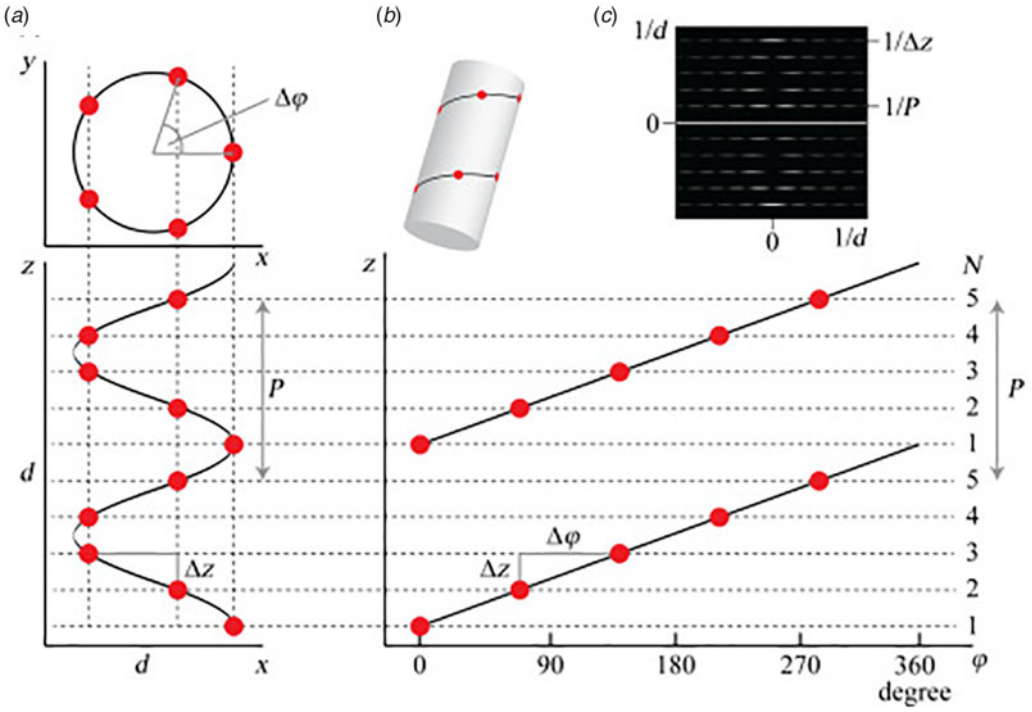

Fig. 1. (*a*) Top and side projections of a helical polymer in which each dot represents an asymmetric unit of the corresponding assembly. (*b*) Helical net diagram corresponding to the symmetry of the helical polymer. A solid line connects protomers within the 1-start helix of the assembly. (*c*) Power spectrum derived from the amplitudes of the Fourier transform of this helical polymer in which layer lines are indicated corresponding to pitch (*P*) and rise (*z*) in reciprocal space. From S. A. Fromm and C. Sachse (2016)*Methods in Enzymology*, 579, 307–328, Academic Press Inc. Reprinted with permission from Elsevier.

resolution has hindered the development of these assemblies as functional materials (Haines-Butterick *et al.*, 2007; Yan *et al.*, 2008; Moore and Hartgerink, 2017; Wu *et al.*, 2017; Gelain *et al.*, 2020).

The key to understanding and emulating the diverse functions of protein filaments resides in the ability to deconvolute the structural principles that enable their highly specific assembly. Native protein and nucleoprotein filaments achieve this specificity through a combination of structural control of interactions at protein–protein interfaces within the assembly and spatiotemporal regulation of the post-synthetic processing of the protein subunits into structurally defined filaments. The latter process enables controlled fabrication of the corresponding protein or nucleoprotein filaments but lies beyond our current capabilities to replicate *in vitro* for synthetic assemblies. In contrast to the majority of synthetic peptide and protein filaments that have been studied *in vitro*, biologically derived protein filaments often *do not self-assemble*, but instead the protomers are fabricated into 'assembled' structures under conditions that are far from equilibrium (Costa *et al.*, 2015).

Synthetic peptide and protein filaments, while differing in the mechanism of formation from native biological assemblies, display similarities in supramolecular structure. Both classes of filaments are based on non-covalent self-association of subunits (protomers) into high aspect-ratio supramolecular polymers (⩾1 μm in length) that display helical symmetry (Fig. 1). This simple symmetry operation involves rotation through a characteristic helical twist or azimuthal angle (ϕ) with a commensurate axial translation (z). Continuous application of this symmetry operation upon successive addition of protomers generates a filamentous assembly, that is, a helical filament or tube. Such filaments can be generated from protomers having any possible molecular structure as long as sufficient interfacial interactions between subunits are present that stabilize the filament vis-à-vis monomers or discrete oligomers. Within these simple geometrical constraints, an infinite number of structural variations are possible that involve different helical symmetries, as well as superimposed rotational and dihedral symmetry. Helical assemblies are usually characterized in terms of the number of subunits per helical turn, N ($=2\pi/\phi$), and the helical pitch, P ($=Nz$). In non-rotationally symmetric cases, i.e. C_1 symmetry, these parameters can be determined from assignment of the 1-start helix, i.e. the helix that passes through every subunit in the assembly (Fig. 1). For helical assemblies containing a rotational symmetry axis C_n, the helical symmetry can be understood in terms of the rise and rotation of the n-start helices subject to this rotational symmetry element.

Helical symmetry can be best understood from consideration of the corresponding helical net diagram, in which the helix is unrolled in two dimensions with the axial rise, z, as the ordinate and the azimuthal angle, ϕ, as the abscissa (Fig. 1*b*). The perspective is usually presented from the outside of the helical assembly and is critical to identification of the helical hand, i.e. right-handed *versus* left-handed screw sense, of the respective n-start helices. Each n-start helix passes through every nth protomer in the helical assembly.

The 1-start helix (solid line in the helical net of Fig. 1*b*) is right-handed since the axial rise increases from left to right in the helical net diagram. In contrast, the same helical net diagram indicates the presence of five 5-start helices within the same assembly, which pass through different sets of subunits at a frequency of every fifth protomer. The 5-start helices are left-handed due to an opposite right-to-left inclination in the helical net diagram. Helical symmetry can be determined from analysis of the

https://doi.org/10.1017/S0033583522000014 Published online by Cambridge University Press

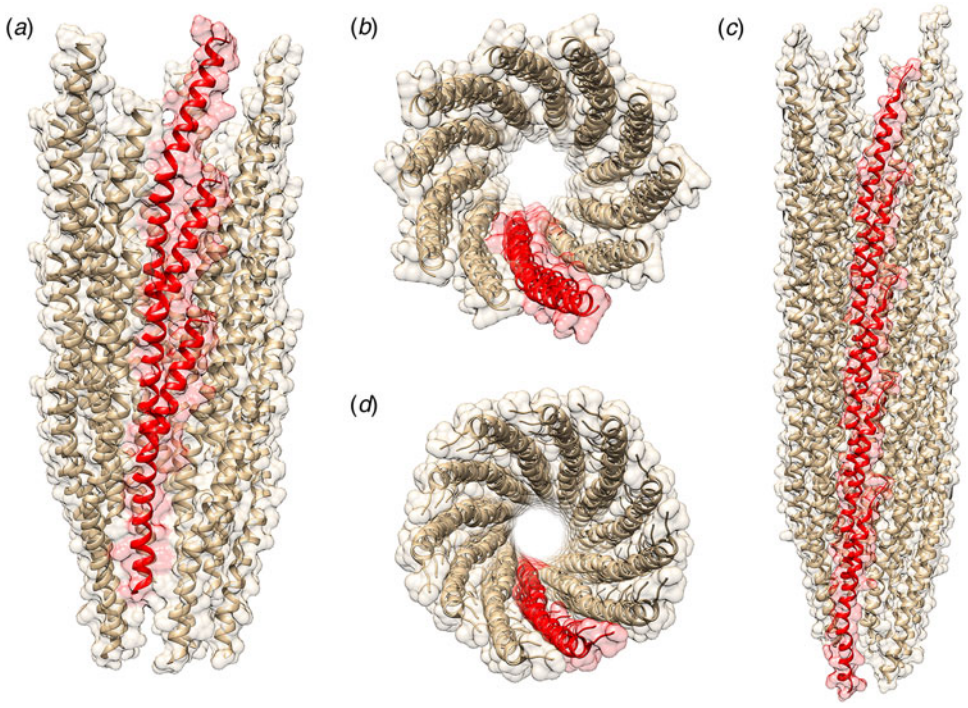

Fig. 2. Side (*a*) and top (*b*) views of the atomic model of the phage IKe capsid. Side (*c*) and top (*d*) views of the atomic model of the phage Pf4 capsid. Single protofilaments corresponding to the 10-start and 11-start helices of the IKe and Pf4 capsids, respectively, are highlighted in red.

averaged power spectrum of the filaments (Fig. 1*c*) (Wang *et al.*, 2006; Egelman, 2010, 2014), which is derived from the Fourier transform of filament segments that are present in the projection images from electron microscopy (EM). The Fourier transform is complex (having both amplitudes and phases), while the power spectrum is simply the intensities (squared amplitudes) of the Fourier transform. As a result, the individual power spectra from each segment can be added together without any need for alignment. The layer lines within the averaged power spectrum correspond to repeat spacings in reciprocal space associated with the spatial frequencies of the different *n*-start helices that are present within the assembly. To assign helical symmetry, two independent orders, *n*, of the corresponding Bessel functions must be assigned to sets of observed layer lines in the averaged power spectrum. This process often relies on a trial-and-error approach in which multiple different helical symmetries are assessed as workable solutions. The details of structural determination using cryo-EM image analysis are beyond the scope of this article. However, a recent review highlights the critical considerations involved in assignment of helical symmetry in the structural analysis of synthetic peptide filaments (Wang *et al.*, 2022).

Prior structural analyses of peptide and protein filaments suggest that helical symmetry can be labile in structural space (Egelman *et al.*, 2015; Lu *et al.*, 2015; Wang *et al.*, 2021*a*). Small changes in packing at the protomer interfaces within the assembly can result in different helical symmetries, even under conditions in which the individual protomer structures are highly conserved. For example, filamentous bacteriophages comprise two distinct structural families that display C_5 and C_1 symmetry, respectively, for the helical arrangement of capsid proteins around the single-stranded DNA genome (Marvin *et al.*, 2014). Helical reconstruction from high-resolution cryo-EM image analysis enabled structural determination of assemblies from representative members of these two classes of filamentous bacteriophage, IKe (C_5) and Pf4 (C_1), at near-atomic resolution (NAR) (Xu *et al.*, 2019; Tarafder *et al.*, 2020). Comparison of the two structures is illustrative of the challenges encountered in the structural analysis of filamentous assemblies. The capsid assemblies consist of simple α-helical protomers. Superimposition of individual protomers derived from the two structures indicated a backbone root-mean-square deviation of ca. 1.5 Å despite low sequence similarity. Since the side-chain interactions define the protein–protein interfaces within the respective assemblies, the differences in higher-order structure presumably result from differences in sequence since the protomer fold is conserved.

The structures of the corresponding helical assemblies of the IKe and Pf4 phage capsids are depicted in Fig. 2 at 3.4 Å (PDB: 6A7F) and 3.2 Å (PDB: 6TUQ) resolution, respectively. In each case, the capsid proteins are arranged in a similar orientation around the central axis of the assembly. Single protofilaments are highlighted in red within the assembly. For phage IKe, the highlighted protofilament coincides with one of the right-handed 10-start helices under C_5 symmetry. In contrast, under the different symmetry of phage Pf4 capsid, the protofilaments coincide with the right-handed 11-start helices.

These differences can be most easily visualized through a comparison of the respective helical net diagrams. The structural subunits associated with the respective protofilaments are highlighted in red (Fig. 3*a* and *b*). For phage IKe, a representative set of protomers related through the C_5 rotational axis is depicted in cyan. Similarly, the right-handed 1-start helix of phage Pf4 is highlighted in the corresponding helical net. Figure 3*c* and *d* depicts a section of calculated power spectra of the respective assemblies, initially sampled at a frequency of 2 Å pixel^{-1}. Arrows indicate the spatial frequencies associated with the axial rise corresponding to the meridional ($n = 0$) for IKe and the 1-start helix ($n = +1$) for Pf4. In either case, the corresponding axial repeats are quite similar between the two assemblies despite the differences in helical symmetry.

https://doi.org/10.1017/S0033583522000014 Published online by Cambridge University Press

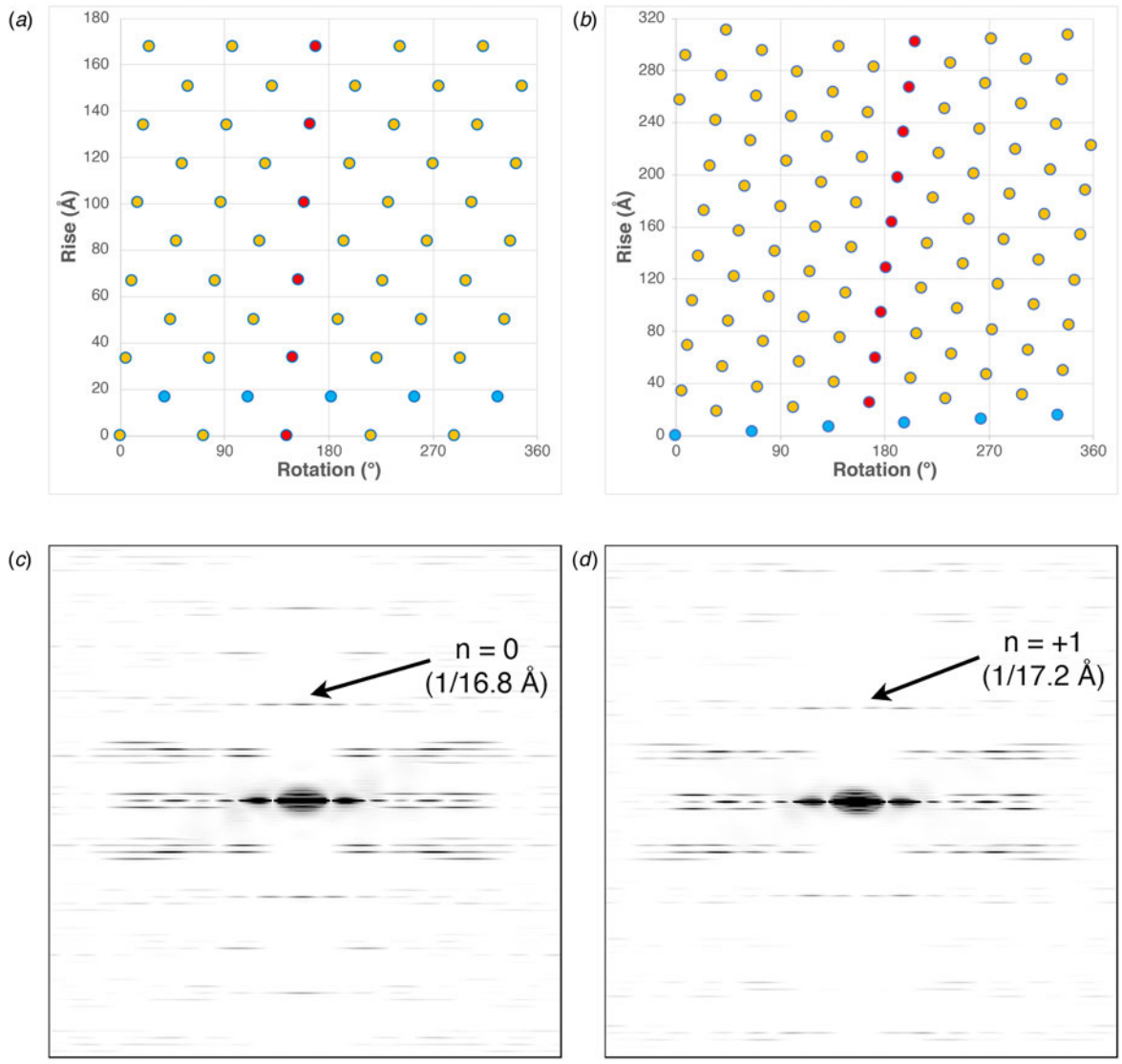

Fig. 3. (*a*) Helical net diagram of IKe phage. (*b*) Helical net diagram of Pf4 prophage. (*c*) Calculated power spectrum of IKe phage. (*d*) Calculated power spectrum of Pf4 phage.

In this review, the term 'helical assemblies' describes supramolecular polymers of proteins, peptides, and structurally related synthetic foldamers that display helical symmetry. This symmetry operation can be applied to protomers based on any structural motif as long as the interfaces between subunits are stable under the set of experimental conditions under which self-assembly occurs. These assemblies need not form closed cylindrical structures, i.e. assemblies in which successive turns of the helix make physical contact through an axial interface. The latter structures are often denoted as nanotubes since self-association generates a water-filled central cavity (lumen) that runs through the structure and is oriented parallel to the helical axis (Bong *et al.*, 2001; Hamley, 2014). Peptide nanotubes can also result from other modes of self-assembly, e.g. axial stacking of cyclic peptides (Ghadiri *et al.*, 1993; Insua and Montenegro, 2020). The latter subject has been reviewed recently and will not be covered here (Song *et al.*, 2021).

This review will discuss the structure of biomimetic helical assemblies derived from synthetic peptides and peptido-mimetics. Where possible, we focus on helical assemblies in which the structures have been solved at high resolution using biophysical methods such as single-crystal diffraction, solid-state nuclear magnetic resonance (ssNMR) spectroscopic measurements, or helical reconstruction from cryo-EM. Such NAR methods for structural determination have revolutionized the study of helical assemblies. These techniques afford atomic models that provide structural insights into the interfacial packing interactions between protomers that guide the formation of these helical assemblies. The information gleaned from structural studies of biological helical assemblies has led to the emergence of a research field focusing on the design of biomimetic helical assemblies from synthetic peptides and structurally related foldamers (i.e. peptido-mimetic oligomers). The goal of the latter studies is to recapture the complex function and responsive behavior of biologically derived helical assemblies using simple structural motifs that are amenable to synthetic control.

The initial discussion will focus on an introduction to high-resolution methods for structural analysis of helical assemblies in conjunction with their relative merits and limitations. Subsequently, different classes of helical assemblies will be

https://doi.org/10.1017/S0033583522000014 Published online by Cambridge University Press

discussed in terms of the conformational features of the protomers. In each case, we will refer to specific examples of helical filaments that have been characterized to NAR.

A recurrent theme in the field of designed filamentous assemblies is the plasticity of quaternary structure in sequence space (Egelman *et al.*, 2015; Lu *et al.*, 2015). Currently, few high-resolution structural models have been generated for filamentous assemblies of designed peptides or proteins (Kajander *et al.*, 2007; Cormier *et al.*, 2013; Egelman *et al.*, 2015; Nagy-Smith *et al.*, 2015, 2017; Chen *et al.*, 2017, 2020; Lee *et al.*, 2017; Shen *et al.*, 2018; Zhang *et al.*, 2018; Hughes *et al.*, 2019; Feng *et al.*, 2020; Wang *et al.*, 2021*a*; Pieri *et al.*, 2022). It has been observed that the experimental structures often display significant differences from the conceptual model upon which the initial design was based. Structural polymorphism is commonly observed for synthetic peptide assemblies or native proteins assembled *in vitro*. The observed structures may depend strongly on the initial conditions, i.e. temperature, pH, ionic strength, etc., that were employed for peptide self-assembly (Close *et al.*, 2018; Guenther *et al.*, 2018; Zhang *et al.*, 2019; Wang *et al.*, 2021*b*). In addition, the experimental methods employed to prepare the sample for high-resolution structural analysis, e.g. crystallization, lyophilization, cryo-vitrification, may bias the system toward a particular structural variant (Egelman *et al.*, 2015).

Structural characterization of synthetic helical filaments

Structural analysis of helical filaments requires application of experimental methods that interrogate structure across multiple length scales. A number of methods can analyze structure at low resolution and are applicable to relatively rapid screening and analysis of peptide specimens for the presence of ordered conformations and the formation of well-defined supramolecular structure. Circular dichroism (CD) spectropolarimetry and Fourier-transform infrared (FTIR) and Raman spectroscopy can provide evidence for the formation of secondary and tertiary structure, which can be subsequently correlated with self-assembly behavior. Atomic force microscopy (AFM) and conventional transmission electron microscopy (TEM) can reveal the presence of supramolecular structure and provide insight into the morphological features of the resultant assemblies at medium resolution. Small-angle X-ray and neutron scattering measurements, i.e. SAXS and SANS, afford information on the structural features of the assemblies in solution at low-to-medium resolution in the range from 1 to 100 nm from analysis of the form factor scattering (Guilbaud and Saiani, 2011). AFM and scanning electron microscopy) (SEM) can also be employed for assignment of the helical hand of peptide assemblies for cases in which the chirality of the surface features can be resolved (Wang *et al.*, 2022). However, only a small set of experimental methods can give information at NAR on filamentous helical assemblies, namely X-ray and electron diffraction methods, ssNMR spectroscopy, and cryo-EM.

NAR structural information is essential for understanding the internal structure of the protomers and the interfacial contacts that stabilize the helical assemblies. The meaning of the term 'near-atomic resolution' is a subject of active debate (Chiu *et al.*, 2017; Wlodawer and Dauter, 2017), especially as regards the level of resolution that can be achieved using different methods of structural analysis (Wlodawer *et al.*, 2017). True atomic resolution, ca. 1.2 Å, refers to the ability to distinguish between separated atoms in an electron density map (Sheldrick, 1990; Morris and Bricogne, 2003). NAR is less well-defined, but it usually employed to describe the resolution of density maps that can serve as the basis for the construction of reliable atomic models. In this latter case, the resolution limit has been claimed to be as low as ca. 4 Å for the corresponding density maps. The reliability of the corresponding atomic model depends on the map quality, which in turn depends on intrinsic properties of the sample, e.g. the thermodynamic stability of the interfacial interactions between protomers within the assembly. Most peptide and protein filaments are intrinsically flexible. Flexibility can introduce disorder into the sample, which can lower the quality of the density maps resulting from helical reconstruction (Egelman *et al.*, 1982; Orlova and Egelman, 1993).

Recent improvements in hardware and software have made the currently available experimental methods for structural determination much more powerful in terms of the limits of resolution and the scope of substrates that can be examined. Until recently, atomic-level structural data could only be obtained on fibrillar assemblies using X-ray diffraction methods (crystallography and fiber diffraction). However, an increasing number of filamentous structures have been solved to NAR using either ssNMR spectroscopic analysis or, more commonly, cryo-EM. In addition, recent developments in microcrystal electron diffraction (MicroED) have enabled a wider application of diffraction methods to protein crystals, especially for situations in which only sub-micron-sized crystals can be obtained as is often the case for peptide filaments (Rodriguez *et al.*, 2015, 2017; Sawaya *et al.*, 2016; Warmack *et al.*, 2019).

Historically, the application of X-ray fiber diffraction enabled the first structural determinations of filamentous protein assemblies at NAR. However, the necessity of generating highly oriented specimens restricted these analyses to filaments that displayed persistent rod-like structures that promoted mesophase formation, which facilitated alignment of the filaments for diffraction experiments. The most common substrates were rigid filamentous viruses such as tobacco mosaic virus (Namba *et al.*, 1989). Specimens that displayed greater flexibility were less amenable to the formation of highly oriented sols. Given that most helical assemblies fall into the category of flexible or semi-flexible filaments, the utility of fiber diffraction for NAR structural determination of helical assemblies remains limited. Nevertheless, fiber diffraction can provide valuable structural information on peptide assemblies. For example, fiber diffraction of oriented amyloid filaments was critical for the identification of the cross-β conformation (Eanes and Glenner, 1968; Sunde *et al.*, 1997; Diaz-Avalos *et al.*, 2003).

Single-crystal X-ray diffraction was the first experimental method to be widely applied to the analysis of peptide assemblies at NAR. This technique has been particularly valuable for structural determination of assemblies derived from short amyloidogenic peptide sequences (Eisenberg and Sawaya, 2017; Ke *et al.*, 2020). However, two distinct challenges are encountered in the application of this method. The first is the experimental difficulty associated with growing suitable single crystals, which is a necessity for high-resolution diffraction experiments. Helical assemblies present several unique challenges to crystallization including limited solubility, length variability, and structural polymorphism. High-throughput screening of crystallization conditions has facilitated identification of effective crystallization conditions. However, crystallization of fibrillogenic peptides and proteins seems to work best under conditions in which the protomers are weakly associated such that self-assembly occurs concurrently with crystal growth. Achieving this condition may require

https://doi.org/10.1017/S0033583522000014 Published online by Cambridge University Press

introduction of mutations that weaken the interfacial interaction between protomers or enhance the solubility of the peptide or protein (Spencer *et al.*, 2013).

The second challenge for single-crystal diffraction analysis is imposition of crystallographic symmetry on the assembly. Helical arrays of chiral rod-like molecules cannot easily accommodate the translational symmetry required for crystallization without imposition of an energy penalty associated with elastic distortion of the protomers (Rodriguez *et al.*, 2015). The resultant packing frustration can limit the dimensions of the crystals. MicroED methods using cryo-EM have alleviated this problem to a degree by allowing single-crystal diffraction experiments to be performed on sub-micron crystals. In addition, crystallographic space symmetry restricts the screw axes to two-, three-, four-, and six-fold rotations. While other helical symmetries can be accommodated in crystal structures (Dauter and Jaskolski, 2018), the protomers cannot occupy symmetry-equivalent positions under these non-crystallographic screw axes. In contrast, the structures of peptide and protein filaments can vary over a wide range of helical symmetries that include non-crystallographic screw symmetry and non-integral helical repeats.

The implication of these limitations can be best understood through comparison of peptide and protein filament structures solved using crystallography *versus* those determined using complementary methods such as ssNMR spectroscopy or cryo-EM, which are not subject to these symmetry restrictions (*vide infra*). Currently, a number of structures are available at comparable resolution for helical assemblies derived from the same peptide sequence using two independent methods of high-resolution structural analysis. In the limited cases in which these comparisons have been made, the crystallographically determined structures have been observed to differ from those determined from ssNMR or cryo-EM (Guenther *et al.*, 2018; Guerrero-Ferreira *et al.*, 2018, 2019). Crystallization imposes conditions that may select for a specific structural form that happens to crystallize well, while a sample of filaments suspended in solution may display significant structural polymorphism. Despite this caveat, crystallography has yielded significant structural insights into the packing of protomers within peptide and protein assemblies and has been especially important in understanding the structural factors that control association of amyloidogenic peptides that adopt cross-β structures (Eisenberg and Sawaya, 2017). In addition to the aforementioned concerns, crystallographic studies of helical filaments often employ mutants or truncations of the native sequences that promote crystallization. The effect of these modifications, vis-à-vis the structure of filaments derived from full-length proteins, needs to be evaluated on an individual basis.

ssNMR measurement has also been applied as a method for structural determination of helical peptide filaments (Huang *et al.*, 2018). Similar to solution NMR structural determination of soluble proteins, selective labeling of the protomers with magnetically active nuclei enables determination of inter-atomic distances between labeled residues within the protein sequence. These distance measurements place constraints on the spatial arrangement of the polypeptide backbone and side chains from which a structural model can be generated. The accuracy of the atomic model depends on the number of constraints, the selectivity of labeling, and the size of the protein.

NMR distance measurements have an upper limit that depends on the identity of labeled nuclei and the experimental method. For ^{13}C–^{15}N contacts, the most commonly employed isotopic spin pair in protein and peptide structural determinations, the upper limit for accurate distance measurements is approximately 6 Å. However, inter-atomic distances up to 10–12 Å can be measured using magnetically active nuclei that are less common in peptides and protein sequences, e.g. ^{19}F and ^{31}P (Mehta *et al.*, 2004). Multiple long-range distance constraints can be challenging to acquire, which hinders assignment of helical symmetry and accurate determination of supramolecular structure. To address this issue, ssNMR structural analysis has been combined with scanning transmission electron microscopy (STEM) mass-per-length measurement or cryo-EM imaging (Colvin *et al.*, 2016).

In addition, the structural polymorphism observed for many helical assemblies can multiply the effective number of resonances in ssNMR experiments, which can complicate structural analysis as it often results in significant spectroscopic overlap and ambiguity in resonance assignment. Therefore, monomorphic filaments represent the best substrates for ssNMR structural analysis, although these may be challenging to isolate and purify to homogeneity due to the intrinsic polymorphism associated with peptide assemblies. Nevertheless, ssNMR methods have been employed for the structural determination of helical assemblies to NAR, including the structures of extended β-sheet filaments such as the HET-s prion domain (Siemer *et al.*, 2005), the Aβ(1-42) amyloid assembly (Colvin *et al.*, 2016), and the α-synuclein (α-syn) polymeric filament (Heise *et al.*, 2005).

Historically, TEM has been one of the most important methods for morphological analysis of peptide and protein filaments. The development of cryo-vitrification methods enabled preservation of isolated and dispersed filaments as thin films in the frozen, hydrated state (Dubochet, 2012). In addition, EM imaging at cryogenic temperatures significantly reduces beam damage due to interaction of the substrate with high-energy electrons. Cryo-EM imaging is less susceptible to introduction of structural artifacts than conventional TEM imaging, which often involves application of a heavy-atom stain (Lepault *et al.*, 1983). However, until the emergence of direct electron detectors, the lower limit of resolution for cryo-EM structural determination was ∼10 Å, which was insufficient to resolve secondary structure elements (Li *et al.*, 2013; Kühlbrandt, 2014; Subramaniam *et al.*, 2016). Higher-resolution reconstructions have been performed using film images (Ge and Zhou, 2011; Sachse, 2015), but this method is labor-intensive and has been superseded by use of direct electron detection cameras with high detective quantum efficiency (Song *et al.*, 2019).

Initially, pseudo-atomic models were built using rigid body modeling of structural subunits into the lower-resolution electron density maps resulting from cryo-EM measurements. The subunit structures were usually determined from X-ray crystallography or solution NMR spectroscopic determinations. These pseudo-atomic models were limited in accuracy due to the incompleteness of individual subunit structures. NMR structures display some degree of disorder in the more flexible regions of the molecule. Crystal structures are often derived from protein fragments rather than the entire peptide sequence. In addition, these input structures often provided little information about the packing interfaces in the helical filament, which are frequently more ordered within the assembly than in the isolated, soluble monomeric precursors.

The development of electron cryo-microscopy with direct electron detection has led to a revolution in structural determination of helical assemblies at NAR (Kühlbrandt, 2014). These detectors can routinely achieve resolutions ⩽4.0 Å. This level of resolution

https://doi.org/10.1017/S0033583522000014 Published online by Cambridge University Press

permits *de novo* building of atomic models of helical filaments from cryo-EM data alone. The main method for structure analysis of helical filaments involves iterative real-space reconstruction from cryo-EM images (Egelman, 2000, 2007, 2010). This single-particle method enables reconstruction from randomly oriented helical filaments that result from immobilization in a thin film of vitreous ice on a cryo-EM grid. Programs such as Relion and cryoSPARC are available to assist in image processing and reconstruction after assignment of helical symmetry (He and Scheres, 2017; Punjani *et al.*, 2017).

Cryo-EM helical reconstruction has many significant advantages for structural analysis of helical assemblies. As a single-particle method, the polymorphism typically observed for helical assemblies can be dealt with through manual or automated classification of the different structural variants. If enough images can be collected, different morphic variants can be structurally analyzed within the same grid. In addition, cryo-EM can tolerate the presence of impurities in the sample as long as the images of the contaminants can be distinguished from those of the analyte (Spaulding *et al.*, 2018). Cryo-EM analysis can be applied to small sample sizes (a few microliters of 0.1–1 mg ml^{-1} solution) and does not require heavy-atom or isotopic labeling as does crystallographic analysis and NMR measurements, respectively. In addition, the method is amenable to structure determinations on helical filaments directly derived from biological samples available in limited quantity, such as tau filaments from human brain tissue (Scheres *et al.*, 2020) or pili harvested directly from bacterial cells (Egelman, 2017). This procedure precludes the necessity of *in vitro* assembly of protein filaments, which can often result in structural polymorphism or deviations from the native filament structure (Wang *et al.*, 2006).

Comparison between NAR structures determined using different experimental methods highlights the challenges associated with the structural polymorphism of helical assemblies. Guenther *et al.* (2018) characterized the structure that resulted from crystallization of an eleven amino acid, amyloidogenic peptide segment, ^{247}DLIIKGISVHI^{257}, from human **T**AR **D**NA-binding **p**rotein 43 (TDP-43). MicroED was employed to determine the structure of ^{247}DLIIKGISVHI^{257} nanocrystals grown at 37 °C in aqueous CHES buffer (pH 8.5) (PDB: 5W52). The resultant structure comprised of a two-fold symmetric filament in which each protofilament displayed a parallel cross-β spine. The two protofilaments interacted through a steric zipper interface in which a face-to-face interaction resulted in side-chain interdigitation.

Surprisingly, at pH values ⩽7.5, cryo-EM analysis of assemblies derived from the same ^{247}DLIIKGISVHI^{257} peptide segment indicated the presence of a multitude of filamentous structures. Helical reconstruction of the most abundant population of filaments resulted in an atomic model that displayed 3_2 screw symmetry (PDB: 5W7V) (Guenther *et al.*, 2018). In addition to the observed difference in helical symmetry between the crystal structure and cryo-EM model, the structure of the protein filament observed in the cryo-EM analysis consisted of three protofilaments that were each based on an asymmetric unit composed of nine peptides. The protofilaments corresponded to the left-handed 3-start helices, in which each of the nine ^{247}DLIIKGISVHI^{257} segments in the asymmetric unit could adopt one of three different possible conformations. This conformational disparity between the crystal structure and cryo-EM structures of ^{247}DLIIKGISVHI^{25} illustrates a critical consideration in the structural analysis of helical assemblies, namely, the potential plasticity of quaternary structure in sequence space and the dependence of the filament structure on the assembly conditions.

Structural differences have also been observed between atomic models generated for assemblies derived from the same peptide using approaches based on either ssNMR spectroscopy or cryo-EM analysis. Colvin *et al.* reported the structure of a monomorphic variant of a peptide assembly of $A\beta_{1\text{-}42}$ using distance constraints derived from ssNMR measurements (Colvin *et al.*, 2016). This peptide has attracted significant scientific interest as it is a primary component of the amyloid fibers associated with the pathology of Alzheimer's disease. The filament structure comprised of an interacting pair of helical assemblies, in which each protofilament displayed the cross-β spine that is typical of amyloid assemblies. Hydrophobic interactions across the mating interface mediated association between protofilaments over an extended interface (Fig. 4).

Independently, Gremer *et al.* employed helical reconstruction from cryo-EM images to build an atomic model of the filament structure for a different monomorphic variant of $A\beta_{1\text{-}42}$ (PDB: 5OQV) (Gremer *et al.*, 2017). The cryo-EM structure differed significantly in detail from that reported by Colvin *et al.* The protofilament displayed a dimeric structure in which the two assemblies were related by the pseudo-2_1 screw axis (Fig. 5) (Scheres, 2020). In addition, a slight left-handed super-helical twist of −1.45° per 4.67 Å axial rise was observed for the protofilament, which resulted in a large helical pitch of circa 1200 Å. The helical reconstruction confirmed both the presence of the cross-β spine within the protofilaments and the steric zipper interactions between protofilaments at the inter-protomer interface. Despite these observations, the details of the packing interaction across the hydrophobic interface and the N-terminal structure of the peptide were distinctly different from the previously reported NMR analysis. The features of the cryo-EM structure were independently confirmed by ssNMR measurements on the corresponding filaments. The two structures represent two distinct morphic variants of $A\beta_{1\text{-}42}$. The experimental conditions for self-assembly differed significantly between the two $A\beta_{1\text{-}42}$ preparations, which reinforces the idea that specimen preparation has a critical influence on the structure of the corresponding filaments.

Structures of helical peptide assemblies

The diverse functional properties and exquisite responsive behaviors of biologically derived protein filaments have stimulated interest in the design of synthetic peptide assemblies that mimic the structure and function of the native congeners (Bowerman and Nilsson, 2012; Hamley, 2014; Beesley and Woolfson, 2019). However, rational and predictive design of helical assemblies remains a significant challenge, primarily due to the lability of helical symmetry in structural space and the resultant potential for structural polymorphism. Through necessity, the design of synthetic peptide filaments has primarily drawn from sequence–structure correlations established from structural analysis of super-secondary and tertiary structures of soluble proteins and discrete oligomers. Several examples of these peptide designs are described in the following sections. However, recent structural evidence suggests this approach may be insufficient to uniquely specify the supramolecular structure of the corresponding filaments. Supramolecular polymerization can result in the formation of helical filaments that display periodic chemical functionality along the contour length of the assembly. The high density of functional groups along the surface of the filaments can often

https://doi.org/10.1017/S0033583522000014 Published online by Cambridge University Press

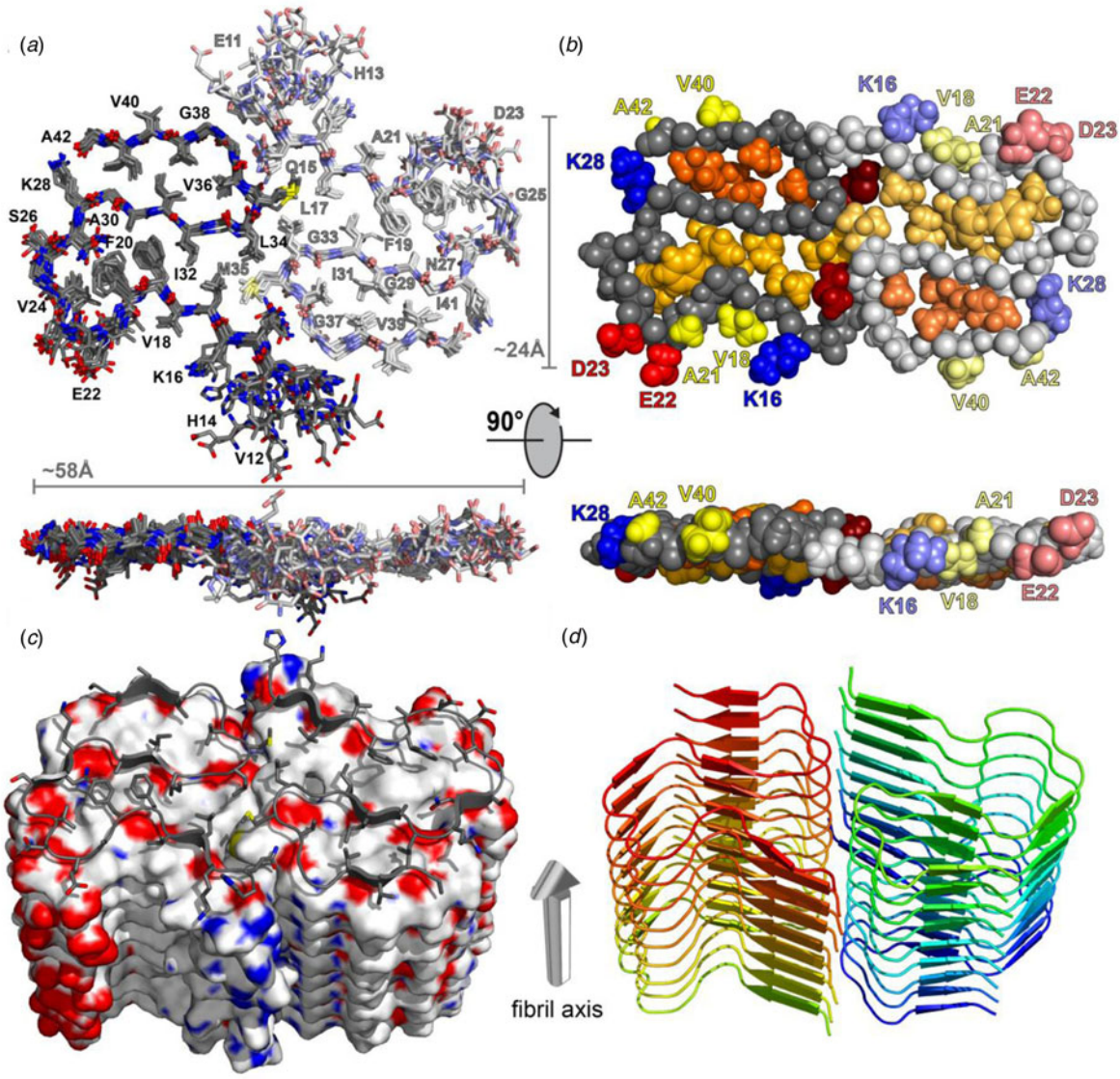

Fig. 4. Dimeric structure of $A\beta_{1\text{-}42}$ as solved by Colvin *et al*. by ssNMR measurements. Only residues Q15-A42 are shown. (*a*) Overlay of the 10 lowest-energy NMR structures. Left monomer is shown in dark colors; right monomer is shown in pale colors. (*b*) CPK model showing backbone in gray, hydrophobic side chains are shown in yellow (solvent-exposed), gold, and orange (buried clusters). (*c*) Surface model of $A\beta_{1\text{-}42}$. (*d*) Ribbon model of $A\beta_{1\text{-}42}$. Reprinted with permission from Colvin *et al*. (2016). *Journal of the American Chemical Society*, 138(30), 9663–9674. DOI: 10.1021/jacs.6b05129. Copyright 2016 American Chemical Society.

promote self-association into higher-order structures (Wang *et al*., 2021*a*). The influence of these interactions can be difficult to accurately predict since, in isolation, the energetic contributions of such local interactions to filament stability may be relatively small. In addition, researchers have observed that a small number of directed mutations at surface positions may convert soluble proteins into filamentous assemblies without perturbing the folded structure of the protomer (Garcia-Seisdedos *et al*., 2017, 2019). Due to the lability of helical symmetry and the resultant plasticity of quaternary structure, many synthetic peptide filaments display structural heterogeneity, often in conjunction with kinetically controlled and potentially chaotic self-assembly behavior (Wang *et al*., 2021*b*). High-resolution structural analysis provides critical structural insight that can inform experimental studies directed toward development of a mechanistic understanding of the elements that determine supramolecular structure and that can potentially enable control of function.

In subsequent sections, representative structural analyses of different classes of synthetic filaments are described in order to convey our current understanding of the relationship between sequence design and structure. Since the majority of assemblies described here derived from chiral substrates, i.e. peptides and enantiopure peptido-mimetics, these structural studies can potentially provide insight into the relationship between molecular chirality and supramolecular chirality. However, while chiral monomers may display a preference for a given helical hand in the corresponding assemblies, this correlation is not necessarily absolute (Harper *et al*., 1997; Chamberlain *et al*., 2000). Twist polymorphism, in which a chiral peptide monomer can assemble into either a right-handed or left-handed supramolecular enantiomorph, has been observed for amyloid fibrils assembled *in vivo* or *in vitro* (Usov *et al*., 2013; Kollmer *et al*., 2019; Wu *et al*., 2021). This phenomenon may also apply to helical filaments derived from self-assembly of designed peptides and peptido-mimetic

https://doi.org/10.1017/S0033583522000014 Published online by Cambridge University Press

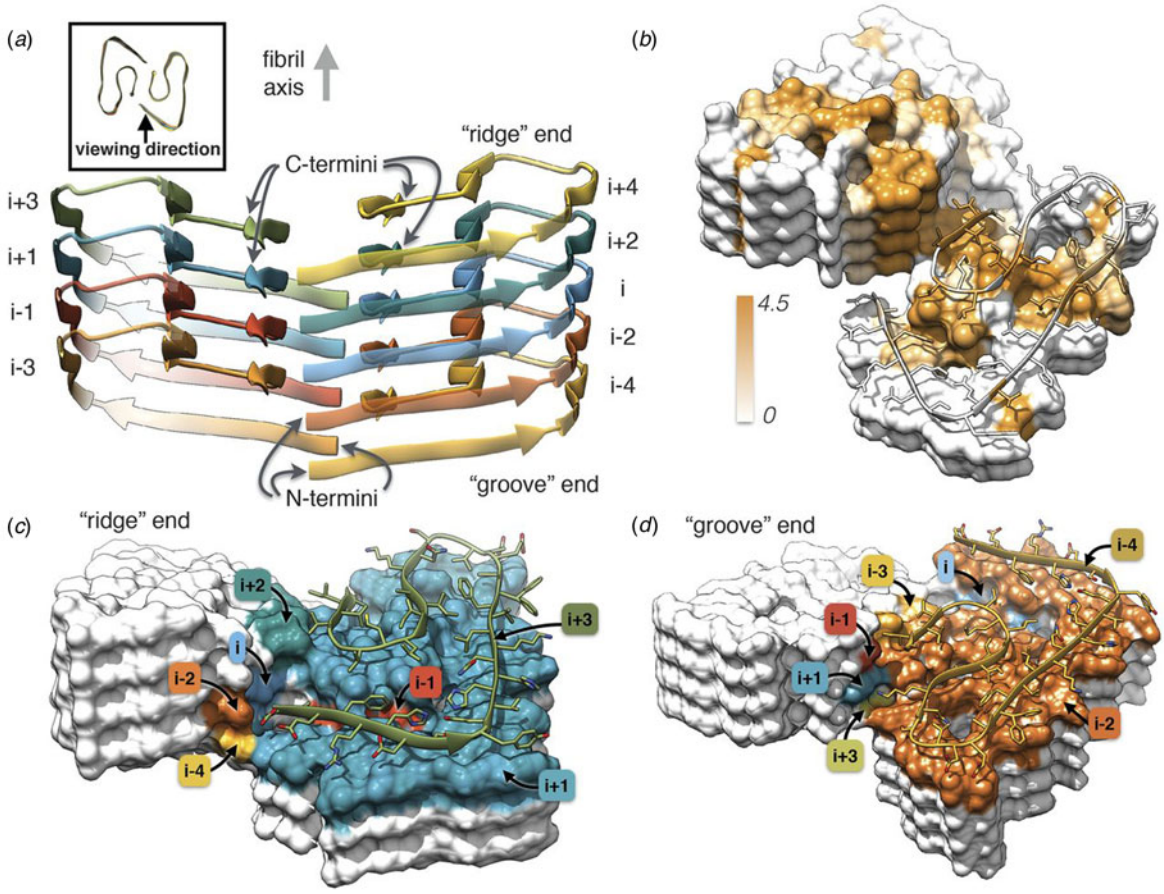

Fig. 5. Dimeric structure of $A\beta_{1\text{-}42}$ as solved by Gremer *et al*. by cryo-EM with helical reconstruction. (*a*) Opposing assemblies are staggered, producing a pseudo-2_1 screw axis in the filament. (*b*) Surface hydrophobicity of a representative segment the $A\beta_{1\text{-}42}$ peptide filament. Brown represents hydrophobicity value of 4.5, white represents 0.0 according to the Kyte–Doolittle scale. (*c*, *d*) Model of the 'ridge' and 'groove' ends of the $A\beta_{1\text{-}42}$ filament. Colors correspond to layers in (*a*). From Gremer *et al*. (2017). *Science*, 358(6359), 116–119. Reprinted with permission from AAAS.

foldamers. Helical hand information is lost in two-dimensional (2D) projection images obtained from TEM and cryo-EM analysis and in many cases cannot be recovered through building of the atomic model into the two enantiomorphic representations of the three-dimensional (3D) volume (Wang *et al*., 2022). In the absence of structural determinations at true-atomic resolution or easily resolved helical surface features, it may not be possible to unambiguously assign the helical hand of synthetic helical filaments and tubes.

Short-peptide assemblies

The conventional wisdom in peptide science posits that oligopeptides of length less than five amino acids might represent the least attractive substrates for construction of synthetic assemblies. Due to their limited size, these peptides would not be expected to adopt persistent secondary structures or form stable, structurally ordered assemblies. However, dipeptides and tripeptides can be more easily crystallized than longer-peptide sequences and the corresponding crystal structures often exhibit extensive intermolecular interactions between peptides that mimic the interfaces proposed to exist within self-assembled peptide filaments. Similar to crystallographic analyses reported for amyloidogenic peptides, high-resolution data from these crystal structures can provide insight into the nature of the interfacial interactions between peptides that can potentially inform the design of more complex sequences. Consequently, the structural analysis of assemblies derived from short peptides has been important to the intellectual development of the field of peptide self-assembly.

Structural investigations of simple dipeptides date back more than two decades and reveal surprisingly complex supramolecular arrangements between peptides in the crystalline state. In 2001, Görbitz demonstrated that simple dipeptides could crystallize into nanotube arrays (Görbitz, 2001). Subsequently, Reches and Gazit analyzed the self-assembly behavior of the Phe–Phe dipeptide and observed that it could self-associate into high aspect-ratio, nanoporous crystalline filaments (Reches and Gazit, 2003). Since these initial reports, significant research effort has been directed toward exploration of the potential of short peptides for the formation of filamentous assemblies for diverse applications (Raeburn *et al*., 2013). Oligopeptides have several advantages as materials, most notably ease of preparative-scale synthesis, which provides access to sufficiently large quantities of pure oligopeptides for detailed experimental studies. In addition, Tuttle, Ulijn, and co-workers demonstrated that coarse-grain molecular dynamics simulations could be employed to screen combinatorial sequence space *in silico* to identify dipeptides and tripeptides that might display the potential to form ordered supramolecular assemblies (Frederix *et al*., 2011, 2015). Subsequent experimental studies have borne out the hypothesis that these

https://doi.org/10.1017/S0033583522000014 Published online by Cambridge University Press

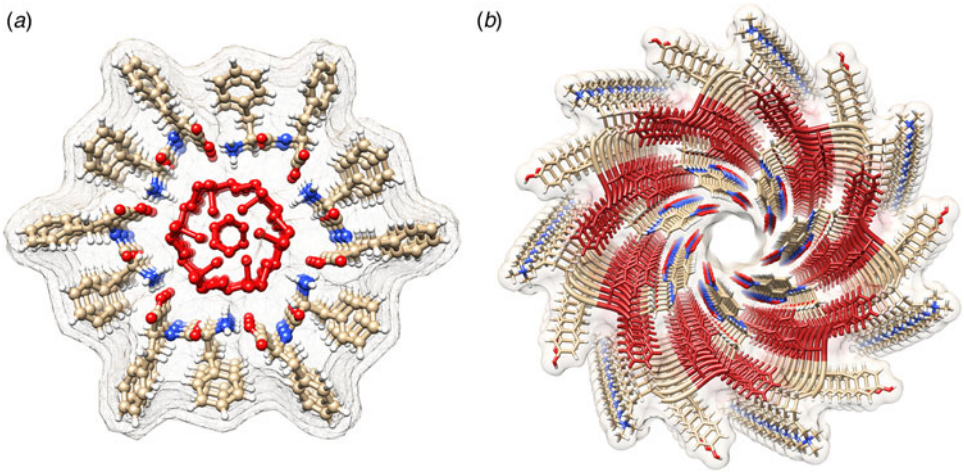

Fig. 6. (*a*) View down the helical channel within the crystal structure of the Phe–Phe dipeptide. Density due to water molecules can be observed in the lumen of the tube. (*b*) View down the channel in the atomic model of the C7 helical filament derived from self-assembly of tetrapeptide 1-KMe$_3$. The ^{D}Phe–^{D}Phe segment of each protofilament is highlighted in red.

computationally screened peptides can form ordered supramolecular assemblies.

Phe–Phe, the best studied synthetic dipeptide system, crystallizes in a unit cell with $P6_1$ space symmetry (Görbitz, 2001). The dipeptide subunits form a head-to-tail supramolecular polymer in the crystal (Fig. 6*a*). The chain of Phe–Phe molecules winds into a helical arrangement that defines a water-lined channel. Within a helical turn, the dipeptide segments are held together through a network of hydrogen-bonding interactions. The phenylalanine side chains are directed outward from the nanotube core and mediate lateral interactions between the helical arrays. Reches *et al.* described conditions that enabled the Phe–Phe peptide to self-assemble into crystalline nanotubes with an average diameter of 100–150 nm. Self-assembly of Phe–Phe from a mixed solvent system promoted crystal growth preferentially along the long axis of the tubular filament (Reches and Gazit, 2003). Subsequently, Görbitz and Kim, and co-workers, independently demonstrated that the peptide structure within the self-assembled tubes was identical to that observed in single crystals of the Phe–Phe dipeptide (Görbitz, 2006; Kim *et al.*, 2010).

Many examples of peptides containing Phe–Phe segments have been prepared and examined in terms of their self-assembly behavior and potential use as nanomaterials (Marchesan *et al.*, 2015). These systems display significant promise as hydrogelators, especially under conditions in which a solution pH change drives filament formation (Raeburn *et al.*, 2013). Recently, Feng *et al.* reported the cryo-EM analysis of helical filaments derived from a fluorophore-modified tetrapeptide containing a ^{D}Phe–^{D}Phe sequence (Feng *et al.*, 2020). The non-natural stereochemistry of the Phe–Phe sequence was employed to stabilize the resultant assemblies with respect to proteolysis *in vivo*. Two distinct structural polymorphs were observed for the resultant filaments, which were based on either C_7 or C_2 (distorted C_6) helical symmetry. An atomic model (PDB: 6X5I) was generated for the C_7 filament at 4.3 Å resolution (Fig. 6*b*). A superficial similarity was observed between this filament structure and the crystal structure of the Phe–Phe peptide. In both assemblies, the protofilaments were based on stacking of peptides such that the backbone was oriented in a plane perpendicular to the central helical axis. In either case, the protofilaments associated to form an oligomeric nanotube that defined a solvent-accessible central lumen. However, the structure of the tetrapeptide assembly was distinct from the crystal structure of Phe–Phe nanotube in that the peptide backbone of 1-KMe$_3$ extended radially outward with respect to the helical axis of the nanotube, in contrast to the circumferential arrangement observed in the crystal structure of the Phe–Phe dipeptide. These results suggested that while Phe–Phe may be employed as a minimalist self-assembling peptide segment, the helical structures of the resultant assemblies can vary significantly depending on the sequence context even for relatively short peptides.

In further support of this hypothesis, Bera *et al.* recently reported the structural analysis of assemblies derived from two related tripeptides, Pro–Phe–Phe and Hyp–Phe–Phe in which imino acids were positioned N-terminal to the well-studied Phe–Phe sequence (Bera *et al.*, 2019). The presence of proline derivatives within a peptide sequence has often been observed to disrupt periodic secondary structures due to conformational restrictions, particularly in the accessible range of ϕ torsions, and the inability of the endocyclic imide group to serve as a hydrogen bond donor (Reiersen and Rees, 2001). Crystallographic analysis of the respective peptides indicated that they adopted similar structures that displayed a local helical conformation rather than an extended, β-strand conformation that is more typically observed for peptides containing Phe–Phe segments. The tripeptide units were stacked into an extended helix in which the phenylalanine side chains radiating outward. Peptide helices interacted laterally through formation of a phenylalanine zipper at the respective helix–helix interfaces. In contrast, the sequence permuted variants, Phe–Pro–Phe and Phe–Phe–Pro, formed β-sheet structures. As observed for longer peptides (*vide infra*), small sequence modifications can drive the assembly down an alternative folding pathway that results in different quaternary structures.

Cross-β filaments

Cross-β filaments were the first synthetic peptide assemblies that were investigated that resulted from rational design efforts. Initial designs focused on sequences that, when assembled into a β-strand, displayed facial amphiphilicity such that self-assembly resulted in the formation of an amphipathic β-sheet (Bowerman and Nilsson, 2012). These sequences usually comprised alternating patterns of hydrophobic and hydrophilic amino acids such

https://doi.org/10.1017/S0033583522000014 Published online by Cambridge University Press

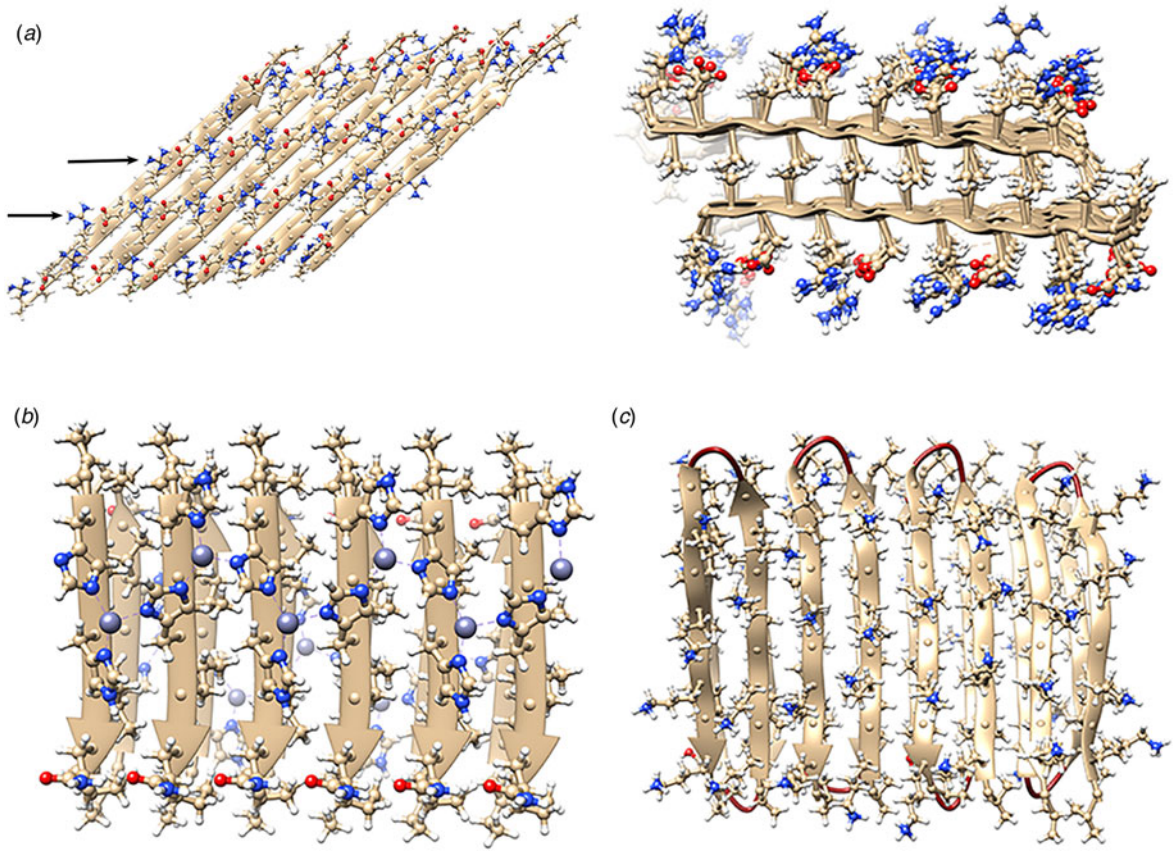

Fig. 7. (*a*) Facial and side views within the atomic model corresponding to the tilted bilayer filament of peptide RADA-16. Arrows indicate the complementary electrostatic interactions between cross-strand arginines and aspartic acid residues. (*b*) Facial view of the atomic model of the cross-β fibrils of peptide HHQ. Zinc ions (gray spheres) bridge adjacent strands through coordination to histidine residues. (*c*) Facial view of the atomic model of the MAX1 bilayer filament. Adjacent hairpins in each layer are *syn* to each other, but *anti* to the corresponding hairpin in the other layer.

that the polar repeat pattern reinforced the fiber repeat of a β-sheet (Pauling and Corey, 1951). The β-strands readily self-associate into cross-β filaments through hydrogen bonding interactions. Pairwise association of protofilaments usually accompanies self-assembly, which results in burial of the hydrophobic surfaces of the two sheets at the interface between protofilaments.

The rational design of synthetic cross-β filaments was initially reported in the 1990s when several research groups realized that introduction of self-complementary electrostatic and hydrogen-bonding interactions between side chains could strongly bias an oligopeptide sequence toward formation of a stable β-sheet filament (Zhang *et al.*, 1993, 1994; Aggeli *et al.*, 1997, 2001; Marini *et al.*, 2002). Zhang and co-workers were among the early entrants in this field and demonstrated that ionic self-complementary peptide sequences could form robust β-sheet assemblies. Most of these peptide designs assumed that β-strands would pack in an antiparallel arrangement in the fibrils, which would result in cross-strand pairing of oppositely charged residues (Zhang *et al.*, 1993). However, Cormier *et al.* demonstrated, using ssNMR measurements, that RADA-16, one of the most thoroughly investigated of these peptides, assembled into a bilayer filament derived from self-association of parallel β-sheet protofilaments (Cormier *et al.*, 2013). The atomic model of the filament was based on a face-to-face (homotypic) sheet packing interface between two protofilaments corresponding to the individual β-sheets. Peptides within a protofilament adopted a progressive two-residue shift that enabled electrostatic interaction between oppositely charged arginine and aspartic acid residues on adjacent strands in the parallel β-sheet (Fig. 7*a*). To accommodate this registry shift, the chain axes of the peptides within the filament were tilted 35° with respect to a plane parallel to the fibril axis.

Since these initial studies, a number of β-sheet-forming peptides have been designed based on similar sequence considerations (Bowerman and Nilsson, 2012). However, only a few of these synthetic cross-β filaments have been structurally investigated at NAR. Lee *et al.* reported the ssNMR structure (PDB: 5UGK) of a cross-β fibril based on an amphipathic heptapeptide sequence, HHQ (Ac-IHVHLQI-NH_2) (Lee *et al.*, 2017). In the presence of Zn^{2+} ions, the peptide assembled into cross-β fibril in which the parallel, in-register alignment was maintained through coordination of zinc ions by facially proximal histidine residues (Fig. 7*b*). These results demonstrate that metal ion coordination can serve as a method to introduce structural specificity within a peptide filament as well as a selective mechanism to drive peptide self-assembly.

Schneider, Pochan, and co-workers, designed a series of synthetic peptides in which a synthetic type-II′ β-turn enforced a β-hairpin conformation between two antiparallel β-sheet strands (Schneider *et al.*, 2002). MAX1 (Ac-VKVKVKVKV^{D}P^{L}PTKVK VKVKV-NH_2), a typical peptide in this series, undergoes pH-driven or salt-driven self-assembly into hydrogels that involved the formation of cross-β fibrils. The MAX1 peptide design was based on an alternating sequence of hydrophilic and hydrophobic amino acids. This polar patterning should favor the formation of

https://doi.org/10.1017/S0033583522000014 Published online by Cambridge University Press

an amphipathic β-sheet upon charge neutralization or electrostatic screening. The heterochiral turn sequence, V^DP^LPT, limits the accessible conformational space of the peptide and serves as a constraint that promotes self-assembly (Lamm *et al.*, 2005). Nagy-Smith *et al.* reported the structural analysis of MAX1 using ssNMR measurements (PDB: 2N1E) (Nagy-Smith *et al.*, 2015), which indicated that MAX1 formed a monomorphic bilayer fibril in which adjacent β-hairpins within a fibril adopted a *syn* geometry (Fig. 7*c*). The two protofilaments pack face-to-face and are oriented in an *anti*-arrangement such that the turn surfaces are on opposite edges of the protofilaments that comprise the bilayer fibril. Self-assembly is driven through burial of hydrophobic surface area at the interface between the cross-β protofilaments. These results demonstrate the power of NAR structural methods to interrogate the details of peptide packing within synthetic β-sheet fibrils.

While cryo-EM analysis has been employed extensively for structural analysis of amyloid fibrils (Gallardo *et al.*, 2020), it has not been extensively applied to the structural analysis of designed cross-β assemblies (see the following section for examples of the cryo-EM analysis of β-sheet nanotubes). While these designed assemblies have been routinely employed for the construction of synthetic biomaterials for medical applications, the limited availability of structural information at NAR hinders the development of this field (Wang *et al.*, 2021*b*). One potential benefit of these analyses would be to gain insight into the surface structure of the filament, which has a critical role in mediating interactions at the cell–biomaterial interface. This structural information is essential for development of functional biomaterials for biomedical applications. Cryo-EM may represent the best experimental approach for the structural analysis of synthetic cross-β fibrils in that it can potentially unravel the speciation of different structural polymorphs, as has been accomplished for amyloid fibrils (Zhang *et al.*, 2019).

Cross-β nanotubes

Structural analyses of filaments derived from self-assembly of a number of β-sheet forming peptides have provided evidence for the formation of thin-walled, wide-diameter nanotubes based on a cross-β fibril supramolecular architecture. Initial studies focused on oligopeptides derived from amyloidogenic peptide sequences. While not resulting from *de novo* design, the corresponding peptide sequences assembled into filamentous structures that appeared quite distinct from the cross-β fibrils typically observed from self-assembly of amyloidogenic peptides and proteins having much longer sequences. The short length of these peptide sequences provided an opportunity to examine the effect of site-directed mutagenesis on self-assembly within a well-defined sequence context. *De novo* design of oligopeptide sequences for cross-β nanotube formation has lagged to some degree due to the absence of structural information at NAR. However, cryo-EM analysis has provided the opportunity to generate reliable atomic models for β-sheet nanotubes, as recently illustrated for two separate peptide assemblies (Wang *et al.*, 2021*b*; Pieri *et al.*, 2022).

In 2003, Lynn and coworkers reported the formation of wide-diameter, thin-walled nanotubes from self-assembly of a hydrophobic heptapeptide derived from the Aβ sequence. This experimental study represented a tipping point in the structural analysis of β-sheet nanotubes from biologically derived to bio-inspired assemblies (Lu *et al.*, 2003). The truncated sequence Ac-^{16}KLVFFA^{22}E-NH_2 ($A\beta_{16\text{-}22}$) self-associated into nanotubes under acidic conditions (pH 2) in which the negative charge of the carboxylate side chain of the terminal glutamic acid was neutralized. The outer diameter of the nanotubes was estimated as ~520 Å with a wall thickness of 40 Å. In contrast, at neutral pH, $A\beta_{16\text{-}22}$ formed thin filaments consisting of a pair of twisted protofilaments of ~50 Å in diameter. The latter assemblies were consistent with the ultrastructure typically observed in low-resolution TEM images of amyloid fibrils (Schmidt *et al.*, 2016).

A combination of SAXS/SANS measurements, powder X-ray and electron diffraction, and ssNMR was employed to provide insight into the structural differences between the two morphological forms (Mehta *et al.*, 2008). The protofilament structure at neutral pH was based on a stack of five cross-β fibrils (Fig. 8*a* and *b*), in which adjacent $A\beta_{16\text{-}22}$ peptides were arranged in exact registry in an antiparallel β-sheet. In contrast, the $A\beta_{16\text{-}22}$ nanotubes are arranged in an antiparallel β-sheet in which adjacent peptides adopt an alternating single-residue offset (Fig. 8*c* and *d*). Each nanotube consists of an indeterminate number of cross-β protofilaments based on a bilayer structure. Individual protofilaments are oriented at an angle of ~23° with respect to the helical axis of the tube. Conventional TEM and AFM measurements, performed under acidic conditions, indicated that bilayer ribbons formed in solution within 30 h. The ribbons eventually closed to form the nanotube through fusion of the edges. The evolution of morphology from twisted ribbons to helical ribbons to tubes has been observed often for self-assembly processes involving chiral monomers, including amyloidogenic peptides and proteins (Selinger *et al.*, 2004; Ziserman *et al.*, 2011; Adamcik and Mezzenga, 2018).

Like Aβ, α-synuclein (α-syn) is a natural protein that self-assembles into cross-β fibrils. The presence of these fibrils has been associated with degeneration of dopaminergic neurons that is a symptom of Parkinson's disease (Spillantini *et al.*, 1997). Morris *et al.* demonstrated that an eight-residue truncation product derived from α-syn, α-Sβ1, NH_2-^{37}VLYVGSK^{44}T-COOH, was able to form a helical ribbon structure (Fig. 9*a*) (Morris *et al.*, 2013). The initial assemblies evolved over time; subsequently forming a closed nanotube through sealing of the edges of the tape (Fig. 9*b*). Structural models were constructed for the ribbon and tube using medium-resolution data acquired from a combination of conventional TEM, FTIR, and X-ray fiber diffraction analyses (Fig. 9*c*–*e*). The peptide sequence displays contour-length amphiphilicity with a hydrophobic N-terminal segment and hydrophilic C-terminal segment. Self-assembly resulted in the formation of a nanotube based on an amphiphilic bilayer in which the hydrophobic segments were sequestered in the interior and the hydrophilic segments decorated the convex and concave surfaces. Each leaflet within the bilayer consisted of peptides packed in parallel β-sheet in which the peptides were oriented in an antiparallel arrangement across the bilayer interface. The α-Sβ1 tubes were ~2400 Å in diameter, which was significantly wider than most peptide-based nanotubes resulting from self-assembly of either biologically derived or synthetic β-sheet peptides.

The self-association behavior of the α-Sβ1 peptide was similar to that of $A\beta_{16\text{-}22}$ in that wide-diameter, thin-walled nanotubes resulted from *in vitro* assembly under ambient conditions. While the sequences were different, both peptides displayed contour-length amphiphilicity, i.e. the sequence could be formally parsed into distinct polar and non-polar segments along the peptide backbone. This sequence pattern more closely resembled conventional amphiphiles such as phospholipids or amphiphilic block copolymers, rather than the facially amphiphilic cross-β fibrils described in the preceding section. Consequently, the

https://doi.org/10.1017/S0033583522000014 Published online by Cambridge University Press

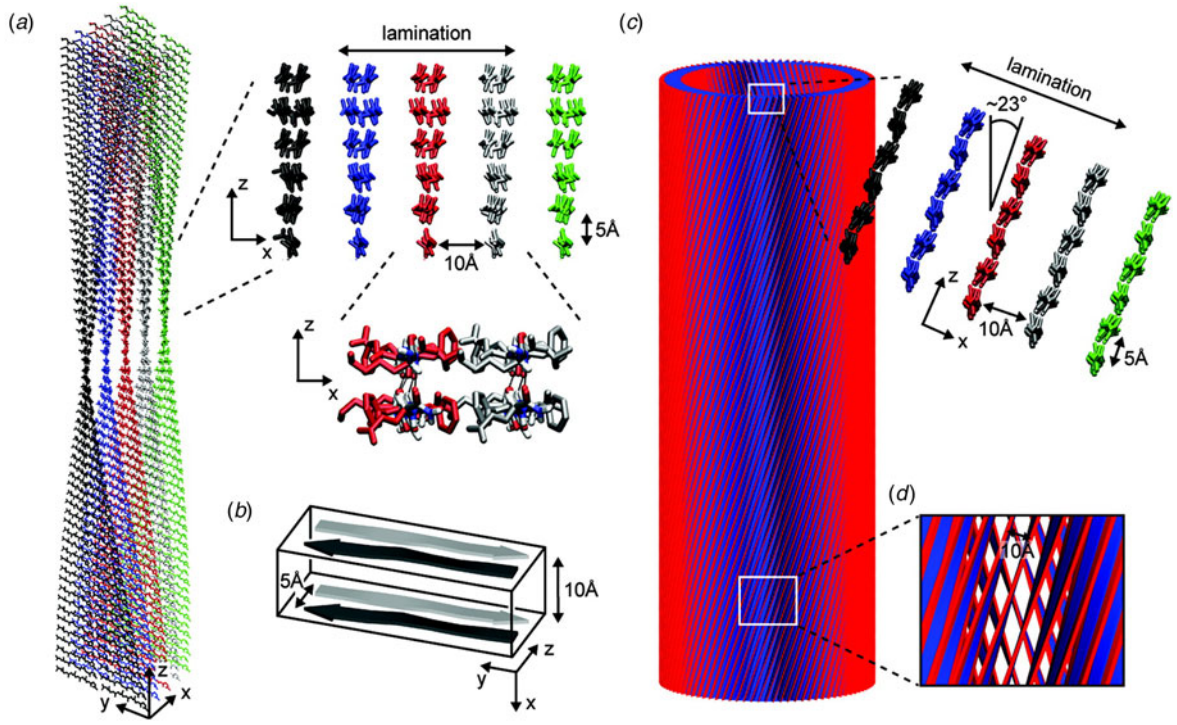

Fig. 8. Morphological variants of $A\beta_{16\text{-}22}$. (*a*) Atomic model of the laminated filament of $A\beta_{16\text{-}22}$ observed at neutral pH. (*b*) Proposed unit cell describing the packing of peptides in the laminated filament of $A\beta_{16\text{-}22}$. (*c*) Atomic model of the bilayer nanotube of $A\beta_{16\text{-}22}$ observed at acidic pH. (*d*) Expanded representation of the tilted packing of β-strands within a bilayer nanotube of $A\beta_{16\text{-}22}$. Reprinted with permission from Mehta *et al.* (2008), *Journal of the American Chemical Society*, 130(30), 9829–9835. Copyright 2021 American Chemical Society.

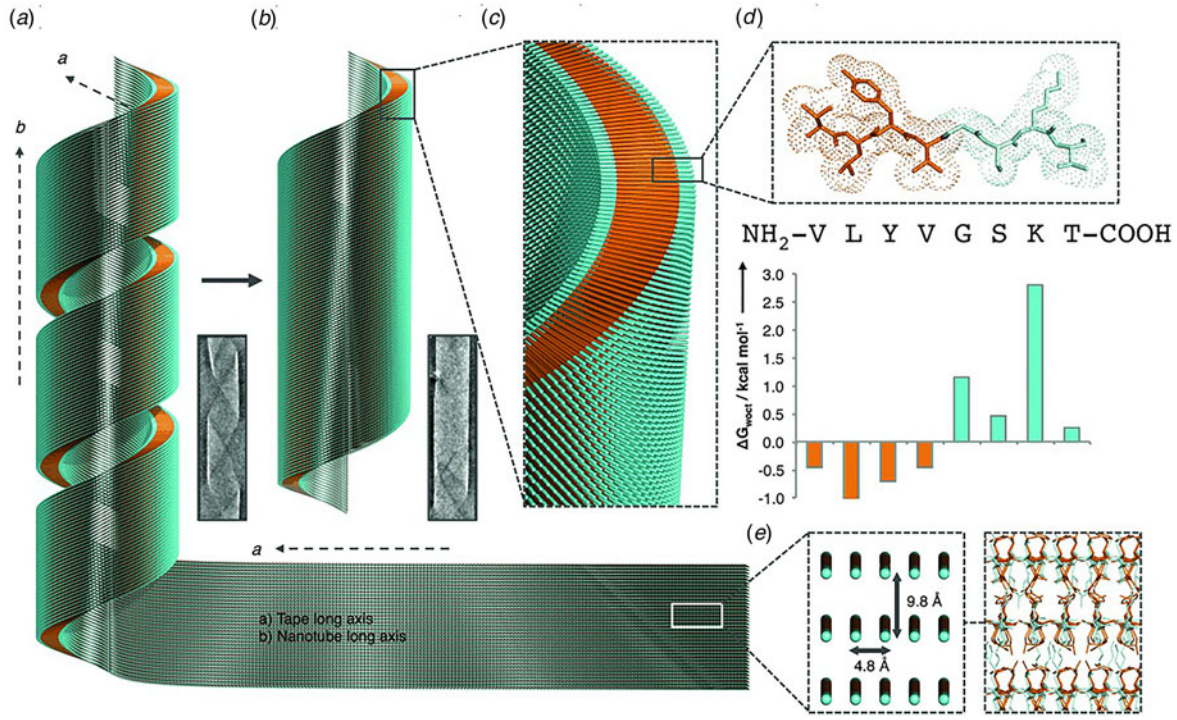

Fig. 9. Proposed mechanism of assembly and structural model of nanotubes derived from self-assembly of α-Sβ1 peptides. (*a*) Model of the initially formed helical ribbon with associated TEM image. (*b*) Model of the mature tubes with associated TEM image. (*c*) Cross-sectional depiction of the mature tube indicating the packing arrangement of peptides in the amphiphilic monolayer. (*d*) Sequence and stick model of the α-Sβ1 peptide. Residues are colored to indicate amphiphilic character based on water-octanol transfer free energies. (*e*) The orientation of the α-Sβ1 strands are shown in the context of the tape then leading to the nanotubes. The single peptides are represented as lines with hydrophobicity and hydrophilicity shown as orange and cyan, respectively. Reprinted with permission from Morris *et al.* (2013), *Angewandte Chemie International Edition*, 52(8), 2279–2283.

https://doi.org/10.1017/S0033583522000014 Published online by Cambridge University Press

layered packing of peptides within the respective nanotubes is reminiscent of the leaflet structure of lipids, in which the hydrophobic portions of the peptide sequence are buried in the core of a monolayer or bilayer with the polar groups decorating the solvent-contacting surfaces (Figs 8 and 9).

Amyloidogenic peptide segments can be incorporated into more complex sequence architectures to promote unique modes of nanotube self-assembly. Nowick and coworkers reported the crystal structure of a macrocyclic β-sheet peptide, 1, derived from the $A\beta_{16\text{-}22}$ sequence (PDB: 5VF1) (Chen *et al.*, 2017). The KLVFFAE sequence was combined with EAFFVLK, its retro-sequence, in a cyclic arrangement in which the two peptide segments were covalently connected with δ-ornithine amide-bond linkages (Fig. 10*a*). For this peptide sequence, macrocyclization limited the accessible conformational space that the peptide could adopt, which presumably restricted the range of supramolecular structures that could result from self-assembly. Crystallographic analysis revealed the presence of nanotubes that formed a porous, hexagonally close-packed lattice under the $P6_122$ space group symmetry of the crystal structure (Fig. 10*b*). Individual nanotubes within the crystal were double-walled and the asymmetric unit consisted of six macrocyclic peptides, in which the inner (concave) and outer (convex) walls of the nanotube were composed of helical arrays of structurally distinct dimers and tetramers, respectively. The dimers at the concave surface self-associated through the formation of hydrogen bonds between the backbone of each monomer and were further stabilized through complementary charge interactions between β-strands (Fig. 10*c* and *d*). The tetramers associated via a combination of hydrogen bonds and hydrophobic interactions in a β-barrel-like structure (Fig. 10*c* and *e*). Each tetramer was associated with four other tetramers by hydrogen bonds. The hexagonal close-packed arrangement of tubes, viewed along the crystallographic *c*-axis, was consistent with the formation of assemblies in solution and subsequent lateral association in the crystal structure. A similar mechanism has been proposed for the formation of nematic liquid crystalline phases in the self-assembly of nanotubes from the A6K peptide (*vide infra*) (Bucak *et al.*, 2009). It is interesting to note that despite the conformational constraints that macrocyclization imposed on the peptide sequence, the resultant structure, especially the outer wall of the nanotube, would have been difficult to predict based on our current knowledge of peptide and protein quaternary structure.

Contour-length amphiphilicity has been employed as an explicit design principle to engineer the sequences of synthetic self-assembling peptides. When these designs incorporate amino acids that display a preference for the formation of β-strand conformation, self-assembly of the corresponding sequences often resulted in supramolecular architectures based on β-sheet formation. Zhang and co-workers were the first researchers to employ this concept to design a class of synthetic surfactant-like peptides (SLPs) based on sequences that displayed contour-length amphiphilicity (Vauthey *et al.*, 2002). In contrast to the adventitious amphiphilicity of the $A\beta_{16\text{-}22}$-derived and α-Sβ1 peptides, Zhang's SLP designs were directly analogous to small-molecule amphiphiles. The peptide sequences consisted of a polar head group of one or two charged amino acid residues, and a non-polar tail composed of a short sequence of hydrophobic amino acids. The properties of these peptide surfactants have been studied extensively over the past two decades (Hamley, 2011). Thus far, however, the structures of the resultant assemblies have not been described at NAR.

The surfactant peptide, NH_2-AAAAAAK-COOH (A6K), has been the most thoroughly investigated member of this class (Bucak *et al.*, 2009; Castelletto *et al.*, 2010; Cenker *et al.*, 2012; Middleton *et al.*, 2013). Above a critical volume fraction, A6K formed a nematic meso-phase composed of an apparently homogeneous population of nanotubes with an approximate mean diameter of 550 Å and an estimated shell thickness of 33 Å. SAXS, cryo-EM, ssNMR, and X-ray diffraction of flow-aligned nanotube solutions contributed structural insights that have led to a proposed structural model for the tubes in which protofilaments derived from antiparallel β-sheet architectures were arranged in an amphiphilic monolayer. In the proposed model, structurally adjacent A6K peptides within the cross-β protofilaments were oriented in register (Fig. 11*a*). Tube formation was proposed to result from lamination of the protofilaments. The H-bonded network of the protofilaments was determined to be oriented at a pitch angle of ~52° with respect to the central axis of the nanotube. In contrast to A6K, the longer-peptide variants, A8K and A10K, form twisted ribbon architectures despite remarkably similar local packing interactions within the unit cells of the respective peptide systems (Rüter *et al.*, 2020) (Fig. 11*b*).

Peptide surfactants based on bolaamphiphile architectures have also been demonstrated to self-assemble into cross-β nanotubes. Bolaamphiphiles display an alternate mode of contour-length amphiphilicity, in which the sequence was composed of a hydrophobic core with flanking terminal polar residues, e.g. RFL_4FR, EFL_4FE, or KI_4K (Zhao *et al.*, 2013; Da Silva *et al.*, 2015*a*, 2015*b*; Hamley *et al.*, 2017). For example, the bolaamphiphilic peptide Ac-KI_4K-NH_2 assembled into wide-diameter, thin-walled nanotubes, despite the potential for electrostatic repulsion between the terminal lysine residues. In contrast, the amphiphilic peptide Ac-I_4K_2-NH_2, in which charges are localized at the C-terminus, formed thin, twisted filaments, which suggested that the polar sequence pattern had an influence on supramolecular structure despite the fact that both peptides adopted a β-sheet conformation in the assembled state. Zhao *et al.* demonstrated that, in aqueous solution, hydrophobic interaction between the isoleucines in Ac-KI_4K-NH_2 drove the formation of nanotubes (Zhao *et al.*, 2015). In contrast, upon addition of acetonitrile (ACN), the peptides assembled into twisted tapes (20% ACN) or thin fibrils (80% ACN). According to CD data, the β-sheet structure was not disrupted in the presence of ACN. However, the addition of ACN reduced the polarity and dielectric constant of the aqueous solvent, which weakened the hydrophobic interaction between the side chains of the isoleucine residues. The weakening of the hydrophobic interactions was proposed to result in a lower degree of sheet lamination, which was hypothesized to underlie the morphological transition from tubes to ribbons to fibrils.

The short sequences of these bolaamphiphilic peptides represent a flexible platform to examine the effect of mutagenesis on the resultant supramolecular structure of the corresponding nanotubes. Interestingly, substitution of residues within the hydrophobic core was observed to influence the diameter of the corresponding nanotubes (Zhao *et al.*, 2018). The parent sequence, Ac-KI_4K-NH_2, was modified through introduction of hydrophobic amino acids having different steric properties. In the series Ac-$KI_nV_{4\text{-}n}K$-NH_2 ($n = 1$–4), SANS, TEM, and cryo-EM measurements indicated that the diameter of the corresponding tubes decreased as the number of isoleucine residues (n) decreased, i.e. with increasing numbers of valine residues within the sequence (Fig. 12). A similar effect was observed for

https://doi.org/10.1017/S0033583522000014 Published online by Cambridge University Press

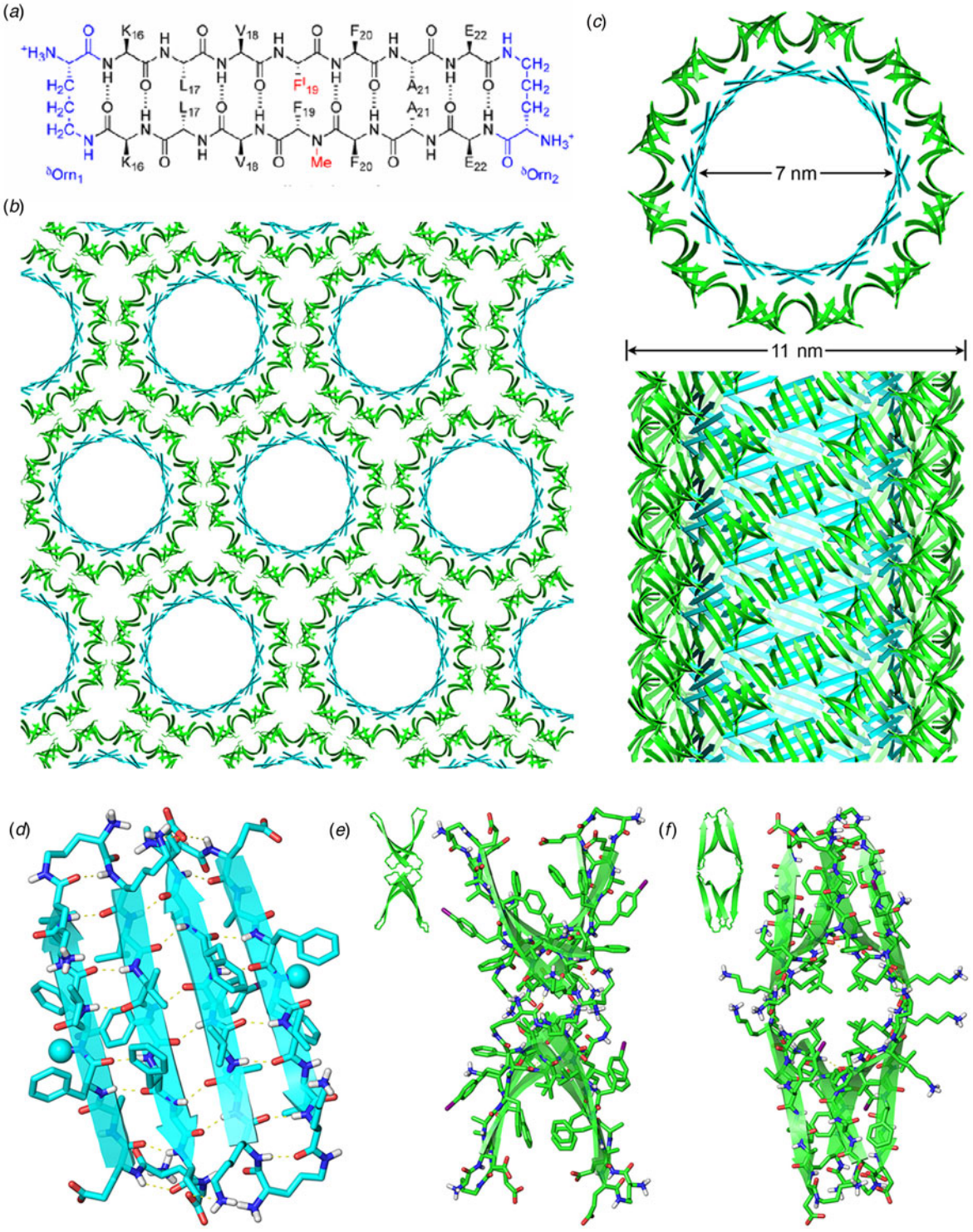

Fig. 10. (*a*) Sequence of macrocyclic β-sheet **1**. (*b*) Macrocyclic β-sheet **1** nanotubes pack into a honeycomb-like crystal lattice. (*c*) Top and side views of nanotube formed by macrocyclic β-sheet **1**. (*d*) Structure of dimeric subunit at the inner wall of the nanotube. (*e*, *f*) Different views of the tetrameric subunit at the outer wall of the nanotube. Reprinted with permission from Chen *et al*. (2017), Journal of the American Chemical Society, 139(24), 8102–8105. Copyright 2021 American Chemical Society.

substitutions of the C-terminal isoleucine in the parent sequence with either leucine or norleucine. In the latter situation, the peptides differed from isoleucine in the side-chain structure, which resulted in constriction of the diameter of the resultant nanotubes. Although the structures were not analyzed at NAR, these results indicated that the supramolecular structure of the nanotubes could be rationally varied through sequence modifications. More detailed structural analyses should provide insight into the interplay of factors that control higher-order assembly within this peptide family.

https://doi.org/10.1017/S0033583522000014 Published online by Cambridge University Press

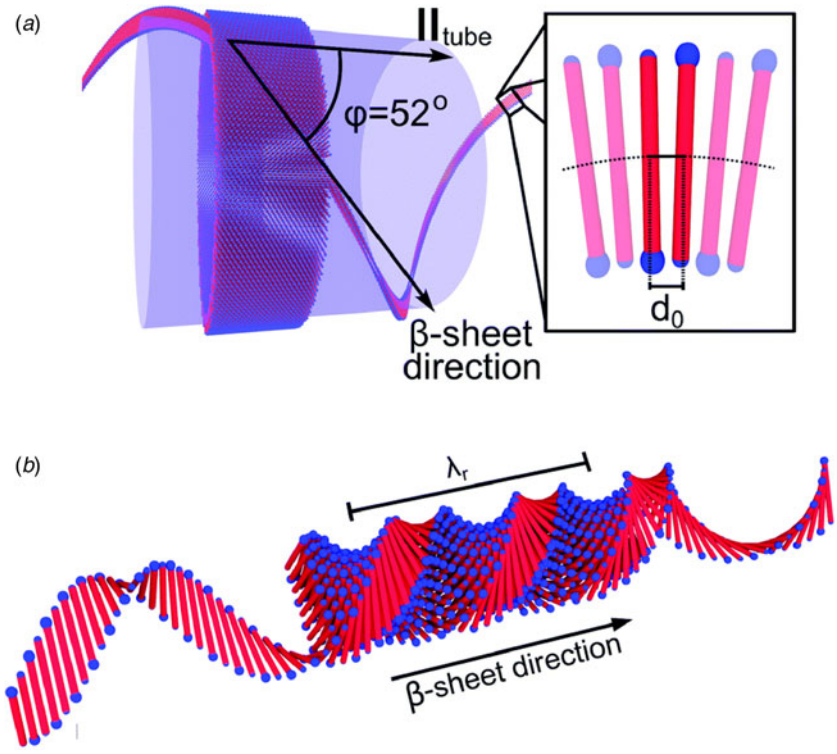

Fig. 11. (*a*) Structural model of a nanotube derived from self-assembly of peptide A_6K. A single protofilament within the nanotube inclines at an angle of 52° with respect to the long axis of the assembly. Inset indicates the proposed antiparallel packing arrangement of peptides within a cross-β protofilament. (*b*) Structural model of a laminated ribbon derived from self-assembly of peptide A_8K or $A_{10}K$. The trajectory of single cross-β protofilament within the ribbon is highlighted. The quantity λ_r corresponds to the helical pitch of the ribbon. In both representations, the imposed helical hand was based on an arbitrary decision. Reproduced from Rüter *et al.* (2020), *Physical Chemistry Chemical Physics*, 22(33), 18320–18327, with permission from the Royal Society of Chemistry.

Nanotube formation was also observed in a series of amphiphilic block co-polypeptides Ac-$[ALV]_x$-*b*-$[KGE]_y$-NH_2 ($x + y = 7$) (Van Rijt *et al.*, 2019). TEM analysis indicated that peptide Ac-$[ALV]_3$-*b*-$[KGE]_4$-NH_2 self-assembled to form high aspect-ratio nanotubes of ∼90 Å in diameter that were stable over a wide pH range (pH = 2–12) and at temperatures up to 80 °C. Cryo-EM and SAXS analysis confirmed the nanotube morphology, while FTIR spectroscopy supported the formation of β-sheet within the assembly. The proposed structure was based on a monolayer nanotube in which adjacent peptides were aligned in an antiparallel orientation such that the hydrophilic blocks decorated the inner and outer surfaces of the tube. A sequence with a smaller hydrophobic block, Ac-$[ALV]_2$-*b*-$[KGE]_5$-NH_2, remained as an unassociated monomer under the same conditions. Longer hydrophobic blocks resulted in kinetically trapped mixtures of nanotubes and cylindrical micelles or in macro-phase separation. In analogy to synthetic amphiphilic block copolymers, these results suggested that the hydrophilic–hydrophobic balance could be employed as a parameter to control self-assembly and supramolecular structure as has been observed for synthetic block copolymers (Jiao *et al.*, 2020). In the cases of peptide-based and peptido-mimetic materials based on sequence-specific oligomers, the hydrophilic–hydrophobic balance should be easily amenable to synthetic control.

Lanreotide acetate, an 8-residue, disulfide-linked, cyclic peptide hormone, has also been demonstrated to form nanotubes of homogeneous diameter (∼280 Å) above a critical aggregation concentration in aqueous solution (Valéry *et al.*, 2003, 2004; Pouget *et al.*, 2010). Nanotube assembly coincided with formation of a hexagonal columnar meso-phase. The structure of the lanreotide nanotubes was initially investigated using a combination of EM, FTIR spectroscopy, and SAXS/WAXS diffraction analysis. Based on this evidence, the octapeptide was proposed to fold into a conformationally constrained β-hairpin. Monomers were suggested to initially associate to form face-to-face dimers (Fig. 13) due to attraction between hydrophobic residues and repulsion between positively charged residues. The dimers were hypothesized to subsequently assemble into helical ribbons through aromatic interactions and hydrogen bonds (Valéry *et al.*, 2003, 2004; Pouget *et al.*, 2010). For the parent lanreotide sequence, the initial structural model for the lanreotide nanotubes was based on the self-association of 26 bilayer protofilaments, in which the peptide backbones are arranged circumferentially around the periphery of the nanotube (Chervy *et al.*, 2019).

The structure of the lanreotide tubes has been recently determined using cryo-EM analysis (Pieri *et al.*, 2022). Helical reconstruction from the projection images afforded a 3D density map at 2.5 Å resolution (PDB: 7Q5A), which represented the highest resolution achieved thus far for a synthetic peptide nanotube. At this level of resolution, the helical hand of the symmetry could be assigned directly based on a structural comparison of atomic models constructed through direct fitting into the two different enantiomorphs that resulted from mirroring the density map. The helical symmetry of the lanreotide model was best described in terms of a right-handed 1-start helix with a rise of 1.04 Å and a rotation of 26.2° (Fig. 14). Surprisingly, the asymmetric unit was based on eight peptides arranged in a monolayer shell in which the peptide backbones extend radially outward from the central axis of the assembly. The hydrogen-bonding direction, corresponding to the cross-β structural interaction, occurs between peptides in every 27th asymmetric unit. The left-handed twist (−12.1°) of this 27-start helix is consistent with the left-handed twist observed for β-sheet in globular proteins and amyloid fibers (Chothia, 1973; Chamberlain *et al.*, 2000). The lanreotide nanotube structure differed significantly from the original model and highlighted the necessity of high-resolution structural analysis to fully understand peptide packing within helical filaments. In addition, unlike many synthetic peptide filaments, the population

https://doi.org/10.1017/S0033583522000014 Published online by Cambridge University Press

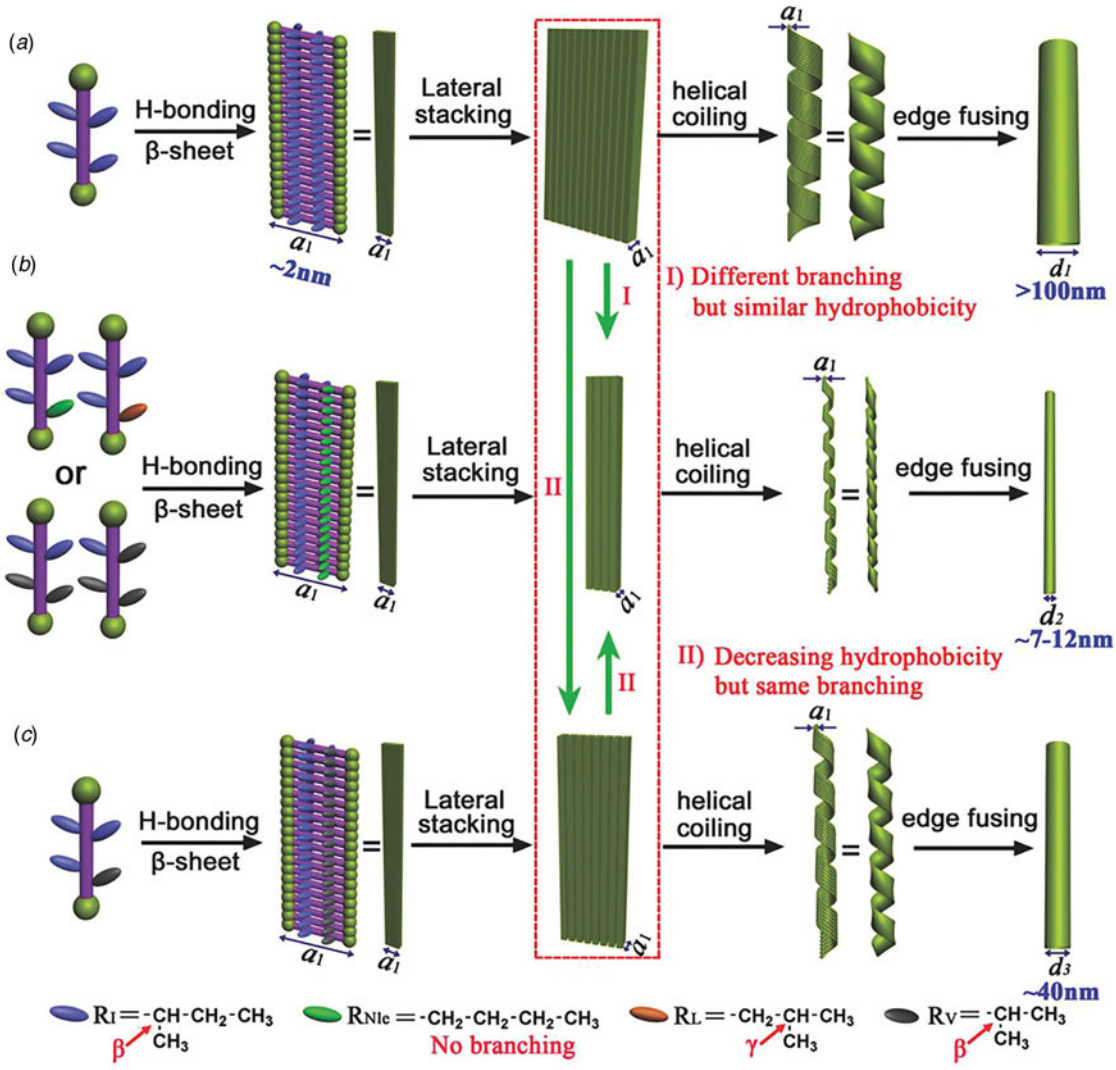

Fig. 12. Schematic illustration of the self-assembly of peptide nanotubes derived from site-directed mutagenesis of peptide Ac-KI$_4$K-NH$_2$. (*a*) Proposed model for self-assembly of the parent peptide Ac-KI$_4$K-NH$_2$. (*b*) Thin tubes are formed by changing side-chain branching and hydrophobicity, which influences the degree of lateral stacking of β-sheets. (*c*) A single mutation of isoleucine to valine in Ac-KI$_3$VK-NH$_2$ leads to an intermediate degree of sheet lamination and modest decrease in nanotube diameter. The assignment of helical hand was based on AFM measurements. Reprinted with permission from Zhao *et al.* (2018), *Small*, 14(12), 1703216.

of lanreotide nanotubes was uniform in diameter with negligible polymorphism. The high degree of structural uniformity within the assembly may have derived from the conformational constraints of the cyclic peptide monomer, which could have restricted interfacial interactions to specific geometries within the assembly through pre-organization.

The small size and constrained conformation of lanreotide acetate made it an attractive substrate to investigate the effect of sequence modifications and counterion effects on nanotube structure. Tarabout *et al.* demonstrated that substitution of the D-Trp4 residue with other aromatic amino acids led, in most cases, to retention of nanotube formation (Tarabout *et al.*, 2011). However, the diameter of the resultant monodisperse nanotubes depended on the size of the amino acid side chain at position 4 and ranged from 100 to 360 Å. Larger side chains increased the nanotube diameter, while smaller side chains had the opposite effect. The observed results were rationalized in terms of the influence of the molecular size parameter of the residue on the curvature at the concave interface between protofilaments. Counterion identity was also observed to influence diameter, although the effect could not be rationalized solely in terms of counterion size (Gobeaux *et al.*, 2012). The high-resolution structure of the parent lanreotide nanotubes should prompt a re-analysis of these mutagenesis results in terms of the structural influence of the substitutions on the packing of peptides in atomic model (Fig. 14).

Paternostre and coworkers (Valery *et al.*, 2015) subsequently reported the structural analysis of assemblies derived from triptorelin, a decapeptide that acts as a gonadotropin-releasing hormone agonist. Like lanreotide, the sequence of triptorelin contains a D-Trp residue, which was proposed to be involved in the formation of a reverse turn. In aqueous solution, triptorelin formed nanotubes in which the diameter depended on the pH of the buffer. At low pH (<6.5), small diameter (~11 Å) tubes were formed, while larger diameter (~50 Å) tubes were formed at higher pH (>7.5). This transition was proposed to involve a switch in the protonation state of a histidine side chain within the peptide sequence, which induced a structural transition within the protomer. X-ray crystallographic analysis was performed on

https://doi.org/10.1017/S0033583522000014 Published online by Cambridge University Press

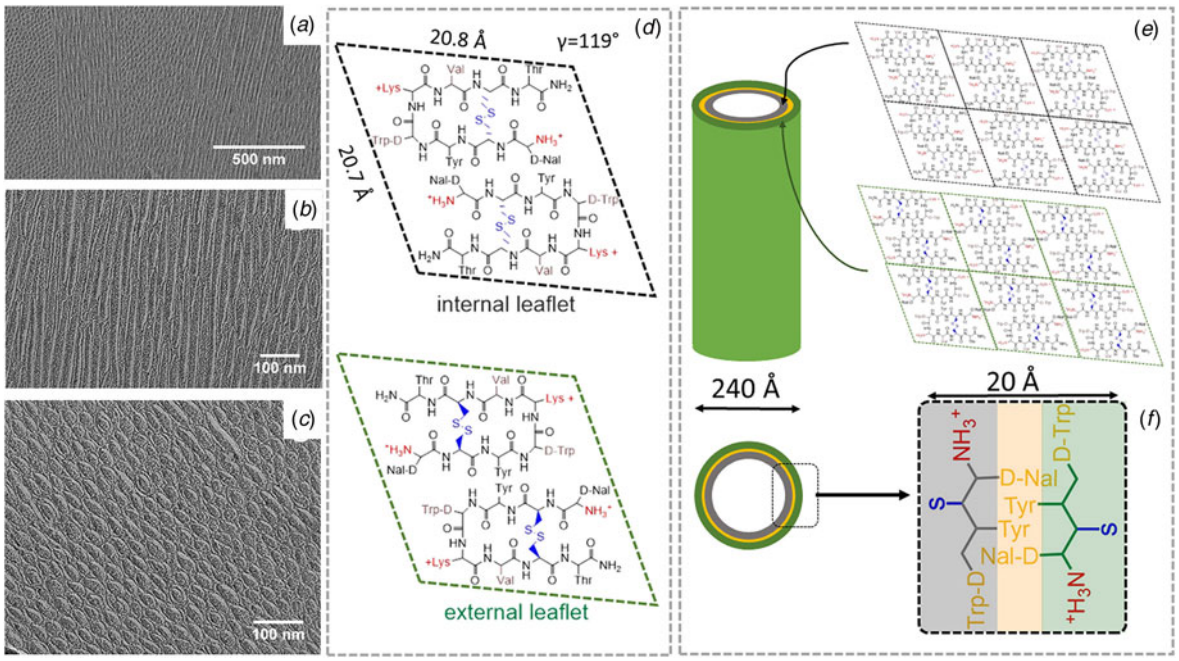

Fig. 13. Initial model for the self-assembled nanotubes of the lanreotide peptide. Freeze-fracture micrographs of longitudinally (*a*, *b*) and transversely (*c*) fractured nanotubes indicated the formation of uniform-diameter assemblies. (*d*) Proposed arrangement of lanreotide monomers in the internal and external leaflets of the bilayer nanotube. (*e*) Initial structural model of the bilayer nanotube with an expansion of the internal and external leaflets corresponding to 2 × 3 asymmetric units. (*f*) Cross-sectional model of the bilayer nanotube indicating the proposed side-chain packing arrangement between monomers at the leaflet interface. Reproduced from Chervy *et al.* (2019), *Langmuir*, 35(32), 10648–10657, with permission from the American Chemical Society.

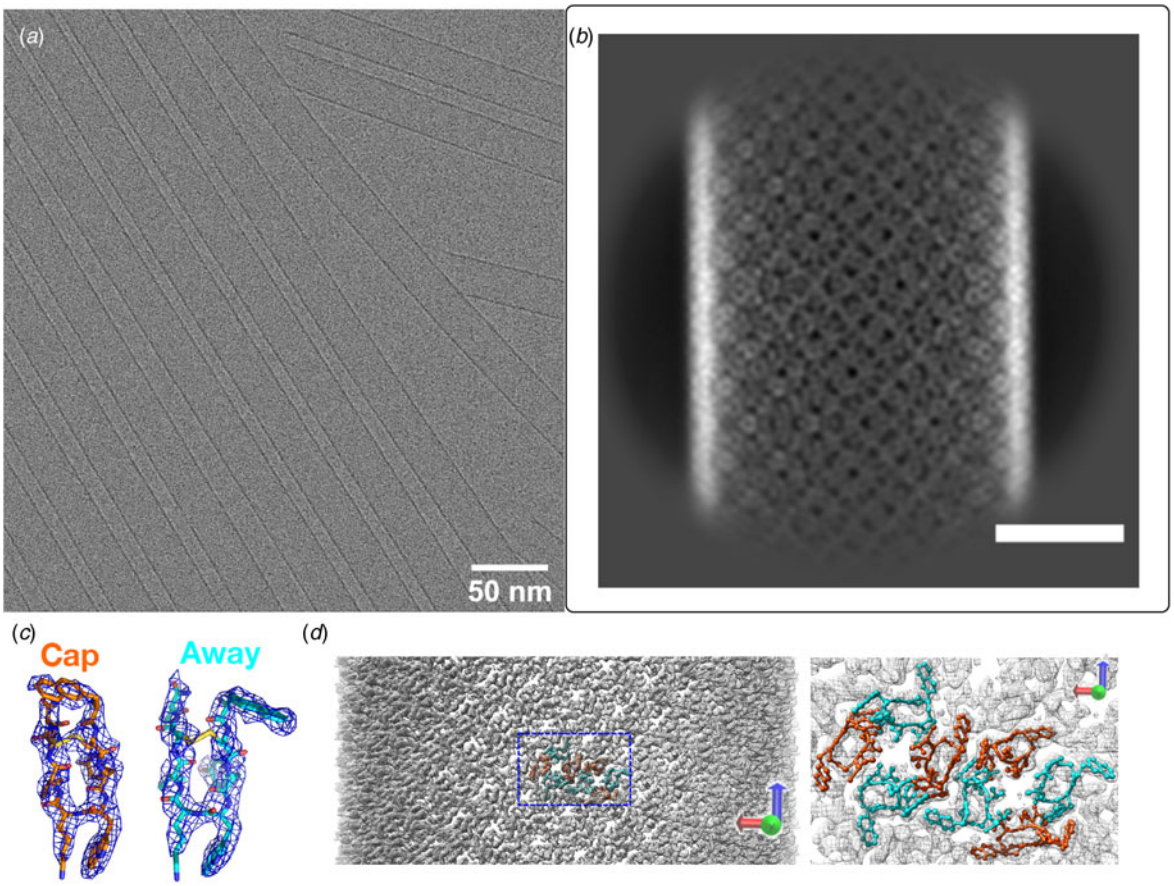

Fig. 14. Cryo-EM structure of lanreotide nanotubes. (*a*) Representative cryo-EM image of peptide nanotubes derived from self-assembly of lanreotide acetate. (*b*) Representative 2D class average derived from cryo-EM analysis of lanreotide nanotubes. (*c*) Density maps for the two main conformations, capped *versus* away, of the lanreotide peptide within the nanotubes. (*d*) Density map for the lanreotide nanotube in which the eight peptides in an asymmetric unit are highlighted within the assembly. An expansion of the asymmetric unit is depicted on the right in which the capped (orange) and away (cyan) conformations are indicated.

https://doi.org/10.1017/S0033583522000014 Published online by Cambridge University Press

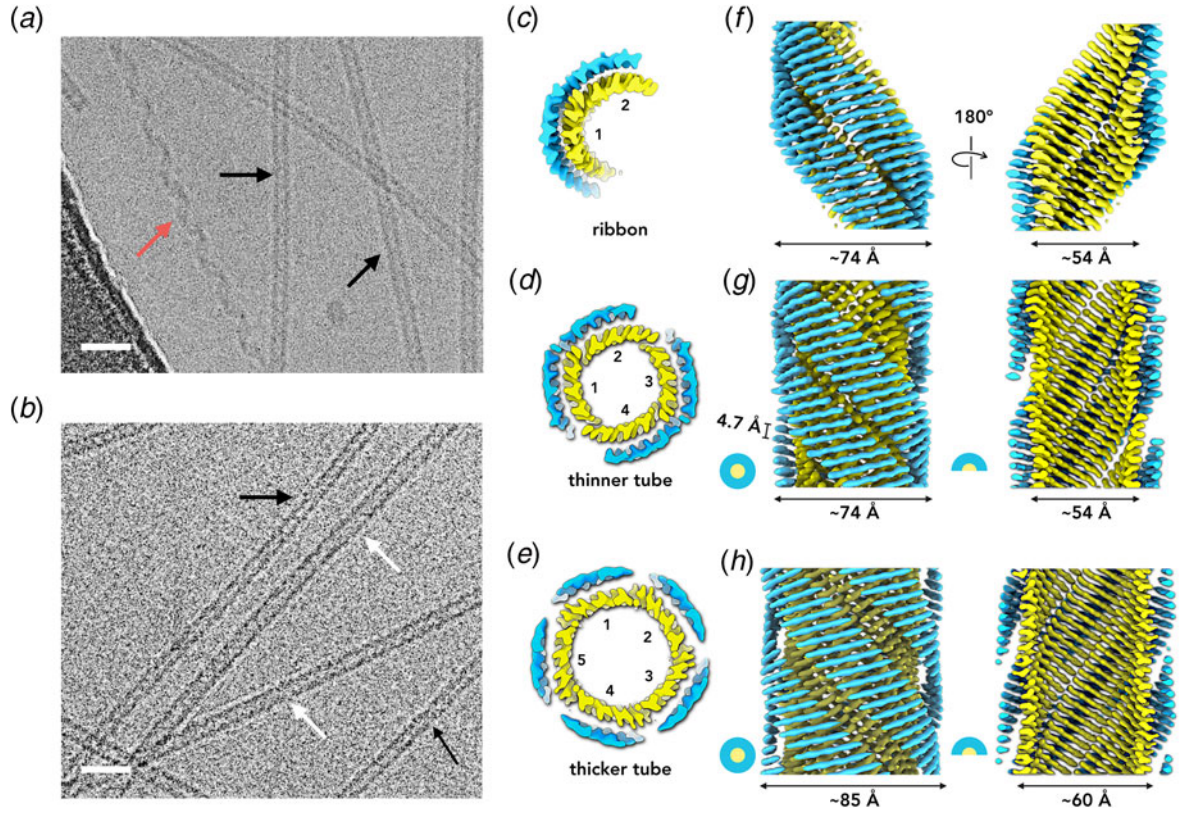

Fig. 15. Peptide **KFE8** self-assembles into helical ribbons and nanotubes. Representative cryo-EM images of **KFE8** assembled at ambient temperature (*a*) or annealed at 90 °C (*b*). Scale bar = 20 nm. Red, black, and white arrows indicate the presence of bilayer ribbons, thinner tubes, and thicker tubes, respectively. Cross-sectional and transverse views of the atomic models for the ribbons (*c*, *f*), thinner tubes (*d*, *g*), and thicker tubes (*e*, *h*). The helical hand was assigned based on imaging data from AFM measurements. Reference: Wang, F.; Gnewou, O.; Wang, S.; Osinski, T.; Zuo, X.; Egelman, E. H.; Conticello, V. P. Deterministic chaos in the self-assembly of β-sheet nanotubes from an amphipathic oligopeptide. *Matter*, DOI:10.1016/j.matt.2021.06.037.

triptorelin at high pH under conditions that resulted in flat lamellar structures rather than wide-diameter nanotubes. The structure (PDB: 4D5M) indicated the absence of β-sheet and the formation of a small globular fold that was stabilized through a hydrogen bonding interaction between the side chains of His(2) and Ser (4). The authors suggested that this interaction was lost at low pH, which resulted in the formation of β-sheet conformation.

Conticello and coworkers reported the cryo-EM structural analysis of assemblies derived from an amphipathic peptide KFE8, Ac-FKFEFKFE-NH_2 (Wang *et al.*, 2021*b*). This peptide had been previously reported to self-assemble into left-handed helical ribbons (Marini *et al.*, 2002; Hwang *et al.*, 2003). However, over the course of assembly, ribbons and nanotubes were observed, although the structure of the nanotubes depended on the assembly conditions. Cryo-EM analysis was employed to generate NAR models for two ribbons and three nanotubes (PDB: LQE, 7LQF, 7LQG, 7LQH, and 7LQI). At ambient temperature, the nanotubes were based on a bilayer structure consisting of four β-sandwich protofilaments, while under annealing the peptide assembled into nanotubes comprising five β-sandwich protofilaments (Fig. 15). Although the structures of the nanotubes differed, each protofilament was based on an unprecedented packing arrangement in which an inner layer of parallel β-sheet was packed against an outer layer of antiparallel β-sheet. The dependence of nanotube structure on minor changes under preparative conditions suggested that self-assembly was a kinetically controlled process. The resultant polymorphism could critically impact use of these resultant assemblies in biological applications through alteration of the structural interactions at the cell–biomaterial interface.

Taken together, these data results provide convincing evidence that helical filaments and nanotubes can result from self-assembly of appropriately designed peptides that adopt a cross-β conformation. Thus far, it has been challenging to reliably and accurately predict the supramolecular structure of such helical filaments from peptide sequence information, which contrasts with recent advances in prediction of tertiary structure (Baek *et al.*, 2021; Jumper and Hassabis, 2022). The structural information within the Protein Data Bank may not be sufficient at present to provide insight that would enable reliable prediction of atomic structure for most assemblies described here. In combination with the frequently observed polymorphism of β-sheet assemblies, the opportunities for reliable *de novo* design of synthetic β-sheet filaments remain relatively limited at present. However, the explosive growth of high-resolution structural data on amyloids over the past two decades provides evidence that supramolecular structural prediction might at some point in the near future become a tractable problem that would enable *de novo* design of β-sheet assemblies.

Coiled-coil filaments

Similar to β-sheet assemblies, α-helical filaments can be constructed through molecular design approaches based on polar sequence patterns (Beesley and Woolfson, 2019). However, in

https://doi.org/10.1017/S0033583522000014 Published online by Cambridge University Press

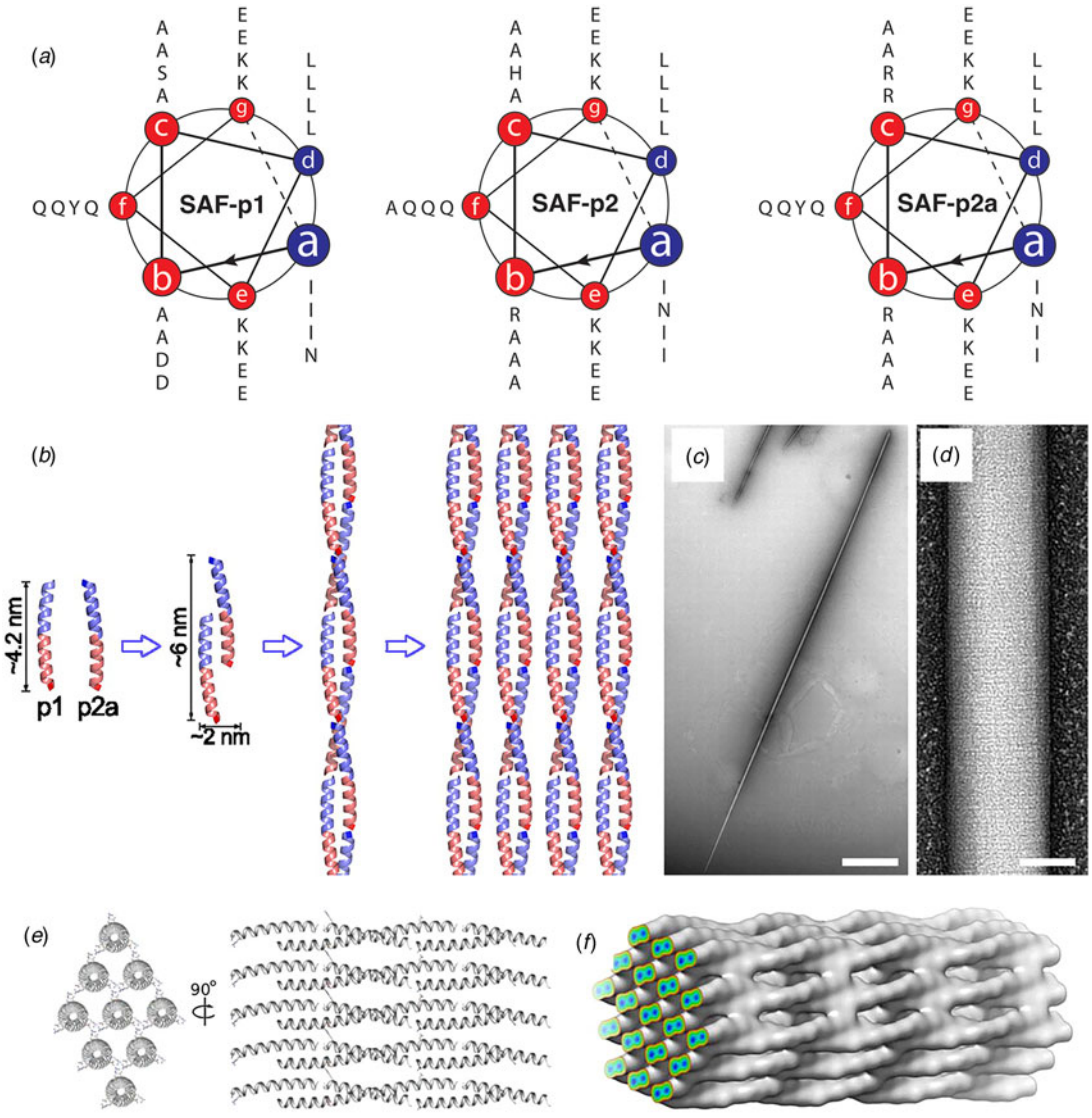

Fig. 16. (*a*) Helical-wheel diagrams of the **SAF-p1**, **SAF-p2**, and **SAF-p2a** peptides indicating the heptad periodicity. (*b*) Proposed model for the heteromeric association of **SAF-p1** and **SAF-p2(a)** peptides into a dimeric coiled-coil through sticky-ended self-assembly. (*c*, *d*) Transmission electron micrographs of the *para*-crystalline assembly of **SAF-p1** and **SAF-p2a** co-assembly. (e, *f*) Simulated model of the packing of coiled-coil peptides within the **SAF** assembly. Reprinted from Sharp *et al.* (2012), *Proceedings of the National Academy of Sciences of the United States of America*, 109(33), 13266–13271.

contrast to β-strands, the hydrogen bonding interactions in α-helices occur within, rather than between, secondary structure elements. Consequently, α-helical sequences can potentially adopt a stable conformation without self-association, while β-strand formation usually requires self-association between two or more intra- or intermolecular peptide segments. Conversely, β-sheet assemblies derived from short peptides are often more stable than α-helical assemblies, as self-association in the former case is primarily driven through directional hydrogen-bonding between β-strands rather than the weaker hydrophobic interactions that hold together α-helical assemblies (Knowles *et al.*, 2007).

The most common mode of self-association between α-helices involves coiling of multiple helices into super-helical architectures known as coiled-coils (Lupas and Bassler, 2017; Woolfson, 2017). Coiled-coil sequences are defined by repeat patterns based on a heptad motif (*a*-*b*-*c*-*d*-*e*-*f*-*g*), in which the residues at the *a*- and *d*-positions of the heptad repeat are usually hydrophobic amino acids. Self-association of helices is mediated through 'knobs-into-holes' packing interactions, which were first proposed by Crick in 1953 (Crick, 1953). The knobs correspond to the side chains of residues at *a*- and *d*-positions, which pack into complementary holes on adjacent helices in the assembly. The pitch of an α-helix corresponds to 3.6 residues, which differs slightly from the 3.5 residues/turn of a coiled-coil. Therefore, the helices in coiled-coil super-coil with a left-handed helical sense to accommodate the 'knobs-into-holes' interactions at the hydrophobic interface within the assemblies. In the helical wheel diagram of a coiled-coil, lettered positions are used to describe the architecture of individual α-helices (Fig. 16*a*). Sighting down the helix with the amino-terminus closest to the viewer, each residue is represented as a vertex of the helical wheel diagram in super-helix space. This diagram represents the relative orientation of residues that form the interacting faces within a given helix with respect to other helices in the axial projection of the coiled-coil.

The self-association of coiled-coil sequences usually results in discrete oligomeric states displaying rotational, i.e. cyclic (C_n),

https://doi.org/10.1017/S0033583522000014 Published online by Cambridge University Press

symmetry. The degree of oligomerization depends on the identity of the core (*a*, *d*) and proximal (*e*, *g*) residues of the heptad repeat sequences. Directed mutagenesis and computational design were employed to identify sequences that form C_n-symmetric homomeric oligomers consisting of two to nine α-helices (Zaccai *et al.*, 2011; Thomson *et al.*, 2014; Rhys *et al.*, 2018; Dawson *et al.*, 2021). In contrast to native coiled-coil filaments, e.g. intermediate filaments, tropomyosin, etc., designed coiled-coils usually form blunt-ended assemblies due to the short length of synthetic peptides, the in-register alignment of helices within the assembly, and the absence of discrete terminal interaction domains.

A convenient strategy to promote the formation of helical filaments from simple helical bundles involves alteration of the helix–helix registry within the assembly to promote staggered self-association between the α-helices (Pandya *et al.*, 2000; Potekhin *et al.*, 2001; Zimenkov *et al.*, 2004). Strand registry can be specified through the pattern of electrostatic interactions between helices, which usually occur between the residues at *e*- and *g*-positions on structurally adjacent helices. In addition, buried polar interactions can be introduced at either the *a*- or *d*-positions within the sequences of the helical protomers to control helix–helix alignment within the assembly (Oakley and Kim, 1998; Akey *et al.*, 2001).

Woolfson and co-workers employed this approach to fabricate helical assemblies based on a heterodimeric coiled-coil motif (Pandya *et al.*, 2000; Smith *et al.*, 2006). A pair of peptides, SAF-p1 and SAF-p2, was designed such that selective heteromeric association would result in a two-heptad offset between the pair of four-heptad peptides. This staggered orientation was enforced through a combination of complementary electrostatic interactions and a buried polar interaction (Fig. 16*b*). The formation of high aspect-ratio helical filaments was observed through sticky-ended association. The width of the filaments suggested that the dimeric coiled-coil protofilaments associated into bundles through weak non-specific lateral interactions. To promote a more specific lateral association, a modified peptide sequence, SAF-p2a, was designed to introduce electrostatic interactions between filaments through incorporation of arginine and aspartic acid at surface-exposed positions in the dimeric coiled-coil. Self-assembly resulted in the formation of highly ordered, *para*-crystalline filaments (Fig. 16*c* and *d*). Cryo-EM analysis of these filaments at intermediate resolution indicated that the dimers packed in a parallel, hexagonal array. The individual protofilaments within the *para*-crystalline assemblies corresponded to pseudo-infinite heterodimeric coiled-coils, which were arranged in parallel along the long axis of the *para*-crystalline assembly (Fig. 16*e* and *f*) (Papapostolou *et al.*, 2007; Sharp *et al.*, 2012).

A similar approach has been employed for the design of coiled-coil filaments based on homomeric self-association of peptides derived from coiled-coil dimer and trimer sequences (Zimenkov *et al.*, 2004, 2006; Gribbon *et al.*, 2008). However, reliance on a single-peptide sequence significantly constrained design space due to the necessity to incorporate the intermolecular interactions that specify a staggered orientation into single-peptide sequences. In the case of coiled-coil trimers, metal ion binding motifs could be incorporated into the sequence to direct or reinforce helix alignment to trigger assembly or disassembly in response to the presence of specific metal ions (Dublin and Conticello, 2008; Anzini *et al.*, 2013).

An alternative strategy for the fabrication of filamentous coiled-coil assemblies involved the stacking of discrete oligomeric bundles. Crystallographic analyses of coiled-coil structures provided evidence that discrete helical bundles could stack to form continuous superhelices along the highest order rotational axis (Ogihara *et al.*, 1997; Zaccai *et al.*, 2011; Lanci *et al.*, 2012). While these coiled-coil assemblies do not usually persist outside of the crystal, the termini of the peptide sequences could be modified to promote axial interactions that would result in the formation of thermodynamically stable helical filaments. This approach is particularly appealing for larger oligomers since the interfacial surface area buried upon the formation of helical stacks would be sufficient to stabilize the resultant assemblies, especially if coupled with other non-covalent interactions, e.g. electrostatic attraction between oppositely charged termini (Xu *et al.*, 2013; Burgess *et al.*, 2015). An additional advantage of this approach is that larger helical bundles, i.e. oligomerization states greater than a tetramer, encompass a central cavity of sufficient size to encapsulate appropriately shaped small molecules (Thomas *et al.*, 2018).

The latter approach was employed for the design of a helical filament based on a seven-helix bundle structure. Starting with the natural two-stranded coiled-coil **GCN4** leucine zipper, Lu and coworkers replaced residues at *e* and *g* with alanine, which generated the modified peptide **GCN4-pAA** (Liu *et al.*, 2006), which assembled into a heptameric coiled-coil. The seven-helix bundle displayed a successive single-residue offset between structurally adjacent α-helices, which resulted in a discrete helically symmetric structure that resembled a lock washer (Fig. 17). The heptameric lock washers remained unassociated in solution and in the corresponding crystal structure of **GCN4-pAA** (PDB: 2HY6). A positively charged arginine at the C-terminal position served as a gatekeeper residue, which prevented axial stacking through introduction of repulsive interactions between the termini of the seven-helix bundles.

Conticello and coworkers designed a self-assembling peptide nanotube by rationally modifying the sequence of **GCN4-pAA** (Xu *et al.*, 2013). The C-terminal arginine at the *d*-position was replaced with a leucine, in accord with the canonical sequence preferences for coiled-coils. This substitution restored the continuous hydrophobic interface. In addition, residues at the *b*- and *c*-positions of the heptad repeat sequence of **GCN4-pAA** were replaced with glutamate and lysine, respectively, to introduce electrostatic interactions that reinforced the association between helices in the heptamer. Two arginine residues were added at *f*-positions to prevent lateral association between helical bundles. The peptide termini were uncapped to promote axial stacking of lock washers through electrostatic interactions (Fig. 17*a* and *b*). Spectroscopic analysis of the corresponding peptide, **7HSAP1**, confirmed the presence of α-helical assemblies. TEM measurements indicated that **7HSAP1** spontaneously formed long fibrils under a wide range of monomer concentrations. STEM determined that most fibrils were ~31 Å in diameter, which was consistent with the diameter of the heptameric **GCN4-pAA** bundle observed in the corresponding crystal structure. X-ray fiber diffraction was employed to analyze the structure of the filament, which indicated the presence of stacked helical bundles in the fibril. ssNMR distance measurements on labeled **7HSAP1** peptides provided evidence that the registry shift between helices was retained in the filament. The solvatochromic fluorophore 6-propionyl-2-(*N*,*N*-dimethylamino)-naphthalene (PRODAN) was used to probe the accessibility of the lumen of the **7HSAP1** nanotube toward guest molecules. A dose-dependent shift in the PRODAN fluorescent emission was observed that was consistent with encapsulation within the hydrophobic lumen of the **7HSAP1** nanotube.

https://doi.org/10.1017/S0033583522000014 Published online by Cambridge University Press

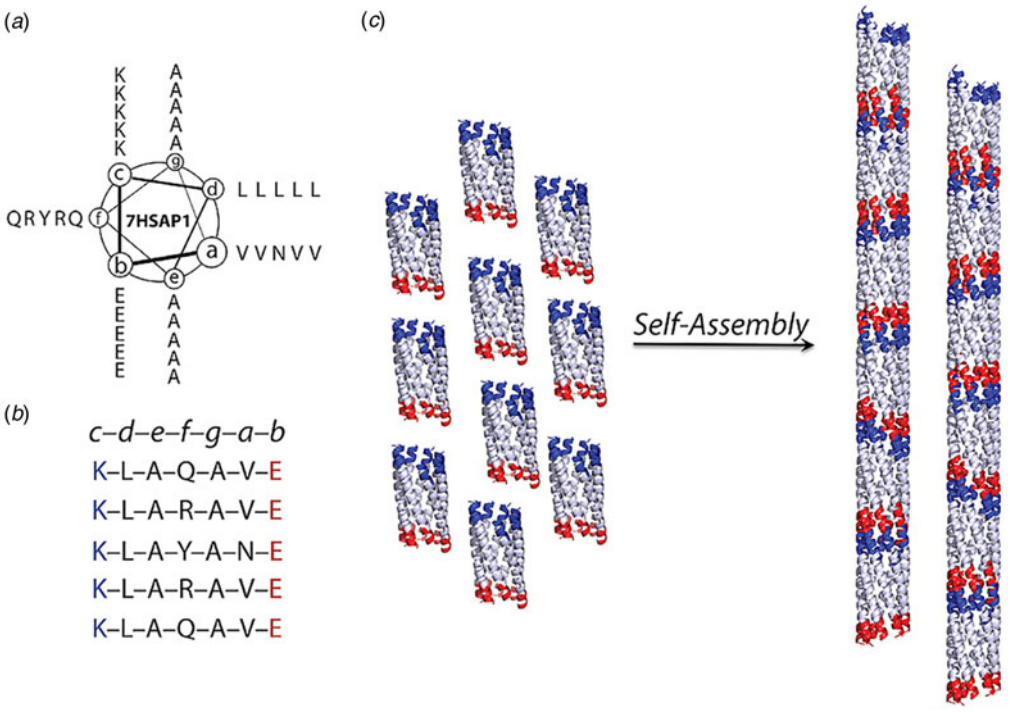

Fig. 17. Mechanism of self-assembly of coiled-coil lock washers into helical filaments. (*a*) Helical wheel diagram of designed coil-coil peptide **7HSAP1**. (*b*) Sequence of the **7HSAP1** peptide indicating the heptad registry. Basic and acidic residues involved in the intra-bundle and inter-bundle (axial stacking) interactions are highlighted in blue and red, respectively. (*c*) Proposed mechanism of self-assembly of heptameric lock washers of **7HSAP1** into filaments through electrostatic interactions between oppositely charged termini. The seven-helix bundle structure was derived from the crystal structure of **GCN4-pAA** (PDB: 2HY6). Reproduced with permission from Xu *et al*. (2013), *Journal of the American Chemical Society*, 135(41), 15565–15578. Copyright 2021 American Chemical Society.

Woolfson and coworkers significantly advanced this approach by extending the scope of the process to a range of different blunt-ended coiled-coil oligomers (Burgess *et al*., 2015). The self-assembly of helical filaments was observed for coiled-coils having oligomeric states from three to seven, i.e. trimers through heptamers (Fig. 18*a* and *b*). TEM measurements indicated that the extent of lateral association was variable between the different peptide systems. However, filaments derived from a hexameric coiled-coil, **CC-Hex_T** (Fig. 18*c*), were observed to form highly ordered, *para*-crystalline assemblies (Fig. 18*d* and *e*). X-ray fiber diffraction and cryo-EM analysis provided evidence that the hexameric barrels stack axially in the filament and were arranged in a 2D lattice based on a tetragonal unit cell (Fig. 18*f*). The high degree of internal order within the assembly was rationalized based on the observation that the super-helical pitch of the hexameric coiled-coil corresponded to an integral number of six stacked assemblies, which would result in the formation of a continuous superhelical array along the contour length of the protofilaments. The ordered presentation of function groups at the periphery of the protofilaments could potentially reinforce lateral association into a *para*-crystalline assembly. Fluorescence binding assays demonstrated that the linear hydrophobic dye 1,6-diphenylhexatriene could bind within the lumen of filamentous nanotubes derived from the larger barrels ($n = 5–7$), which suggested that the internal channel of the assemblies was accessible to appropriately shaped substrates.

The coiled-coil assemblies described thus far display the classical architecture in which the individual helices were aligned nearly parallel to the superhelical axis (Lupas and Bassler, 2017; Woolfson, 2017). Tayeb-Fligelman *et al*. recently reported the first example of a cross-α fibril structure from crystallographic analysis of PSMα3, a short cytolytic peptide secreted from virulent strains of *Staphylococcus aureus* (Tayeb-Fligelman *et al*., 2017). The helices were observed to pack in a stacked bilayer array, in which individual peptides were oriented perpendicular to the long axis of the crystallographically defined filament. Subsequently, Zhang *et al*. reported a series of peptides based on designed coiled-coil sequences that assembled into filaments (Zhang *et al*., 2018). Crystallographic analyses demonstrated that the peptides formed cross-α super-helical arrays through stacking of parallel dimers in an alternating antiparallel orientation. However, these filaments displayed limited interfaces over which KIH packing was observed between protomers.

Egelman *et al*. employed helical reconstruction from cryo-EM images to characterize two cross-α filaments based on coiled-coil peptide sequences (Egelman *et al*., 2015). Two 29-residue peptide sequences were designed based on a type 3 coiled-coil architecture, first proposed by Walshaw and Woolfson (2001), from analysis of the coiled-coil region of the bacterial protein tolC and subsequently observed in bacteriophage transit tubes (Koronakis *et al*., 2000; Sun *et al*., 2014). To decrease the degree of curvature and create a larger nanotube, residues at the interface between protomers (*c*- and *d*-positions, Fig. 19*a* and *b*) were replaced with larger isoleucine and leucine, and residues on the outside (*a*- and *f*-positions) were exchanged for smaller alanine. Charged residues were substituted at the *b*- and *e*-positions to increase solubility and direct heterotypic facial interaction between adjacent helices in a parallel orientation. The resulting peptides, **Form I** and **Form II**, differed only in the presence of arginine *versus* lysine at identical positions within the respective sequences.

https://doi.org/10.1017/S0033583522000014 Published online by Cambridge University Press

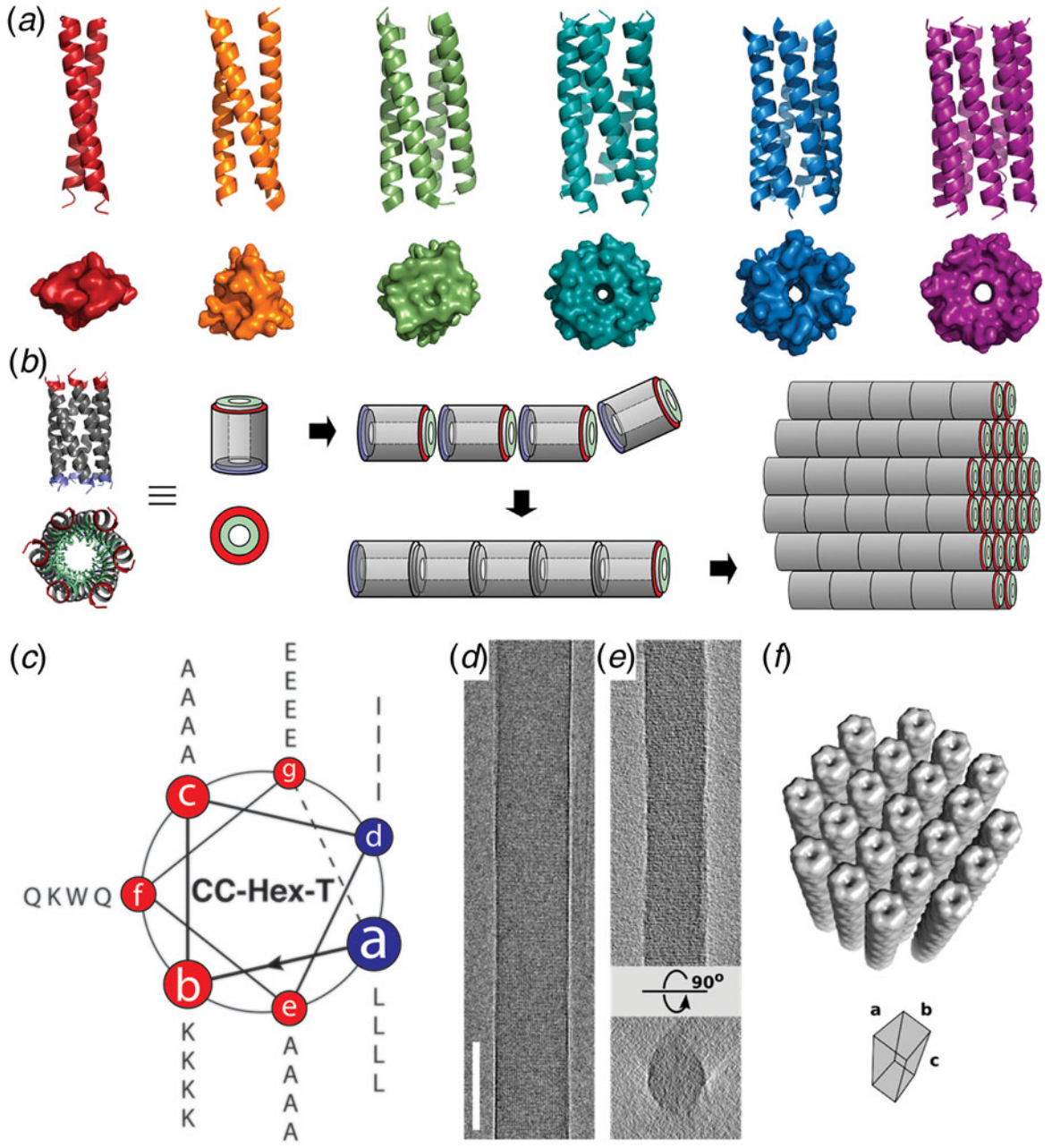

Fig. 18. Blunt-ended coiled-coil oligomers self-assemble into peptide nanotubes. (*a*) Ribbon diagrams and orthogonal views of space-filling models for designed coiled-coil oligomers; CC-Di (red; PDB: 4DZM), CC-Tri (orange; 4DZL), CC-Tet (green; 3R4A), CC-Pent (turquoise; 4PN8), CC-Hex (blue; 3R3K), and CC-Hept (purple; 4PNA). (*b*) Proposed model for self-assembly of CC-Hex-T involving axial stacking of hexameric barrels into a filament. (*c*) Helical wheel diagram depicting the heptad register of the CC-Hex-T sequence. (*d*) Representative cryo-EM image of thermally annealed CC-Hex-T assemblies (scale bar = 100 nm). (*e*) Tomographic slice of a CC-Hex-T assembly from cryo-ET analysis depicting an approximately cylindrical cross section. (*f*) Tetragonal lattice model for packing of CC-Hex-T filaments in a *para*-crystalline array. Reprinted with permission from Burgess *et al*. (2015), Journal of the American Chemical Society, 137(33), 10554–10562. Copyright 2021 American Chemical Society.

The **Form I** and **Form II** peptides assembled into nanotubes from buffered aqueous solution at ambient temperature. CD spectropolarimetry indicated the presence of an α-helical conformation, which was consistent with the formation of a coiled-coil assembly. However, conventional TEM and SAXS measurements provided evidence that the diameter of the **Form II** filaments (~120 Å) was double the diameter of the **Form I** filaments (~60 Å). These results suggested that the two structures must be different despite the similarity between the two peptide sequences. Cryo-EM analysis with direct electron detection was employed to generate 2D projection images for helical reconstruction of the thin filaments (Fig. 19*c* and *d*). Helical reconstruction afforded distinct atomic models for the **Form I** and **Form II** filaments (Fig. 19*e* and *f*). This work represented an early success for single-particle cryo-EM structural analysis of designed peptide filaments.

While similar in sequence and identical in apparent secondary structure, **Forms I** and **II** assembled into different quaternary structures. The structure of the **Form I** nanotubes (PDB: 3J89)

https://doi.org/10.1017/S0033583522000014 Published online by Cambridge University Press

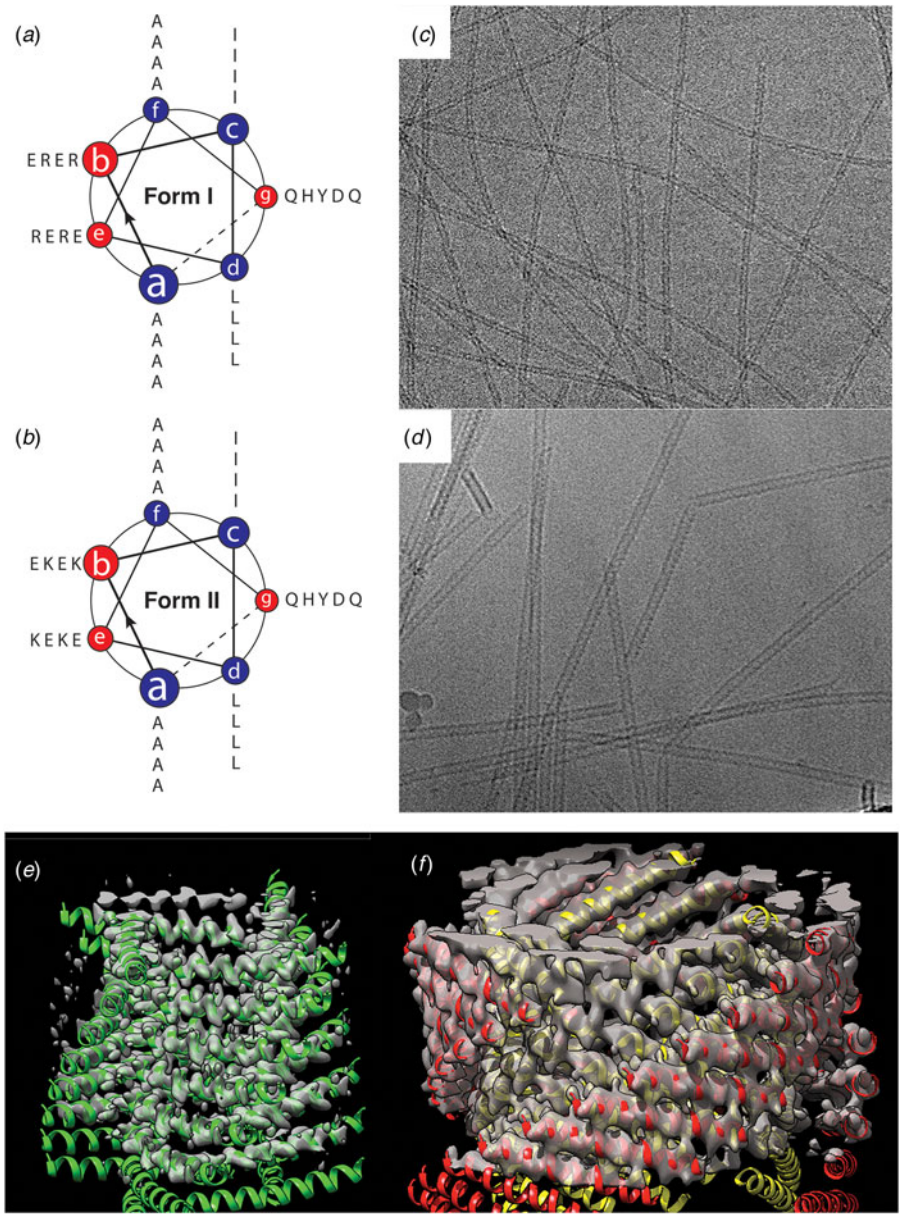

Fig. 19. (*a*, *b*) Helical wheel diagrams indicating the heptad register of the **Form I** and **Form II** peptide sequences. (*c*, *d*) Representative cryo-EM images of the **Form I** (*c*) and **Form II** (*d*) nanotubes. (*e*, *f*) Atomic models fit into the 3D reconstructions of the **Form I** (*e*) and the **Form II** (*f*) nanotubes derived from cryo-EM analysis. Reprinted with permission from Egelman *et al*. (2015), *Structure*, 23(2), 280–289.

was solved at 3.6 Å resolution and was based on a left-handed, 1-start helix (~4.1 subunits per turn). The asymmetric unit corresponded to a single α-helix, which resulted in formation of a single-walled nanotube with a helical pitch of ca. 9.0 Å and a helical twist of ca. −88°. The **Form I** nanotube has a nearly square cross section in which the subunits were arranged into four protofilaments that coincided with the right-handed 4-start helices of the nanotube.

In contrast, the initial reconstruction of the **Form II** nanotube afforded a density map at relatively low resolution (~7 Å), but clearly displayed an asymmetric unit based on a pair of α-helices that resulted in a double-walled nanotube. Subsequent cryo-EM data collection on **Form II** filaments resulted in a higher-resolution (~4.2 Å) reconstruction, which resulted in a more reliable atomic model (PDB: 6WL8). The structure was based on a right-handed 1-start helix with a helical pitch of 5.6 Å and a helical twist of 124.4°. The individual protofilaments within the nanotube corresponded to the right-handed 3-start helices. The reconstruction had sufficient resolution to determine that the pair of helices in the asymmetric unit was oriented in parallel across the inner-outer interface of the bilayer.

The primary difference between the **Form I** and **Form II** assemblies resided in the nature of the cohesive interactions between protofilaments that correspond to the cross-α helical stacks. The stacking interactions along a protofilament were quite similar between the two assemblies and corresponded to the KIH interactions that are typically observed for coiled-coil motifs. In contrast, the interactions between protofilaments involved side-to-end helical association and end-to-end association for **Form I** and **Form II**, respectively. The **Form I**

https://doi.org/10.1017/S0033583522000014 Published online by Cambridge University Press

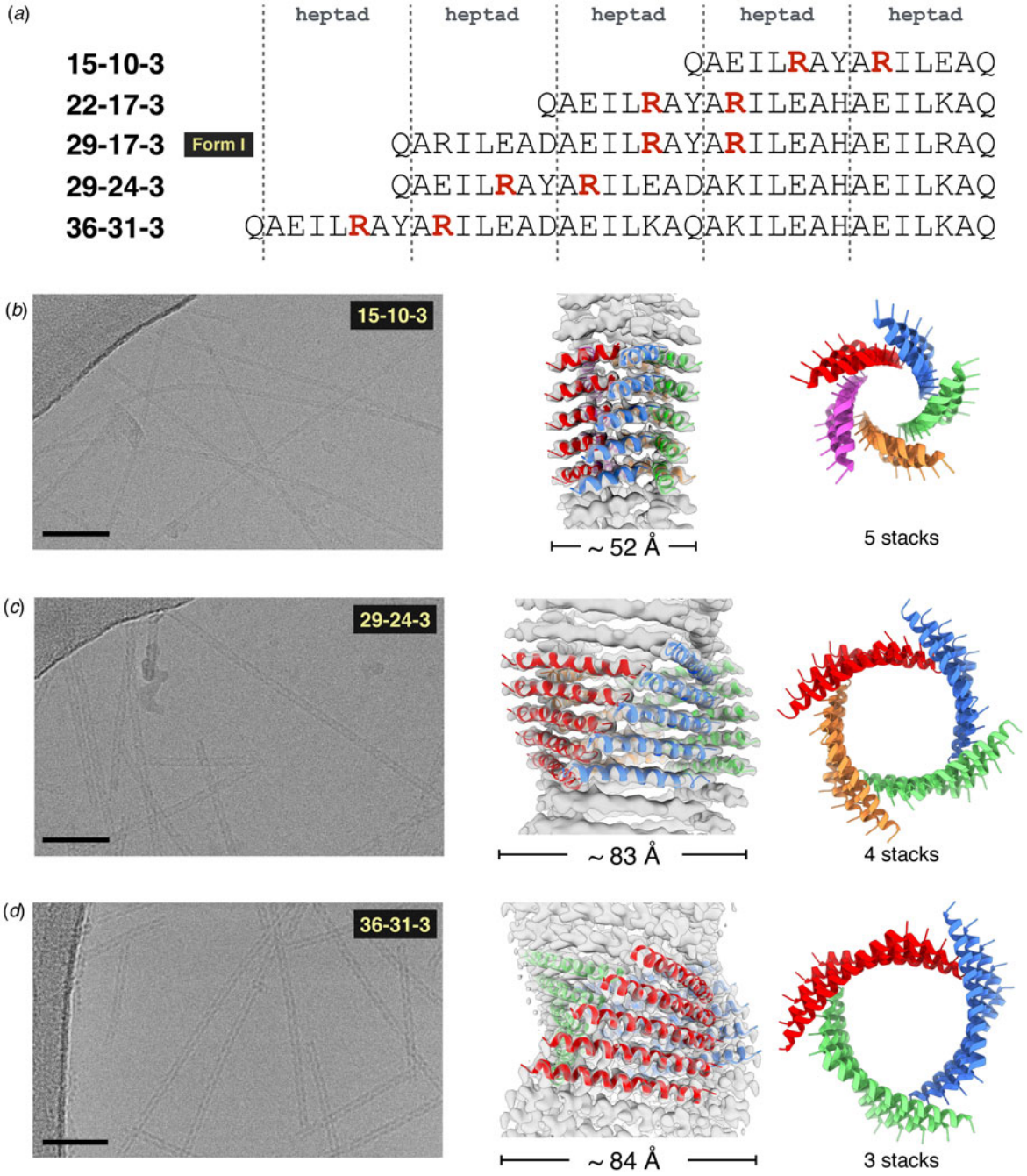

Fig. 20. (*a*) Peptide sequences of **Form I** variants in which the position of the arginine clasp motif is highlighted in red. Structural analyses of the **15-10-3** (*b*), the **29-24-3** (*c*), and the **36-31-3** (*d*) filaments. Representative cryo-EM images are shown on the left (scale bar = 50 nm). Atomic models fit into the respective 3D reconstructions are in the middle. Top views of the respective assemblies are shown on the right. Reproduced under the Creative Commons License from Wang *et al.* (2021*a*). *Nature Communications*, 12(1), 407.

interactions involved a pair of arginine residues, R13 and R17, that capped the C-terminus of a helix on an adjacent protofilament through a network of hydrogen-bonding interactions. This unique interaction, which was designated as an arginine clasp, does not appear to have been evolutionarily sampled as an interaction motif between helices in native protein structures (Wang *et al.*, 2021*a*). Lateral association between protofilaments in the **Form II** structure was based on a much weaker hydrogen bonding between Q29 and Q1 on structurally adjacent helices at the concave (inner) interface. The two structures can be interconverted through limited mutagenesis at these structurally critical positions within the respective peptide sequences (Egelman *et al.*, 2015).

The arginine clasp motif defined the number of protofilaments in the **Form I** structure and consequently its diameter. A series of peptides based on the **Form I** sequence was synthesized in which the length of the peptide was varied from two to five heptad repeats (Fig. 20*a*) (Wang *et al.*, 2021*a*). Each sequence preserved a single arginine clasp motif within the most N-terminal heptad. This peptide series was observed to self-assemble into high aspect-ratio filaments. Cryo-EM imaging (Fig. 20*b–d*) was

https://doi.org/10.1017/S0033583522000014 Published online by Cambridge University Press

employed to determine the structures of the two-heptad (**15-10-3**), four-heptad (**29-24-3**), and five-heptad (**36-31-3**) peptides at resolutions 4.2, 4.1, and 4.0 Å, respectively (PDB: 6WKX, 6WKY, and 6WL0). In combination with the **Form I** structure, these filaments represent a homologous series in which the arginine clasp interaction is conserved between laterally associating protofilaments within the respective structures. However, the number of protofilaments within the respective structures depended on the length of the peptide and decreased with an increasing number of heptad repeats (Fig. 20).

Finally, alternative strategies can be conceived for the fabrication of nanotubes from self-association of discrete helical bundles. Zhang *et al.* reported the computational design of antiparallel four-helix bundles that could self-associate into crystalline 2D assemblies of defined layer symmetry through optimization of protein–protein interactions at the interfaces between the tetrameric protomers (Zhang *et al.*, 2016). However, in lower pH buffers (10 mM sodium acetate, pH 4.5), one of these peptides assembled into nanotubes of defined diameter (Tian *et al.*, 2018). Multiple analytical measurements (TEM, SAXS, AFM, cryo-EM, and STEM) supported the formation of apparently homogeneous nanotubes, although the nature of the cohesive interactions between tetramers remains speculative in the absence of high-resolution structural information. The tubes were observed to slowly convert into sheets over extended periods of time. The sheet form was dominant at neutral pH, which suggested that the tubes represented a kinetic product. A similar pH-dependent transition between sheets and scrolled tubes was reported for a series of designed collagen-mimetic peptides (Merg *et al.*, 2020). These data suggested that preformed supercoiled peptide motifs could serve as protomers for the creation of shape-shifting nanomaterials that could toggle between sheet-like and tubular forms. Further structural characterization at high-resolution would enable a more detailed understanding regarding the supramolecular structural parameters that underlie these morphological transitions.

Tandem repeat assemblies

Tandem repeat proteins (TRPs) consist of concatenated sequences of relatively short secondary structure motifs, e.g. α-helical hairpins, that form extended folded structures displaying helical symmetry (Kobe and Kajava, 2000; Kajava, 2012). Within a given TRP class, sequence features that mediate interactions between the repeats are often highly conserved, while non-structurally integral amino acid positions are usually hypervariable. These protein families represent attractive substrates for the design of synthetic helical assemblies, especially for roles in substrate recognition and binding.

One of the most studied classes of TRPs is derived from the tetratricopeptide repeat (TPR) motifs, which are naturally occurring TRPs based on a helix–turn–helix structural motif. Regan and co-workers identified the consensus repeat sequence for a 34 amino acid TPR motif (Main *et al.*, 2003). Synthetic concatemers based on different lengths of this consensus TPR (**CTPR**) were prepared and structurally characterized. Single-crystal X-ray diffraction analysis of **CTPR8** indicated that it crystallized in three different unit cells corresponding to different space groups with distinct crystallographic symmetry elements (PDB: 2AVP, 2FO7, and 2HYZ) (Kajander *et al.*, 2007). In each case, the CTPR units stacked in a polar, head-to-tail fashion to form a continuous right-handed superhelix. The main-chain atoms within the respective CTPR subunits of the three crystal structures were superimposable. The right-handed superhelix consisted of eight TPR motifs per helical turn and therefore a **CTPR8** polypeptide corresponded to a single turn of the superhelix. The crystal structure of the longer **CTPR20** indicated that it adopted an identical helical structure with respect to individual superhelical filaments within stacked unit cells along the central axis of the assembly. SAXS measurements of **CTPR8** in aqueous buffers did not provide evidence for the formation of persistent filamentous structures in solution, although the local helical conformation was conserved. However, Grove and coworkers demonstrated that a concatemer of different length, **CTPR18**, could spontaneously self-associate into oriented thin solid films that display multi-scale order and stimulus responsive behavior (Carter and Grove, 2015, 2018).

In an attempt to create synthetic helical filaments based on minimal-length tandem repeat motifs, Conticello and coworkers (Hughes *et al.*, 2019) designed two peptides based on sequences derived from a leucine-rich repeat variant (**LRV**) (Peters *et al.*, 1996) and a thermostable HEAT repeat (**PBS_HEAT**) (Urvoas *et al.*, 2010) sequences, respectively. While single-repeat motifs have been postulated to be thermodynamically unstable toward self-association at ambient temperature, the resulting sequences, **LRV_M3Δ1** and **HEAT_R1**, assembled into high aspect-ratio helical filaments in aqueous buffers over a wide pH range (Fig. 21). Synchrotron SAXS measurements on solutions of the respective peptides confirmed the presence of narrow diameter filamentous assemblies. Cryo-EM was employed to investigate the structures of the two filaments derived from these structurally related tandem repeat motifs.

Structural analysis of the **LRV_M3Δ1** filaments (PDB: 6HQE) indicated that it formed a left-handed, 1-start helix (Fig. 21*a–c*). The helical hand of the **LRV** filament differed from the native right-handed helical twist of a crystallographically characterized LRV repeat concatemer (PDB: 1LRV). In addition, while the asymmetric unit corresponded to a single-repeat motif, the repeat units adopted an α-helix–loop–α-helix conformation, which contrasted with the α-helix–loop–3_{10}-helix conformation of the tandem repeat motifs in the crystal structure of a native LRV concatemer. The lateral interaction between adjacent LRV repeat motifs stabilized the assembly along the direction of the 1-start helix of the assembly and provided the primary driving force for polymerization. The formation of the closed nanotube involved the interaction between arginine residues on protomers at the interface between adjacent turns of the helical assembly (Fig. 21*b*). Notably, this axial interaction buried about twice as much surface area per subunit as the **HEAT_R1** filaments (*vide infra*).

In contrast, the structure of the **HEAT_R1** filament (PDB: 6MK1) displayed right-handed 1-start helical symmetry (Fig. 21*d–f*) in which the periodicity was similar to the superhelical structure observed within the crystal structure of a concatemer based on a consensus **PBS_HEAT** repeat (PDB: 3LTJ). However, the arrangement of protomers in the **HEAT_R1** filament differed from the crystal structure of the soluble concatemers. The asymmetric unit of the **HEAT_R1** filament was based on non-covalent association between two peptide motifs (Fig. 21*e*). One helical hairpin in the asymmetric unit could be aligned with repeat units derived from **PBS_HEAT** motifs in the crystal structure of the synthetic concatemer. The structure of the other peptide was distinct from that of the canonical **PBS_HEAT** repeats due to the need to accommodate a Trp–

https://doi.org/10.1017/S0033583522000014 Published online by Cambridge University Press

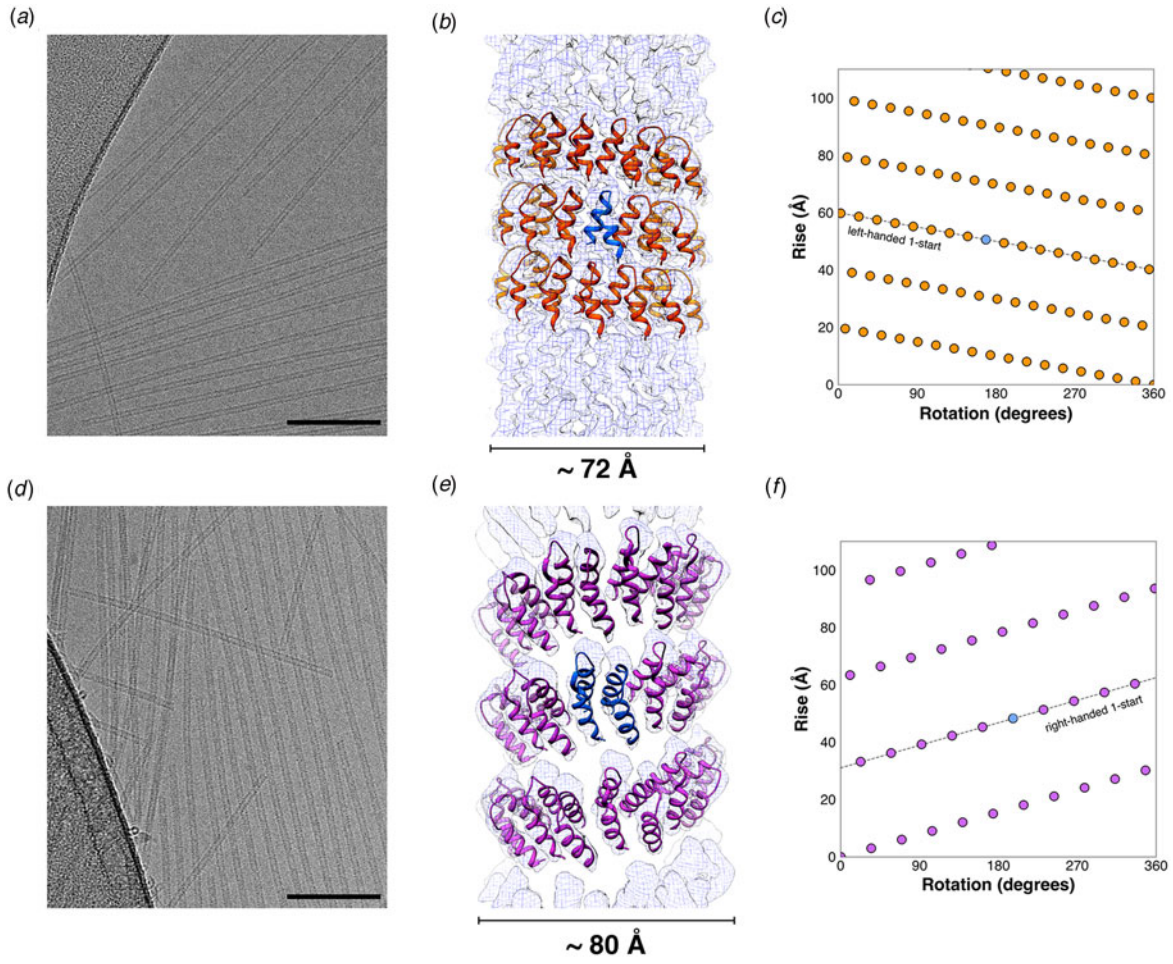

Fig. 21. Single tandem repeat motifs self-assemble into stable nanotubes. (*a*, *d*) Representative cryo-EM images of **LRV_M3Δ1** (*a*) and **HEAT_R1** (*d*) filaments. (Scale bar = 100 nm.) (*b*, *e*) Atomic models fit into the 3D reconstructions of the **LRV_M3Δ1** (*b*) and **HEAT_R1** (*e*) nanotubes. The asymmetric units are highlighted for the respective filaments in blue, which, in the case of **HEAT_R1**, corresponds to a dimer of peptides. (*c*, *f*) Helical net diagrams for the **LRV_M3Δ1** (*c*) and **HEAT_R1** (*f*) nanotubes, in which the difference in helical hand between the respective 1-start helices is apparent. The helical nets show the unrolled surface lattice viewed from the outside of the filament. From Hughes *et al*. (2019), *Proceedings of the National Academy of Sciences of the United States of America*, 116 (29), 14456–14464.

Trp interaction between the two peptides in the asymmetric unit. PISA (proteins, interfaces, surfaces, and assemblies) (Krissinel and Henrick, 2007) analysis showed that the buried surface area of the lateral interface was significantly larger than the corresponding value for axial interface. This difference arises because of the structural distortions induced by the Trp–Trp interaction between the two peptides in the asymmetric unit. TEM imaging indicated that the **HEAT_R1** filaments would frequently unwind on the grid, presumably because of the weak axial interaction between adjacent helical turns of the assembly. While these results confirmed that stable helical filaments could be constructed from self-assembly of tandem repeat sequences, the structural analysis also highlighted the plasticity of helical symmetry within supramolecular assemblies. Slight differences in local interactions and peptide conformation led to differences in peptide packing at the lateral and axial interfaces within a filament, which altered the helical symmetry of the assembly vis-à-vis the corresponding soluble oligomers.

Shen *et al*. reported successful *de novo* design of helical filaments (DHFs) derived from computationally optimized synthetic tandem repeat oligomers based on helix–turn–helix motifs (Shen *et al*., 2018). The design algorithm screened for self-assembling proteins by selecting an arbitrary asymmetric protomer and randomly sliding an identical protomer into contact. The screen employed 15 structurally distinct, computationally designed folded protomers, which resulted in 124 target sequences that were expressed in *Escherichia coli*. Filamentous nanomaterials were observed from expression of 34 of these synthetic constructs. Cryo-EM was employed to analyze the structure of the six most promising filaments. The helical reconstructions ranged in resolution from 3.4 to 7.8 Å (Fig. 22). The geometry of the experimentally determined structural interfaces matched well to the computational designs for four of the six designed filaments, while the overall supramolecular architectures were retained for all of the designs. Despite these observations, even the most accurate computational predictions cannot recapture helical symmetry precisely since slight differences in interfacial interactions may lead to changes in helical symmetry (*vide supra*). The latter represents a known but unappreciated phenomenon in the design of helical peptide and protein assemblies (Egelman *et al*., 2015; Lu *et al*., 2015). Nevertheless, this observation does not diminish the impact of these results, which represent the most reliable and

https://doi.org/10.1017/S0033583522000014 Published online by Cambridge University Press

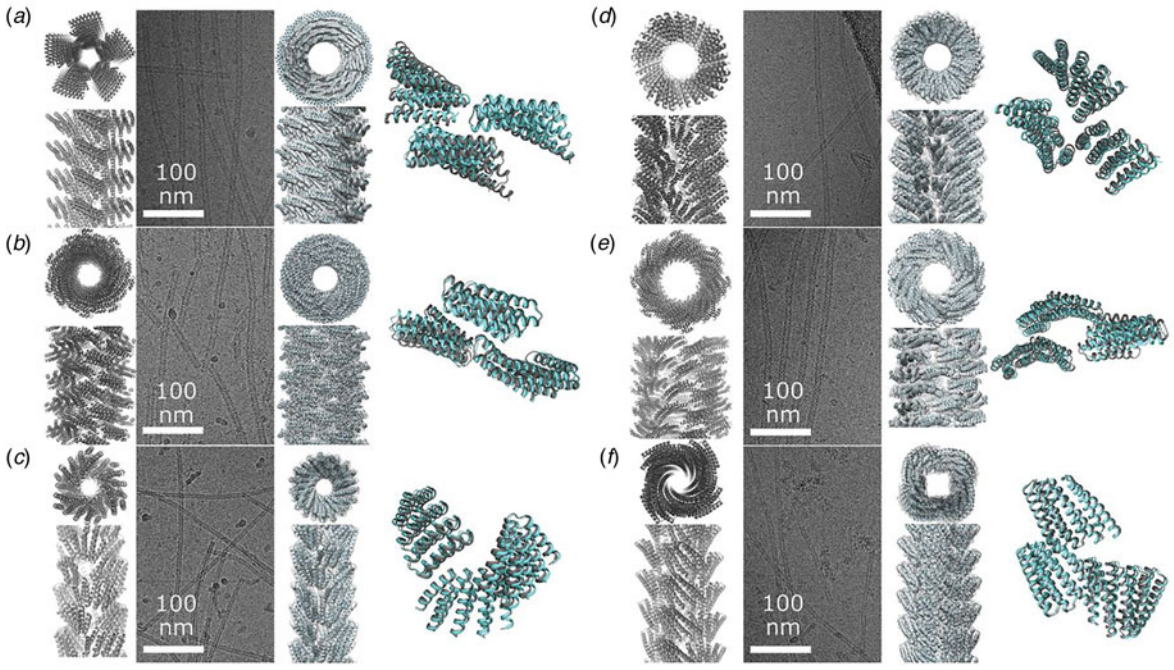

Fig. 22. Computational design of helical filaments from designed TRPs. Left to right: Computational models, representative cryo-EM images, cryo-EM-derived atomic models, and structural overlays between the computational model and experimental structure for designed helical filaments DHF58 (*a*), DHF119 (*b*), DHF91 (*c*), DHF46 (*d*), DHF79 (*e*), and DHF38 (*f*). From Shen *et al.* (2018), *Science*, 362(6415), 705–709. Reprinted with permission from AAAS.

accurate predictive design of helical filaments that has been reported thus far.

The stability and persistent tertiary structures of the synthetic protomers enabled rational control of filament structure as well as the dynamics of filament assembly. For one designed helical filament, DHF58 (PDB: 6E9T), the number of repeats in the concatemer was employed to control filament width, while preserving the designed inter-protomer interfaces (Fig. 23). Kinetic analysis of another designed filament, DHF119 (PDB: 6E9Z), indicated that the self-assembly process was concentration-dependent and reversible below a ceiling concentration. Filament disassembly resulted upon dilution below this critical concentration. Synthetic capping proteins were designed in which one interface in the protomer was prevented from self-association. Addition of these capping agents prevented further addition at the blocked terminus, but also initiated a concentration-dependent disassembly of the filaments due to the dynamically reversible association/dissociation of kinetically competent protomers. Green fluorescent protein-tagged monomers of DHF58 could assemble into filaments in live and phage-lysed *E. coli* expression strains, which suggested that these assemblies could be employed for *in cellulo* applications.

While TRPs based on α-helical motifs have been more extensively examined for the fabrication of synthetic peptide and protein filaments, β-sheet tandem repeat motifs commonly occur as structural elements in native proteins as well (Kajava and Steven, 2006). These β-solenoid or β-helix motifs consist of two, three, or four β-strands that are linked through short turn or β-arc segments. The individual repeat motifs often occur as extended concatemers within native proteins, which form the turns of a parallel cross-β helix. Stacking of the repeats is mediated through the formation of hydrogen-bonded β-sheet along the helical axis of the structure and is reinforced through hydrophobic interactions that occur within the core of the helix. In contrast to cross-β filaments such as amyloids, uncontrolled polymerization in native β-solenoid proteins is prevented through the presence of N- and C-terminal globular domains that prevent end-to-end association.

Toney and co-workers (Peralta *et al.*, 2015; Peng *et al.*, 2017*b*, 2020), have employed native β-solenoid domains as the starting point for the design of synthetic β-helical filaments. Manual and computational designs were used separately or in combination to create discrete-length concatemeric sequences based on two-strand and three-strand solenoid repeats. The proteins were obtained from bacterial expression from synthetic genes. To promote assembly of extended filaments, the corresponding proteins lacked N- and C-terminal capping groups. Remarkably, despite their strong aggregation potential, the β-helical proteins could be prepared and purified in reasonable yield (30–40 mg l^{-1} of culture) using recombinant protein expression in an *E. coli* bacterial host.

Protein solutions were meta-stable in the unassociated state but could be driven to self-assemble through incubation at 37 °C. TEM and AFM analysis of the assembled proteins indicated the presence of filaments of similar diameter to the parent β-helices. The CD spectra were consistent with the presence of a high content of β-sheet conformation. The resulting filaments displayed remarkable resistance to elevated temperature, organic solvents, chemical denaturants, and were stable over a wide pH range. In addition, nanomechanical measurements and molecular dynamics simulations provided evidence that mechanical properties of the synthetic filaments, e.g. ultimate tensile strength and Young's modulus, were similar to the corresponding values for other β-sheet materials including amyloids and spider silk (Peng *et al.*, 2017*a*). These results suggested that β-solenoid assemblies present attractive targets for rational design of novel nanomaterials.

Most of the designed filaments described thus far have been derived from relatively simple structural motifs. As protein

https://doi.org/10.1017/S0033583522000014 Published online by Cambridge University Press

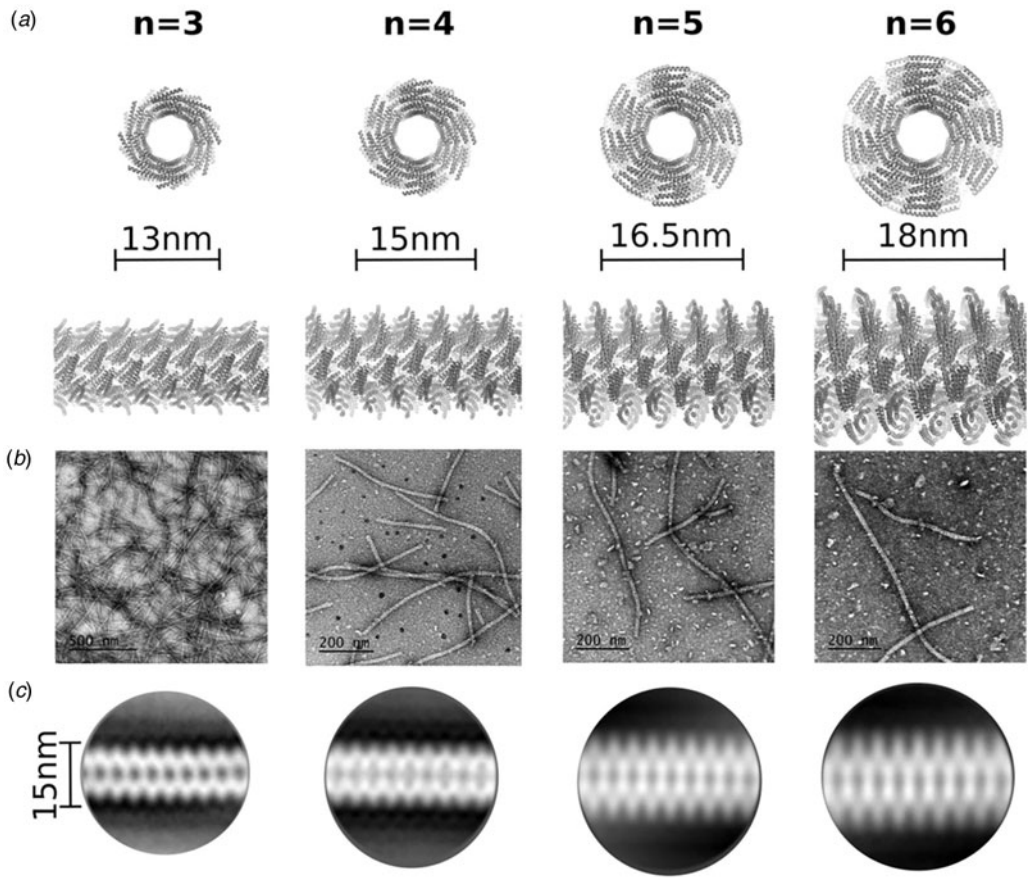

Fig. 23. Diameter of designed helical filament DHF58 can be controlled through the number of tandem repeats in the protomer. (*a*) Cross sections and side views of computational models based on the four-repeat cryo-EM structure. The number of repeats (*n*) is shown at the top. (*b*) Representative negative stain electron micrographs of the corresponding helical filaments. (*c*) 2D-class averages derived from electron micrographs of the respective filaments. From Shen *et al*. (2018), *Science*, 362(6415), 705–709. Reprinted with permission from AAAS.

engineering and computational design efforts advance, more structurally complex subunits may be considered as substrates for the design of synthetic protein filaments. Biological systems often employ globular protein domains as building blocks for the assembly of filaments including F-actin, microtubules, etc. Recent studies suggested that filamentation may represent a mechanism to regulate protein function, including enzymatic catalysis (Lynch *et al*., 2017, 2020).

In this vein, Kaltofen *et al*. (2015) reported the computational design of a small self-assembling βαβ domain (Fig. 24). While technically neither a globular domain nor a tandem repeat motif, this small modular protein fold was constructed from a pair of β-strands that were connected via turns to an α-helix (Fig. 24*a*). The sequence of the β-strand motifs was derived from a self-associating heptapeptide in the N-terminal prion domain of the *Saccharomyces cerevisiae* termination factor Sup35 (Balbirnie *et al*., 2001; Nelson *et al*., 2005). The self-assembly behavior of this oligopeptide sequence was associated with manifestation of the [*PSI*+] prion phenotype in *S. cerevisiae* (Cox *et al*., 1988). The amino acid residues responsible for the polar zipper interface between β-sheets were retained, but the remainder of the structure was designed *de novo* using Rosetta (Huang *et al*., 2011; Leaver-Fay *et al*., 2011). Self-assembly was proposed to occur through dimerization of the computationally designed βαβ motif at the β-sheet interface and subsequent elongation through end-to-end propagation of the β-sheet in a cross-β orientation (Fig. 24*b* and *c*). The computationally designed peptide, βαβZip, was synthesized using solid-phase synthesis (Fig. 24*d*). TEM imaging indicated the presence of high aspect-ratio filaments of apparent width that compared well with the lateral dimensions of the computational model. FTIR spectroscopy and CD spectropolarimetry measurements agreed with a mixed α/β conformational population. While a high-resolution structure was not available to compare to the atomistic model, X-ray fiber diffraction analysis performed on oriented filaments provided evidence for a cross-β structure that agreed well with the computational model.

Foldamer-based helical assemblies

Until now, peptide assemblies derived from discrete length oligomeric α-amino acid sequences, corresponding to native polyamide backbones, have been discussed exclusively. However, these sequences do not represent the sole plausible substrates for design of oligomers competent for self-assembly into structurally defined filaments. Recently, the design of peptido-mimetic foldamers (Goodman *et al*., 2007) has been explored in order to evaluate for the potential formation of structurally defined supramolecular assemblies (Misra *et al*., 2021). While sequence–structure correlations are less well-defined for covalent oligomers based on alternative backbone chemistries, foldamer assemblies offer several potential advantages as substrates for the fabrication of

https://doi.org/10.1017/S0033583522000014 Published online by Cambridge University Press

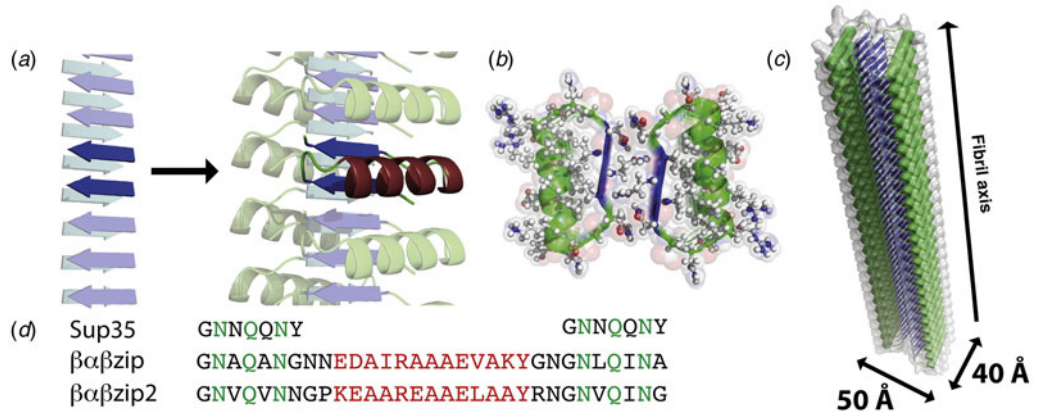

Fig. 24. De novo design of self-assembling βαβ peptides. (*a*) The computational design is based on the crystal structure of the amyloidogenic heptapeptide sequence GNNQQNY derived from the sup35 N-terminal prion domain. A loop–helix–loop segment constructed using flexible backbone design connects two β-strands with backbone conformations taken from the sup35 peptide. (*b*) Cross section of the computational model of the fibril in a view perpendicular to the fiber axis. The interactions between the two layers of sheets are stabilized by a steric zipper interface formed by interdigitating side chains at the strand interfaces. (*c*) Structural model the peptide filament with estimated lateral dimensions for a cross section. (*d*) Sequences of computationally designed peptides βαβZip and βαβZip2. Residues highlighted in green correspond to the steric zipper interface, while residues highlighted in red correspond to the α-helix. From Kaltofen *et al*. (2015), *Journal of Molecular Biology*, 427(2), 550–562. Reprinted with permission from Elsevier.

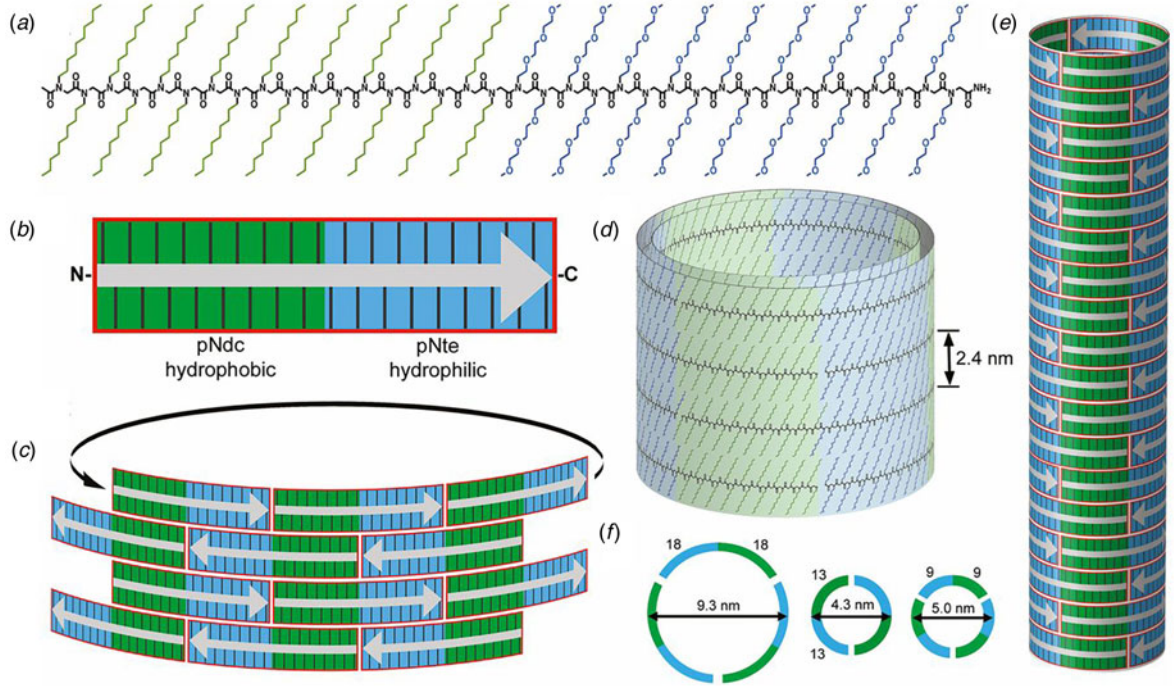

Fig. 25. Amphiphilic peptoids block copolymer tiles self-assemble into hollow nanotubes. (*a*) Sequence and chemical structure of $pNdc_{18}$-*b*-$pNte_{18}$. (*b*) Schematic depiction of the structure of $pNdc_{18}$-*b*-$pNte_{18}$ tile in which the hydrophobic and hydrophilic domains are highlighted in green and blue, respectively. The gray arrow indicates the *N* to *C* chain trajectory. (*c*) Schematic representation of the packing of four layers of peptoid tiles within the proposed nanotube structures. (*d*) Cross section of a four-layer nanotube segment with depiction of side-chain arrangement and the stacking repeat distance. (*e*) Schematic representation of the proposed nanotube structure with amphiphilic tile packing indicated. (*f*) Cross-sectional view of the proposed packing of amphiphilic tiles for three peptoid polymers with approximate tube diameter for each cross section. Reprinted with permission from Sun *et al*. (2016), *Proceedings of the National Academy of Sciences of the United States of America*, 113(15), 3954–3959.

biomimetic helical filaments and nanotubes. The primary consideration that has driven investigation into foldamer assemblies is their potential resistance to proteolytic cleavage in a biological environment as well as a lowered propensity to elicit an immune response. Moreover, synthetic foldamers exhibit a rich structural chemistry that differs from that of conventional α-amino acid oligomers, which may lead to different supramolecular architectures that may be more suited for a particular downstream application.

Polypeptoids, or polymers of *N*-substituted glycines, have been extensively studied as building blocks for construction of supramolecular assemblies (Sun and Zuckermann, 2013). Unlike

https://doi.org/10.1017/S0033583522000014 Published online by Cambridge University Press

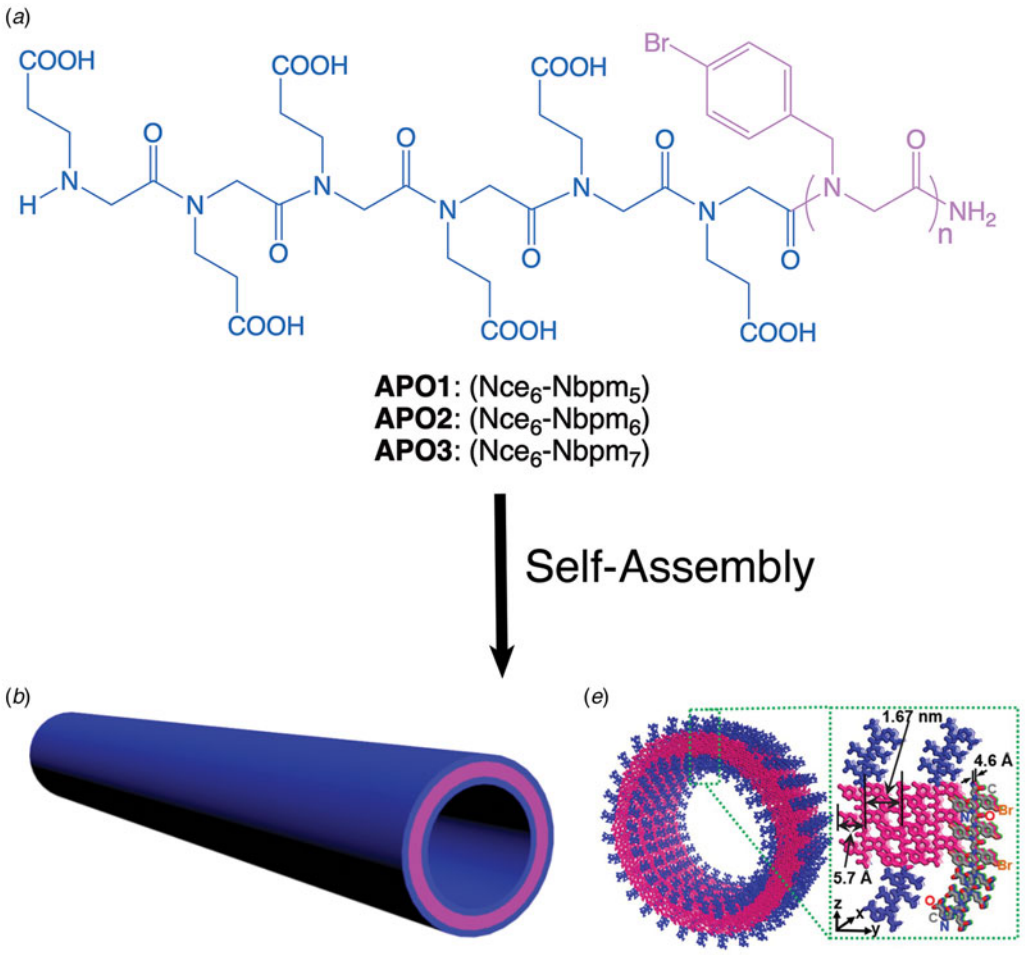

Fig. 26. Amphiphilic peptoid oligomers (APOs) self-assemble into highly ordered, crystalline, single-walled peptoid nanotubes. (*a*) Sequence and chemical structure of the APOs. Hydrophilic and hydrophobic blocks are indicated in blue and magenta, respectively. (*b*) Schematic representation of the proposed structure of the monolayer nanotube with color-coding of the hydrophilic and hydrophobic blocks. (*c*) Cross-sectional representation of the proposed model for the APO2 nanotubes. The molecular packing of the peptoid protomers is depicted along with the critical distances that define the packing arrangement. Reprinted under Creative Commons License from Jin *et al*. (2018), *Nature Communications*, 9(1), 270.

natural proteins they cannot be overexpressed in bacteria, but the chemical synthesis of peptoids is no more difficult than solid-phase peptide synthesis (Culf and Ouellette, 2010). A diverse range of quaternary structures have been prepared from self-assembly of sequence-specific peptoids (Nam *et al*., 2010), but here we focus on the design of filamentous assemblies. Two research groups independently demonstrated that block-like peptoid oligomers (Xuan and Zuckermann, 2020) based on sequence-encoded contour-length amphiphilicity could self-assemble into filamentous nanomaterials. Similar self-assembly behavior was observed for block-like peptide sequences that display contour-length amphiphilicity (Van Rijt *et al*., 2019).

Zuckermann and coworkers described a series of peptoid polymers, $(pNdc)_n$-*b*-$(pNte)_n$ ($n = 9$, 13, 18), that displayed an AB-type amphiphilic block copolymer architecture (Sun *et al*., 2016). The *N*-substituents of the respective blocks had identical length, i.e. number of non-hydrogen atoms, and linear architecture, but differed significantly in polarity (Fig. 25*a* and *b*). The poly-*N*-decylglycine (pNdc) A-block was hydrophobic in character, while the poly-*N*-2-(2-(2-methoxyethoxy)ethylglycine) (pNte) B-block was hydrophilic in nature. The amphiphilic block peptoids self-assembled from a mixed solvent system into structurally well-defined nanotubes. SAXS, TEM, cryo-EM, and cryo-electron tomography (cryo-ET) provided evidence that the nanotubes displayed an unusual supramolecular architecture. The peptoid backbone was arranged circumferentially around the periphery of the nanotubes in an orientation perpendicular to the long axis of the nanotube (Fig. 25*c*–*e*). The side chains projected along the tube axis but segregated into separate hydrophilic and hydrophobic domains, which resulted in a regular pattern of stripes along the contour length of the nanotube. The packing of peptoids within the tubes resembled the stacking of tiles. The tiles were composed of side chains in which the uniform length of the hydrophilic and hydrophobic substituents was proposed to abet the ordered stacking. Three different peptoid block polymers were prepared in which the A and B block lengths were identical in the number of monomers ($n = 9$, 13, and 18). In every case, the axial periodicity of 24 Å was conserved in the corresponding assemblies, although the diameter of the tubes varied depending on the peptoid sequence (Fig. 25*f*).

In contrast, Chen and co-workers described a class of peptoid block copolymer amphiphiles, $(pNce)_6$-*b*-$(pNbpm)_n$ ($n = 5$, 6, 7) (Fig. 26*a* and *b*) in which the length of the hydrophobic block was varied (Jin *et al*., 2018). Self-assembly of these peptoid polymers

https://doi.org/10.1017/S0033583522000014 Published online by Cambridge University Press

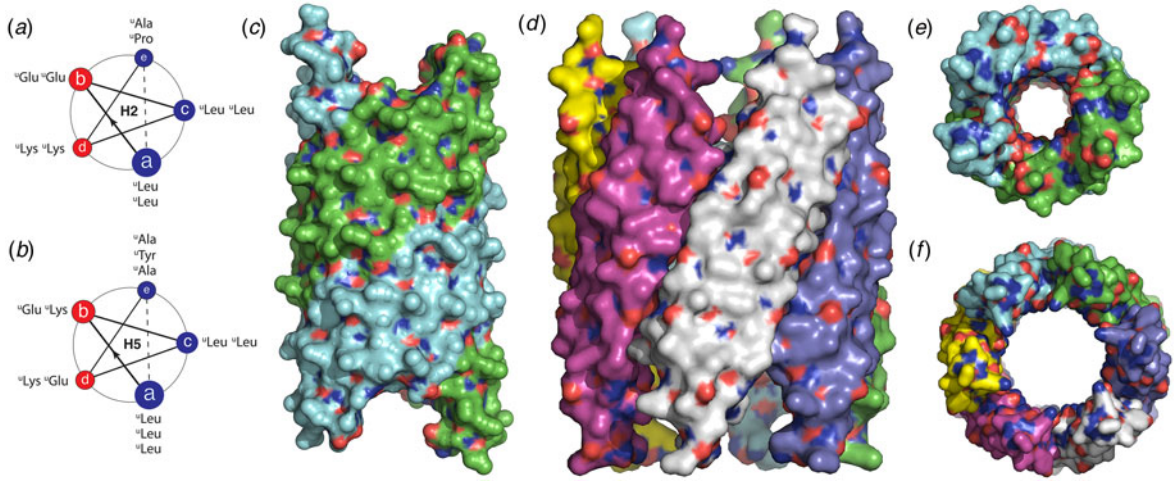

Fig. 27. Oligoureas can adopt amphiphilic helical secondary structures that promote self-assembly into nanotubes. (*a*, *b*) Helical wheel diagrams of the decameric (**H2**) and dodecameric (**H5**) oligourea sequences indicating the pentad registry. The facial amphiphilicity can be detected from the pattern of polar residues (red) and non-polar residues (blue). (^{u}Xaa indicates the urea analog of a canonical amino acid.) (*c*, *e*) Side and top views of the **H2** nanotube derived from the corresponding crystal structure. (*d*, *f*) Side and top views of the **H5** nanotube derived from the corresponding crystal structure. In each case, the individual protofilaments within the respective structures are color coded.

from a mixed solvent system afforded mechanically robust, crystalline nanotubes. TEM analysis indicated that the self-assembly process involved a structural evolution from particles to ribbons to tubes. The wall thickness, diameter, and mechanical properties of the tubes could be controlled through the sequence of the peptoid oligomers, that is, the length of the hydrophobic peptoid segment. Remarkably, the nanotubes were able to undergo a reversible pH-driven expansion and contraction of the tube diameter without any evidence for disassembly. Despite a similar contour-length amphiphilicity to the nanotubes described by Zuckermann and coworkers, these peptoid polymers were arranged in an antiparallel orientation within an amphiphilic monolayer. The peptoid backbones were proposed to be oriented radially within the nanotube rather than circumferentially as proposed for the previously described peptoid block copolymers (Fig. 26*c*). The hydrophobic 4-bromophenylmethyl (pNbpm) B-block substituents were buried in the monolayer core, while the polar 2-carboxyethyl (pNce) A-block segments extended from either surface. TEM measurements of the wall thickness of the tubes supported this structural model, in that the wall thickness increased as the length of the pNbpmn segment increased.

Similarly, foldamers based on aliphatic oligourea backbone (Violette *et al.*, 2005) have been demonstrated to form helical assemblies in which polar sequence patterning was observed to promote selective self-assembly (Collie *et al.*, 2015). In contrast to the peptoids described above, the sequences of the synthetic oligoureas were designed to display conformational, that is, facial, amphiphilicity. Oligoureas had been previously demonstrated to adopt local helical secondary structures based on a pentad repeat motif, which corresponded to five monomers per two helical turns within the conformation (Fig. 27*a* and *b*). Guichard and coworkers (Collie *et al.*, 2015) demonstrated that oligourea foldamers could assemble into either discrete hexameric helical bundles or extended nanotubes. The preference for the respective structures depended on the polar patterning of the urea side chains within the pentad-based sequence of the oligomer. Formation of an extended hydrophobic interface within a helical conformation promoted higher-order assembly of the oligourea protomers into helical assemblies.

Two oligourea oligomers, decamer **H2** and dodecamer **H5**, were synthesized based on the same polar pattern although with slightly different sequences. Single-crystal X-ray diffraction analysis of these two oligourea assemblies revealed the presence of nanotubes in both cases. The structure of **H2** was based on a helical assembly with apparent C_2 symmetry in which the two protofilaments corresponded to pairs of antiparallel helices stacked along the respective 2-start helices (Fig. 27*c* and *e*). The structurally related oligourea **H5** assembled into a nanotube of apparent C_6 symmetry, in which the protofilaments corresponded to the 6-start helices of the assembly (Fig. 27*d* and *f*). Conventional TEM and cryo-EM confirmed the presence of isolated nanotubes of similar dimensions to those observed crystallographically. Notably, slight changes in oligourea sequence could result in dramatic changes in the structure of the assembly, in a manner that was reminiscent of the structural plasticity often observed in peptide assemblies (Yoo *et al.*, 2020). *N*-Methylation of the C-terminal amide resulted in a structural variant of the H2 decamer, **H2′**, which crystallized into two distinctive helical assemblies under different sets of experimental conditions. One form adopted a structure that was identical to that of **H2** (Fig. 27*c* and *e*). However, under a separate set of conditions, a completely different structure was observed with a different helical periodicity although it retained C_2 symmetry.

Finally, higher-order filamentous assemblies have been observed for peptides based on non-α-amino acid sequences. Oligomers of β^3-homoamino acids (Gopalan *et al.*, 2015) have been observed to self-assemble into filaments (Del Borgo *et al.*, 2013; Christofferson *et al.*, 2018), and form lyotropic mesophases based on filamentous assemblies (Pomerantz *et al.*, 2006, 2008, 2011; Pizzey *et al.*, 2008). The sequence determinants responsible for self-assembly have been investigated, but thus far are not well-understood due to the absence of NAR structural information. At least one example of an oligo-β^3-homopeptide sequence has been reported in which formation of hollow cylindrical nanotubes was inferred on the basis of conventional TEM, low-resolution cryo-EM, and SAXS measurements (Pizzey *et al.*, 2008; Pomerantz *et al.*, 2008). The polar patterning of this peptide system does not fit a conventional model that can correlate sequence

https://doi.org/10.1017/S0033583522000014 Published online by Cambridge University Press

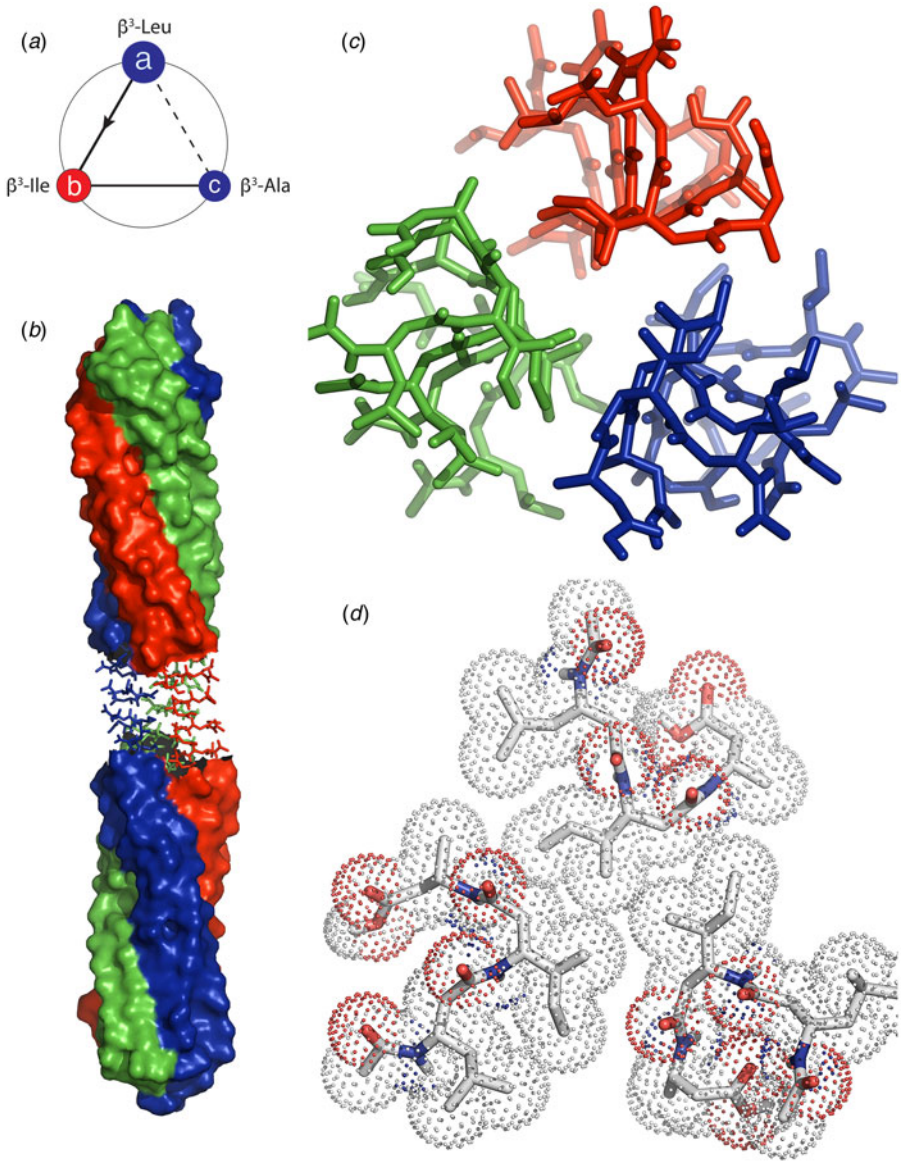

Fig. 28. (*a*) Helical wheel diagram of tripeptide Ac-β³[hLhIhA] indicating the triad registry in a left-handed 14-helix conformation. (*b*) Side view of the triple-helical ribbon model of the Ac-β³[hLhIhA] filament in water. (*c*) Expansion of a four-layer helical stack from (*b*) highlighting packing at the trimeric interface in a stick representation. (*d*) Trimeric packing interface of a single-layer of the triple helix in which inter-residue contacts are indicated using a mesh depiction.

with higher-order structure for the 14-helix conformation (Cheng *et al*., 2001) that is often observed for oligo-β³-homopeptides.

In the case of oligo-β³-homopeptide sequences, complex filamentous structures can arise even from tripeptides (Fig. 28*a*). Christofferson *et al*. reported a detailed structural analysis of assemblies derived from hydrophobic tripeptides composed of different sequence combinations of β³-homoLeu, β³-homoIle, and β³-homoAla (Christofferson *et al*., 2018). X-ray fiber diffraction of oriented samples derived from assemblies of tripeptide Ac-β³[hLhIhA] (hL, homoleucine; hI, homoisoleucine; hA, homoalanine) provided evidence for a supramolecular structure in which three helical protofilaments formed a trimeric superhelix through self-association (Fig. 28*b–d*). X-ray diffraction data on Ac-β³[hLhIhA] were employed to benchmark molecular dynamics simulations, which were extended to the other tripeptide variants that were sequence permutants of Ac-β³[hLhIhA]. MD simulations were compared with AFM measurements and provided evidence that the supramolecular structural variations between the tripeptides originated in differences in the packing details at the helix–helix interface within the corresponding atomic models. Further confirmation of these sequence–structure correlations will await structural determination at NAR.

While the structural analysis of foldamer assemblies is at an early stage in its development, opportunities abound for the creation of structurally defined helical assemblies from sequences based on alternative backbone and side-chain chemistries. High-resolution structural analysis, particularly cryo-EM, offers the ability to provide insight into the sequence determinants that underlie the formation of these chemically and structurally orthogonal helical assemblies, which would enable a better understanding of the local sequence and conformational factors that underlie self-assembly behavior and provide rubrics to better guide the design of such synthetic assemblies.

Conclusions

Helical peptide assemblies offer engineering opportunities that range from peptide design to assembly functionalization. However, the rational design of synthetic helical assemblies is complicated in that minor sequence modifications within the

https://doi.org/10.1017/S0033583522000014 Published online by Cambridge University Press

subunits can have a considerable influence on the quaternary structure of the resultant assemblies. These effects can be difficult to predict *a priori*, in part due to the limited availability of high-resolution structural information on peptide and peptido-mimetic helical filaments and tubes. While the latter situation is rapidly undergoing transformative growth, reliable *de novo* design of helical assemblies remains a significant challenge.

NAR methods for structural determination, i.e. cryo-EM, MicroED, and ssNMR, are revolutionizing the structural analysis of peptide and protein assemblies. As these resources become more widely available, we expect to see increased information from structural studies, which will enable a better understanding of the factors that influence higher-order structure within helical assemblies. Many significant questions remain to be answered, in particular, the role of amphiphilicity in conformational selection and in orientational preferences for packing of protomers within the filaments. A better understanding of structural principles is critical to the development of synthetic helical assemblies that emulate the functional properties of native biological filaments and can be tailored for specific applications.

Acknowledgments. The authors thank Edward Egelman, Fengbin Wang, James Nowick, Louise Serpell, Mibel Aguilar, Gilles Guichard, Anil Mehta, Chunlong Chen, and Ulf Olsson for useful discussions and providing data and graphics for figures.

Financial support. This work was supported by the National Science Foundation (NSF) (V. P. C., grant number DMR-1534317).

Conflict of interest. The authors declare no competing interests.

References

Adamcik J and Mezzenga R (2018) Amyloid polymorphism in the protein folding and aggregation energy landscape. *Angewandte Chemie International Edition* **57**, 8370–8382.

Aggeli A, Bell M, Boden N, Keen JN, Knowles PF, Mcleish TCB, Pitkeathly M and Radford SE (1997) Responsive gels formed by the spontaneous self-assembly of peptides into polymeric β-sheet tapes. *Nature* **386**, 259–262.

Aggeli A, Nyrkova IA, Bell M, Harding R, Carrick L, Mcleish TC, Semenov AN and Boden N (2001) Hierarchical self-assembly of chiral rod-like molecules as a model for peptide β-sheet tapes, ribbons, fibrils, and fibers. *Proceedings of the National Academy of Sciences of the United States of America* **98**, 11857–11862.

Akey DL, Malashkevich VN and Kim PS (2001) Buried polar residues in coiled-coil interfaces. *Biochemistry* **40**, 6352–6360.

Anzini P, Xu C, Hughes S, Magnotti E, Jiang T, Hemmingsen L, Demeler B and Conticello VP (2013) Controlling self-assembly of a peptide-based material via metal-Ion induced registry shift. *Journal of the American Chemical Society* **135**, 10278–10281.

Baek M, Dimaio F, Anishchenko I, Dauparas J, Ovchinnikov S, Lee GR, Wang J, Cong Q, Kinch LN, Schaeffer RD, Millan C, Park H, Adams C, Glassman CR, Degiovanni A, Pereira JH, Rodrigues AV, Van Dijk AA, Ebrecht AC, Opperman DJ, Sagmeister T, Buhlheller C, Pavkov-Keller T, Rathinaswamy MK, Dalwadi U, Yip CK, Burke JE, Garcia KC, Grishin NV, Adams PD, Read RJ and Baker D (2021) Accurate prediction of protein structures and interactions using a three-track neural network. *Science (New York, N.Y.)* **373**, 871–876.

Balbirnie M, Grothe R and Eisenberg DS (2001) An amyloid-forming peptide from the yeast prion Sup35 reveals a dehydrated beta-sheet structure for amyloid. *Proceedings of the National Academy of Sciences of the United States of America* **98**, 2375–2380.

Beesley JL and Woolfson DN (2019) The *de novo* design of α-helical peptides for supramolecular self-assembly. *Current Opinion in Biotechnology* **58**, 175–182.

Bera S, Mondal S, Xue B, Shimon LJW, Cao Y and Gazit E (2019) Rigid helical-like assemblies from a self-aggregating tripeptide. *Nature Materials* **18**, 503–509.

Bong DT, Clark TD, Granja JR and Ghadiri MR (2001) Self-assembling organic nanotubes. *Angewandte Chemie International Edition* **40**, 988–1011.

Bowerman CJ and Nilsson BL (2012) Review self-assembly of amphipathic β-sheet peptides: insights and applications. *Peptide Science* **98**, 169–184.

Bucak S, Cenker C, Nasir I, Olsson U and Zackrisson M (2009) Peptide nanotube nematic phase. *Langmuir* **25**, 4262–4265.

Burgess NC, Sharp TH, Thomas F, Wood CW, Thomson AR, Zaccai NR, Brady RL, Serpell LC and Woolfson DN (2015) Modular design of self-assembling peptide-based nanotubes. *Journal of the American Chemical Society* **137**, 10554–10562.

Carter NA and Grove TZ (2015) Repeat-proteins films exhibit hierarchical anisotropic mechanical properties. *Biomacromolecules* **16**, 706–714.

Carter NA and Grove TZ (2018) Protein self-assemblies that can generate, hold, and discharge electric potential in response to changes in relative humidity. *Journal of the American Chemical Society* **140**, 7144–7151.

Castelletto V, Nutt DR, Hamley IW, Bucak S, Cenker Ç and Olsson U (2010) Structure of single-wall peptide nanotubes: *in situ* flow aligning X-ray diffraction. *Chemical Communications* **46**, 6270–6272.

Cenker ÇÇ, Bomans PHH, Friedrich H, Dedeoğlu B, Aviyente V, Olsson U, Sommerdijk NAJM and Bucak S (2012) Peptide nanotube formation: a crystal growth process. *Soft Matter* **8**, 7463–7470.

Chamberlain AK, Macphee CE, Zurdo J, Morozova-Roche LA, Hill HA, Dobson CM and Davis JJ (2000) Ultrastructural organization of amyloid fibrils by atomic force microscopy. *Biophysical Journal* **79**, 3282–3293.

Chen KH, Corro KA, Le SP and Nowick JS (2017) X-ray crystallographic structure of a giant double-walled peptide nanotube formed by a macrocyclic β-sheet containing $A\beta_{16\text{-}22}$. *Journal of the American Chemical Society* **139**, 8102–8105.

Chen YX, Ing NL, Wang F, Xu D, Sloan NB, Lam NT, Winter DL, Egelman EH, Hochbaum AI, Clark DS and Glover DJ (2020) Structural determination of a filamentous chaperone to fabricate electronically conductive metalloprotein nanowires. *ACS Nano* **14**, 6559–6569.

Cheng RP, Gellman SH and Degrado WF (2001) Beta-peptides: from structure to function. *Chemical Reviews* **101**, 3219–3232.

Chervy P, Petcut C, Rault D, Meriadec C, Bizien T, François K, Richard J, Chassaing C, Benamar N, Artzner F and Paternostre M (2019) Organic nanoscrolls from electrostatic interactions between peptides and lipids: assembly steps and structure. *Langmuir* **35**, 10648–10657.

Chiu W, Holton J, Langan P, Sauter NK, Schlichting I, Terwilliger T, Martin JL, Read RJ and Wakatsuki S (2017) Responses to 'atomic resolution': a badly abused term in structural biology. *Acta Crystallographica Section D: Structural Biology* **73**(Pt 4), 381–383.

Chothia C (1973) Conformation of twisted beta-pleated sheets in proteins. *Journal of Molecular Biology* **75**, 295–302.

Christofferson AJ, Al-Garawi ZS, Todorova N, Turner J, Del Borgo MP, Serpell LC, Aguilar M-I and Yarovsky I (2018) Identifying the coiled-coil triple helix structure of β-peptide nanofibers at atomic resolution. *ACS Nano* **12**, 9101–9109.

Close W, Neumann M, Schmidt A, Hora M, Annamalai K, Schmidt M, Reif B, Schmidt V, Grigorieff N and Fändrich M (2018) Physical basis of amyloid fibril polymorphism. *Nature Communications* **9**, 699.

Collie GW, Pulka-Ziach K, Lombardo CM, Fremaux J, Rosu F, Decossas M, Mauran L, Lambert O, Gabelica V, Mackereth CD and Guichard G (2015) Shaping quaternary assemblies of water-soluble non-peptide helical foldamers by sequence manipulation. *Nature Chemistry* **7**, 871–878.

Colvin MT, Silvers R, Ni QZ, Can TV, Sergeyev I, Rosay M, Donovan KJ, Michael B, Wall J, Linse S and Griffin RG (2016) Atomic resolution structure of monomorphic $A\beta_{42}$ amyloid fibrils. *Journal of the American Chemical Society* **138**, 9663–9674.

Cormier AR, Pang X, Zimmerman MI, Zhou H-X and Paravastu AK (2013) Molecular structure of RADA16-I designer self-assembling peptide nanofibers. *ACS Nano* **7**, 7562–7572.

Costa TRD, Felisberto-Rodrigues C, Meir A, Prevost MS, Redzej A, Trokter M and Waksman G (2015) Secretion systems in Gram-negative bacteria: structural and mechanistic insights. *Nature Reviews Microbiology* **13**, 343–359.

Costa TRD, Ilangovan A, Ukleja M, Redzej A, Santini JM, Smith TK, Egelman EH and Waksman G (2016) Structure of the bacterial sex F

https://doi.org/10.1017/S0033583522000014 Published online by Cambridge University Press

pilus reveals an assembly of a stoichiometric protein–phospholipid complex. *Cell* **166**, 1436–1444.e1410.

Cox BS, Tuite MF and Mclaughlin CS (1988) The psi factor of yeast: a problem in inheritance. *Yeast* **4**, 159–178.

Crick F (1953) The packing of α-helices: simple coiled-coils. *Acta Crystallographica* **6**, 689–697.

Culf AS and Ouellette RJ (2010) Solid-phase synthesis of *N*-substituted glycine oligomers (α-peptoids) and derivatives. *Molecules* **15**, 5282–5335.

Da Silva ER, Alves WA, Castelletto V, Reza M, Ruokolainen J, Hussain R and Hamley IW (2015*a*) Self-assembly pathway of peptide nanotubes formed by a glutamatic acid-based bolaamphiphile. *Chemical Communications* **51**, 11634–11637.

Da Silva ER, Walter MNM, Reza M, Castelletto V, Ruokolainen J, Connon CJ, Alves WA and Hamley IW (2015*b*) Self-assembled arginine-capped peptide bolaamphiphile nanosheets for cell culture and controlled wettability surfaces. *Biomacromolecules* **16**, 3180–3190.

Dauter Z and Jaskolski M (2018) On the helical arrangements of protein molecules. *Protein Science* **27**, 643–652.

Dawson WM, Martin FJO, Rhys GG, Shelley KL, Brady RL and Woolfson DN (2021) Coiled coils 9-to-5: rational *de novo* design of alpha-helical barrels with tunable oligomeric states. *Chemical Science* **12**, 6923–6928.

Del Borgo MP, Mechler AI, Traore D, Forsyth C, Wilce JA, Wilce MCJ, Aguilar M-I and Perlmutter P (2013) Supramolecular self-assembly of *N*-acetyl-capped β-peptides leads to nano- to macroscale fiber formation. *Angewandte Chemie International Edition* **52**, 8266–8270.

Diaz-Avalos R, Long C, Fontano E, Balbirnie M, Grothe R, Eisenberg D and Caspar DL (2003) Cross-beta order and diversity in nanocrystals of an amyloid-forming peptide. *Journal of Molecular Biology* **330**, 1165–1175.

Dublin SN and Conticello VP (2008) Design of a selective metal Ion switch for self-assembly of peptide-based fibrils. *Journal of the American Chemical Society* **130**, 49–51.

Dubochet J (2012) Cryo-EM – the first thirty years. *Journal of Microscopy* **245**, 221–224.

Eanes ED and Glenner GG (1968) X-ray diffraction studies on amyloid filaments. *Journal of Histochemistry & Cytochemistry* **16**, 673–677.

Egelman EH (2000) A robust algorithm for the reconstruction of helical filaments using single-particle methods. *Ultramicroscopy* **85**, 225–234.

Egelman EH (2007) The iterative helical real space reconstruction method: surmounting the problems posed by real polymers. *Journal of Structural Biology* **157**, 83–94.

Egelman EH (2010) Reconstruction of helical filaments and tubes. *Methods Enzymol* **482**, 167–183.

Egelman EH (2014) Ambiguities in helical reconstruction. *Elife* **3**, e04969.

Egelman EH (2017) Cryo-EM of bacterial pili and archaeal flagellar filaments. *Current Opinion in Structural Biology* **46**, 31–37.

Egelman EH, Francis N and Derosier DJ (1982) F-actin is a helix with a random variable twist. *Nature* **298**, 131–135.

Egelman EH, Xu C, Dimaio F, Magnotti E, Modlin C, Yu X, Wright E, Baker D and Conticello VP (2015) Structural plasticity of helical nanotubes based on coiled-coil assemblies. *Structure (London, England: 1993)* **23**, 280–289.

Eisenberg DS and Sawaya MR (2017) Structural studies of amyloid proteins at the molecular level. *Annual Review of Biochemistry* **86**, 69–95.

Feng Z, Wang H, Wang F, Oh Y, Berciu C, Cui Q, Egelman EH and Xu B (2020) Artificial intracellular filaments. *Cell Reports Physical Science* **1**, 100085.

Frederix PWJM, Ulijn RV, Hunt NT and Tuttle T (2011) Virtual screening for dipeptide aggregation: toward predictive tools for peptide self-assembly. *The Journal of Physical Chemistry Letters* **2**, 2380–2384.

Frederix PWJM, Scott GG, Abul-Haija YM, Kalafatovic D, Pappas CG, Javid N, Hunt NT, Ulijn RV and Tuttle T (2015) Exploring the sequence space for (tri-)peptide self-assembly to design and discover new hydrogels. *Nature Chemistry* **7**, 30–37.

Gallardo R, Ranson NA and Radford SE (2020) Amyloid structures: much more than just a cross-β fold. *Current Opinion in Structural Biology* **60**, 7–16.

Garcia-Seisdedos H, Empereur-Mot C, Elad N and Levy ED (2017) Proteins evolve on the edge of supramolecular self-assembly. *Nature* **548**, 244–247.

Garcia-Seisdedos H, Villegas JA and Levy ED (2019) Infinite assembly of folded proteins in evolution, disease, and engineering. *Angewandte Chemie International Edition* **58**, 5514–5531.

Ge P and Zhou ZH (2011) Hydrogen-bonding networks and RNA bases revealed by cryo electron microscopy suggest a triggering mechanism for calcium switches. *Proceedings of the National Academy of Sciences of the United States of America* **108**, 9637–9642.

Gelain F, Luo Z and Zhang S (2020) Self-assembling peptide EAK16 and RADA16 nanofiber scaffold hydrogel. *Chemical Reviews* **120**, 13434–13460.

Ghadiri MR, Granja JR, Milligan RA, Mcree DE and Khazanovich N (1993) Self-assembling organic nanotubes based on a cyclic peptide architecture. *Nature* **366**, 324–327.

Gobeaux F, Fay N, Tarabout C, Meriadec C, Meneau F, Ligeti M, Buisson DA, Cintrat JC, Nguyen KM, Perrin L, Valery C, Artzner F and Paternostre M (2012) Structural role of counterions adsorbed on self-assembled peptide nanotubes. *Journal of the American Chemical Society* **134**, 723–733.

Goodman CM, Choi S, Shandler S and Degrado WF (2007) Foldamers as versatile frameworks for the design and evolution of function. *Nature Chemical Biology* **3**, 252–262.

Gopalan RD, Del Borgo MP, Mechler AI, Perlmutter P and Aguilar M-I (2015) Geometrically precise building blocks: the self-assembly of β-peptides. *Chemistry & Biology* **22**, 1417–1423.

Görbitz CH (2001) Nanotube formation by hydrophobic dipeptides. *Chemistry – A European Journal* **7**, 5153–5159.

Görbitz CH (2006) The structure of nanotubes formed by diphenylalanine, the core recognition motif of Alzheimer's β-amyloid polypeptide. *Chemical Communications* **22**, 2332–2334.

Gremer L, Schölzel D, Schenk C, Reinartz E, Labahn J, Ravelli RBG, Tusche M, Lopez-Iglesias C, Hoyer W, Heise H, Willbold D and Schröder GF (2017) Fibril structure of amyloid-β(1–42) by cryo-electron microscopy. *Science (New York, N.Y.)* **358**, 116–119.

Gribbon C, Channon KJ, Zhang W, Banwell EF, Bromley EHC, Chaudhuri JB, Oreffo ROC and Woolfson DN (2008) MagicWand: a single, designed peptide that assembles to stable, ordered α-helical fibers. *Biochemistry* **47**, 10365–10371.

Guenther EL, Ge P, Trinh H, Sawaya MR, Cascio D, Boyer DR, Gonen T, Zhou ZH and Eisenberg DS (2018) Atomic-level evidence for packing and positional amyloid polymorphism by segment from TDP-43 RRM2. *Nature Structural & Molecular Biology* **25**, 311–319.

Guerrero-Ferreira R, Taylor NM, Mona D, Ringler P, Lauer ME, Riek R, Britschgi M and Stahlberg H (2018) Cryo-EM structure of alpha-synuclein fibrils. *Elife* **7**, e36402.

Guerrero-Ferreira R, Taylor NM, Arteni A-A, Kumari P, Mona D, Ringler P, Britschgi M, Lauer ME, Makky A, Verasdonck J, Riek R, Melki R, Meier BH, Böckmann A, Bousset L and Stahlberg H (2019) Two new polymorphic structures of human full-length alpha-synuclein fibrils solved by cryo-electron microscopy. *Elife* **8**, e48907.

Guilbaud J-B and Saiani A (2011) Using small angle scattering (SAS) to structurally characterise peptide and protein self-assembled materials. *Chemical Society Reviews* **40**, 1200–1210.

Haines-Butterick L, Rajagopal K, Branco M, Salick D, Rughani R, Pilarz M, Lamm MS, Pochan DJ and Schneider JP (2007) Controlling hydrogelation kinetics by peptide design for three-dimensional encapsulation and injectable delivery of cells. *Proceedings of the National Academy of Sciences of the United States of America* **104**, 7791–7796.

Hamley IW (2011) Self-assembly of amphiphilic peptides. *Soft Matter* **7**, 4122–4138.

Hamley IW (2014) Peptide nanotubes. *Angewandte Chemie International Edition* **53**, 6866–6881.

Hamley IW, Burholt S, Hutchinson J, Castelletto V, Da Silva ER, Alves W, Gutfreund P, Porcar L, Dattani R, Hermida-Merino D, Newby G, Reza M, Ruokolainen J and Stasiak J (2017) Shear alignment of bola-amphiphilic arginine-coated peptide nanotubes. *Biomacromolecules* **18**, 141–149.

Harper JD, Lieber CM and Lansbury Jr PT (1997) Atomic force microscopic imaging of seeded fibril formation and fibril branching by the Alzheimer's disease amyloid-beta protein. *Chemistry & Biology* **4**, 951–959.

https://doi.org/10.1017/S0033583522000014 Published online by Cambridge University Press

He S and Scheres SHW (2017) Helical reconstruction in RELION. *Journal of Structural Biology* **198**, 163–176.

Heise H, Hoyer W, Becker S, Andronesi OC, Riedel D and Baldus M (2005) Molecular-level secondary structure, polymorphism, and dynamics of full-length α-synuclein fibrils studied by solid-state NMR. *Proceedings of the National Academy of Sciences of the United States of America* **102**, 15871–15876.

Huang PS, Ban YE, Richter F, Andre I, Vernon R, Schief WR and Baker D (2011) RosettaRemodel: a generalized framework for flexible backbone protein design. *PLoS One* **6**, e24109.

Huang D, Hudson BC, Gao Y, Roberts EK and Paravastu AK (2018) Solid-state NMR structural characterization of self-assembled peptides with selective ^{13}C and ^{15}N isotopic labels. In Nilsson BL and Doran TM (eds), *Peptide Self-Assembly: Methods and Protocols*. New York, NY: Springer New York, pp. 23–68.

Hughes SA, Wang F, Wang S, Kreutzberger MAB, Osinski T, Orlova A, Wall JS, Zuo X, Egelman EH and Conticello VP (2019) Ambidextrous helical nanotubes from self-assembly of designed helical hairpin motifs. *Proceedings of the National Academy of Sciences of the United States of America* **116**, 14456–14464.

Hwang W, Marini DM, Kamm RD and Zhang S (2003) Supramolecular structure of helical ribbons self-assembled from a β-sheet peptide. *The Journal of Chemical Physics* **118**, 389–397.

Insua I and Montenegro J (2020) 1D to 2D self assembly of cyclic peptides. *Journal of the American Chemical Society* **142**, 300–307.

Jiao W, Yang H, Wu Z, Liu J and Zhang W (2020) Self-assembled block polymer aggregates in selective solution: controllable morphology transitions and their applications in drug delivery. *Expert Opinion on Drug Delivery* **17**, 947–961.

Jin H, Ding YH, Wang M, Song Y, Liao Z, Newcomb CJ, Wu X, Tang XQ, Li Z, Lin Y, Yan F, Jian T, Mu P and Chen CL (2018) Designable and dynamic single-walled stiff nanotubes assembled from sequence-defined peptoids. *Nature Communications* **9**, 270.

Jumper J and Hassabis D (2022) Protein structure predictions to atomic accuracy with AlphaFold. *Nature Methods* **19**, 11–12.

Kajander T, Cortajarena AL, Mochrie S and Regan L (2007) Structure and stability of designed TPR protein superhelices: unusual crystal packing and implications for natural TPR proteins. *Acta Crystallographica Section D: Biological Crystallography* **63**(Pt 7), 800–811.

Kajava AV (2012) Tandem repeats in proteins: from sequence to structure. *Journal of Structural Biology* **179**, 279–288.

Kajava AV and Steven AC (2006) Beta-rolls, beta-helices, and other beta-solenoid proteins. *Advances in Protein Chemistry* **73**, 55–96.

Kaltofen S, Li C, Huang PS, Serpell LC, Barth A and Andre I (2015) Computational *de novo* design of a self-assembling peptide with predefined structure. *Journal of Molecular Biology* **427**, 550–562.

Ke PC, Zhou R, Serpell LC, Riek R, Knowles TPJ, Lashuel HA, Gazit E, Hamley IW, Davis TP, Fändrich M, Otzen DE, Chapman MR, Dobson CM, Eisenberg DS and Mezzenga R (2020) Half a century of amyloids: past, present and future. *Chemical Society Reviews* **49**, 5473–5509.

Kim J, Han TH, Kim Y-I, Park JS, Choi J, Churchill DG, Kim SO and Ihee H (2010) Role of water in directing diphenylalanine assembly into nanotubes and nanowires. *Advanced Materials* **22**, 583–587.

Knowles TP, Fitzpatrick AW, Meehan S, Mott HR, Vendruscolo M, Dobson CM and Welland ME (2007) Role of intermolecular forces in defining material properties of protein nanofibrils. *Science (New York, N.Y.)* **318**, 1900–1903.

Kobe B and Kajava AV (2000) When protein folding is simplified to protein coiling: the continuum of solenoid protein structures. *Trends in Biochemical Sciences* **25**, 509–515.

Kollmer M, Close W, Funk L, Rasmussen J, Bsoul A, Schierhorn A, Schmidt M, Sigurdson CJ, Jucker M and Fandrich M (2019) Cryo-EM structure and polymorphism of abeta amyloid fibrils purified from Alzheimer's brain tissue. *Nature Communications* **10**, 4760.

Koronakis V, Sharff A, Koronakis E, Luisi B and Hughes C (2000) Crystal structure of the bacterial membrane protein TolC central to multidrug efflux and protein export. *Nature* **405**, 914–919.

Krissinel E and Henrick K (2007) Inference of macromolecular assemblies from crystalline state. *Journal of Molecular Biology* **372**, 774–797.

Kühlbrandt W (2014) The resolution revolution. *Science (New York, N.Y.)* **343**, 1443–1444.

Lamm MS, Rajagopal K, Schneider JP and Pochan DJ (2005) Laminated morphology of nontwisting beta-sheet fibrils constructed via peptide self-assembly. *Journal of the American Chemical Society* **127**, 16692–16700.

Lanci CJ, Macdermaid CM, Kang SG, Acharya R, North B, Yang X, Qiu XJ, Degrado WF and Saven JG (2012) Computational design of a protein crystal. *Proceedings of the National Academy of Sciences of the United States of America* **109**, 7304–7309.

Leaver-Fay A, Tyka M, Lewis SM, Lange OF, Thompson J, Jacak R, Kaufman K, Renfrew PD, Smith CA, Sheffler W, Davis IW, Cooper S, Treuille A, Mandell DJ, Richter F, Ban YE, Fleishman SJ, Corn JE, Kim DE, Lyskov S, Berrondo M, Mentzer S, Popovic Z, Havranek JJ, Karanicolas J, Das R, Meiler J, Kortemme T, Gray JJ, Kuhlman B, Baker D and Bradley P (2011) ROSETTA3: an object-oriented software suite for the simulation and design of macromolecules. *Methods in Enzymology* **487**, 545–574.

Lee M, Wang T, Makhlynets OV, Wu Y, Polizzi NF, Wu H, Gosavi PM, Stöhr J, Korendovych IV, Degrado WF and Hong M (2017) Zinc-binding structure of a catalytic amyloid from solid-state NMR. *Proceedings of the National Academy of Sciences of the United States of America* **114**, 6191–6196.

Lepault J, Booy FP and Dubochet J (1983) Electron microscopy of frozen biological suspensions. *Journal of Microscopy* **129**, 89–102.

Li X, Mooney P, Zheng S, Booth CR, Braunfeld MB, Gubbens S, Agard DA and Cheng Y (2013) Electron counting and beam-induced motion correction enable near-atomic-resolution single-particle cryo-EM. *Nature Methods* **10**, 584–590.

Liu J, Zheng Q, Deng Y, Cheng C-S, Kallenbach NR and Lu M (2006) A seven-helix coiled coil. *Proceedings of the National Academy of Sciences of the United States of America* **103**, 15457–15462.

Loquet A, Sgourakis NG, Gupta R, Giller K, Riedel D, Goosmann C, Griesinger C, Kolbe M, Baker D, Becker S and Lange A (2012) Atomic model of the type III secretion system needle. *Nature* **486**, 276–279.

Lu K, Jacob J, Thiyagarajan P, Conticello VP and Lynn DG (2003) Exploiting amyloid fibril lamination for nanotube self-assembly. *Journal of the American Chemical Society* **125**, 6391–6393.

Lu A, Li Y, Yin Q, Ruan J, Yu X, Egelman E and Wu H (2015) Plasticity in PYD assembly revealed by cryo-EM structure of the PYD filament of AIM2. *Cell Discovery* **1**, 15013.

Lupas AN and Bassler J (2017) Coiled coils – a model system for the 21st century. *Trends in Biochemical Sciences* **42**, 130–140.

Lynch EM, Hicks DR, Shepherd M, Endrizzi JA, Maker A, Hansen JM, Barry RM, Gitai Z, Baldwin EP and Kollman JM (2017) Human CTP synthase filament structure reveals the active enzyme conformation. *Nature Structural & Molecular Biology* **24**, 507–514.

Lynch EM, Kollman JM and Webb BA (2020) Filament formation by metabolic enzymes – a new twist on regulation. *Current Opinion in Cell Biology* **66**, 28–33.

Main ER, Xiong Y, Cocco MJ, D'Andrea L and Regan L (2003) Design of stable alpha-helical arrays from an idealized TPR motif. *Structure (London, England: 1993)* **11**, 497–508.

Marchesan S, Vargiu AV and Styan KE (2015) The Phe–Phe motif for peptide self-assembly in nanomedicine. *Molecules* **20**, 19775–19788.

Marini DM, Hwang W, Lauffenburger DA, Zhang S and Kamm RD (2002) Left-handed helical ribbon intermediates in the self-assembly of a β-sheet peptide. *Nano Letters* **2**, 295–299.

Marvin DA, Symmons MF and Straus SK (2014) Structure and assembly of filamentous bacteriophages. *Progress in Biophysics and Molecular Biology* **114**, 80–122.

Mehta AK, Shayo Y, Vankayalapati H, Hurley LH and Schaefer J (2004) Structure of a quinobenzoxazine–G-quadruplex complex by REDOR NMR. *Biochemistry* **43**, 11953–11958.

Mehta AK, Lu K, Childers WS, Liang Y, Dublin SN, Dong J, Snyder JP, Pingali SV, Thiyagarajan P and Lynn DG (2008) Facial symmetry in protein self-assembly. *Journal of the American Chemical Society* **130**, 9829–9835.

Merg AD, Touponse G, Genderen EV, Blum TB, Zuo X, Bazrafshan A, Siaw HMH, Mccanna A, Brian Dyer R, Salaita K, Abrahams JP and Conticello

VP (2020) Shape-shifting peptide nanomaterials: surface asymmetry enables pH-dependent formation and interconversion of collagen tubes and sheets. *Journal of the American Chemical Society* **142**, 19956–19968.

Middleton DA, Madine J, Castelletto V and Hamley IW (2013) Insights into the molecular architecture of a peptide nanotube using FTIR and solid-state NMR spectroscopic measurements on an aligned sample. *Angewandte Chemie International Edition* **52**, 10537–10540.

Misra R, Rudnick-Glick S and Adler-Abramovich L (2021) From folding to assembly: functional supramolecular architectures of peptides comprised of non-canonical amino acids. *Macromolecular Bioscience* **21**, e2100090.

Moore AN and Hartgerink JD (2017) Self-assembling multidomain peptide nanofibers for delivery of bioactive molecules and tissue regeneration. *Accounts of Chemical Research* **50**, 714–722.

Morris RJ and Bricogne G (2003) Sheldrick's 1.2 A rule and beyond. *Acta Crystallographica Section D: Biological Crystallography* **59**(Pt 3), 615–617.

Morris KL, Zibaee S, Chen L, Goedert M, Sikorski P and Serpell LC (2013) The structure of cross-β tapes and tubes formed by an octapeptide, αSβ1. *Angewandte Chemie International Edition* **52**, 2279–2283.

Nagy-Smith K, Moore E, Schneider J and Tycko R (2015) Molecular structure of monomorphic peptide fibrils within a kinetically trapped hydrogel network. *Proceedings of the National Academy of Sciences of the United States of America* **112**, 9816–9821.

Nagy-Smith K, Beltramo PJ, Moore E, Tycko R, Furst EM and Schneider JP (2017) Molecular, local, and network-level basis for the enhanced stiffness of hydrogel networks formed from coassembled racemic peptides: predictions from Pauling and Corey. *ACS Central Science* **3**, 586–597.

Nam KT, Shelby SA, Choi PH, Marciel AB, Chen R, Tan L, Chu TK, Mesch RA, Lee BC, Connolly MD, Kisielowski C and Zuckermann RN (2010) Free-floating ultrathin two-dimensional crystals from sequence-specific peptoid polymers. *Nature Materials* **9**, 454–460.

Namba K, Pattanayek R and Stubbs G (1989) Visualization of protein–nucleic acid interactions in a virus: refined structure of intact tobacco mosaic virus at 2.9 Å resolution by X-ray fiber diffraction. *Journal of Molecular Biology* **208**, 307–325.

Nelson R, Sawaya MR, Balbirnie M, Madsen AO, Riekel C, Grothe R and Eisenberg D (2005) Structure of the cross-beta spine of amyloid-like fibrils. *Nature* **435**, 773–778.

Oakley MG and Kim PS (1998) A buried polar interaction can direct the relative orientation of helices in a coiled coil. *Biochemistry* **37**, 12603–12610.

Ogihara NL, Weiss MS, Degrado WF and Eisenberg D (1997) The crystal structure of the designed trimeric coiled coil coil-VaLd: implications for engineering crystals and supramolecular assemblies. *Protein Science* **6**, 80–88.

Orlova A and Egelman EH (1993) A conformational change in the actin subunit can change the flexibility of the actin filament. *Journal of Molecular Biology* **232**, 334–341.

Pandya MJ, Spooner GM, Sunde M, Thorpe JR, Rodger A and Woolfson DN (2000) Sticky-end assembly of a designed peptide fiber provides insight into protein fibrillogenesis. *Biochemistry* **39**, 8728–8734.

Papapostolou D, Smith AM, Atkins EDT, Oliver SJ, Ryadnov MG, Serpell LC and Woolfson DN (2007) Engineering nanoscale order into a designed protein fiber. *Proceedings of the National Academy of Sciences of the United States of America* **104**, 10853–10858.

Pauling L and Corey RB (1951) The pleated sheet, a new layer configuration of polypeptide chains. *Proceedings of the National Academy of Sciences of the United States of America* **37**, 251–256.

Peng Z, Parker AS, Peralta MDR, Ravikumar KM, Cox DL and Toney MD (2017*a*) High tensile strength of engineered beta-solenoid fibrils via sonication and pulling. *Biophysical Journal* **113**, 1945–1955.

Peng Z, Peralta MDR and Toney MD (2017*b*) Extraordinarily stable amyloid fibrils engineered from structurally defined beta-solenoid proteins. *Biochemistry* **56**, 6041–6050.

Peng Z, Peralta MDR, Cox DL and Toney MD (2020) Bottom-up synthesis of protein-based nanomaterials from engineered beta-solenoid proteins. *PLoS One* **15**, e0229319.

Peralta MD, Karsai A, Ngo A, Sierra C, Fong KT, Hayre NR, Mirzaee N, Ravikumar KM, Kluber AJ, Chen X, Liu GY, Toney MD, Singh RR and Cox DL (2015) Engineering amyloid fibrils from beta-solenoid proteins for biomaterials applications. *ACS Nano* **9**, 449–463.

Peters JW, Stowell MHB and Rees DC (1996) A leucine-rich repeat variant with a novel repetitive protein structural motif. *Nature Structural Biology* **3**, 991–994.

Pieri L, Wang F, Arteni AA, Vos M, Winter JM, Le Du MH, Artzner F, Gobeaux F, Legrand P, Boulard Y, Bressanelli S, Egelman EH and Paternostre M (2022) Atomic structure of lanreotide nanotubes revealed by cryo-EM. *Proceedings of the National Academy of Sciences of the United States of America* **119**, 4.

Pizzey CL, Pomerantz WC, Sung B-J, Yuwono VM, Gellman SH, Hartgerink JD, Yethiraj A and Abbott NL (2008) Characterization of nanofibers formed by self-assembly of β-peptide oligomers using small angle X-ray scattering. *The Journal of Chemical Physics* **129**, 095103.

Pomerantz WC, Abbott NL and Gellman SH (2006) Lyotropic liquid crystals from designed helical β-peptides. *Journal of the American Chemical Society* **128**, 8730–8731.

Pomerantz WC, Yuwono VM, Pizzey CL, Hartgerink JD, Abbott NL and Gellman SH (2008) Nanofibers and lyotropic liquid crystals from a class of self-assembling β-peptides. *Angewandte Chemie International Edition* **47**, 1241–1244.

Pomerantz WC, Yuwono VM, Drake R, Hartgerink JD, Abbott NL and Gellman SH (2011) Lyotropic liquid crystals formed from ACHC-rich β-peptides. *Journal of the American Chemical Society* **133**, 13604–13613.

Potekhin SA, Melnik TN, Popov V, Lanina NF, Vazina AA, Rigler P, Verdini AS, Corradin G and Kajava AV (2001) *De novo* design of fibrils made of short alpha-helical coiled coil peptides. *Chemistry & Biology* **8**, 1025–1032.

Pouget E, Fay N, Dujardin E, Jamin N, Berthault P, Perrin L, Pandit A, Rose T, Valéry C, Thomas D, Paternostre M and Artzner F (2010) Elucidation of the self-assembly pathway of lanreotide octapeptide into β-sheet nanotubes: role of two stable intermediates. *Journal of the American Chemical Society* **132**, 4230–4241.

Poweleit N, Ge P, Nguyen HH, Loo RRO, Gunsalus RP and Zhou ZH (2016) CryoEM structure of the methanospirillum hungatei archaellum reveals structural features distinct from the bacterial flagellum and type IV pilus. *Nature Microbiology* **2**, 16222.

Punjani A, Rubinstein JL, Fleet DJ and Brubaker MA (2017) cryoSPARC: algorithms for rapid unsupervised cryo-EM structure determination. *Nature Methods* **14**, 290–296.

Raeburn J, Zamith Cardoso A and Adams DJ (2013) The importance of the self-assembly process to control mechanical properties of low molecular weight hydrogels. *Chemical Society Reviews* **42**, 5143–5156.

Reches M and Gazit E (2003) Casting metal nanowires within discrete self-assembled peptide nanotubes. *Science (New York, N.Y.)* **300**, 625–627.

Reiersen H and Rees AR (2001) The hunchback and its neighbours: proline as an environmental modulator. *Trends in Biochemical Sciences* **26**, 679–684.

Rhys GG, Wood CW, Lang EJM, Mulholland AJ, Brady RL, Thomson AR and Woolfson DN (2018) Maintaining and breaking symmetry in homomeric coiled-coil assemblies. *Nature Communications* **9**, 4132.

Rodriguez JA, Ivanova MI, Sawaya MR, Cascio D, Reyes FE, Shi D, Sangwan S, Guenther EL, Johnson LM, Zhang M, Jiang L, Arbing MA, Nannenga BL, Hattne J, Whitelegge J, Brewster AS, Messerschmidt M, Boutet S, Sauter NK, Gonen T and Eisenberg DS (2015) Structure of the toxic core of α-synuclein from invisible crystals. *Nature* **525**, 486–490.

Rodriguez JA, Eisenberg DS and Gonen T (2017) Taking the measure of MicroED. *Current Opinion in Structural Biology* **46**, 79–86.

Rüter A, Kuczera S, Stenhammar J, Zinn T, Narayanan T and Olsson U (2020) Tube to ribbon transition in a self-assembling model peptide system. *Physical Chemistry Chemical Physics* **22**, 18320–18327.

Sachse C (2015) Single-particle based helical reconstruction – how to make the most of real and Fourier space. *AIMS Biophysics* **2**, 219–244.

Sawaya MR, Rodriguez J, Cascio D, Collazo MJ, Shi D, Reyes FE, Hattne J, Gonen T and Eisenberg DS (2016) *Ab initio* structure determination from prion nanocrystals at atomic resolution by MicroED. *Proceedings of the National Academy of Sciences of the United States of America* **113**, 11232–11236.

Scheres S (2020) Amyloid structure determination in RELION-3.1. *Acta Crystallographica Section D* **76**, 94–101.

https://doi.org/10.1017/S0033583522000014 Published online by Cambridge University Press

Scheres SHW, Zhang W, Falcon B and Goedert M (2020) Cryo-EM structures of tau filaments. *Current Opinion in Structural Biology* **64**, 17–25.

Schmidt A, Annamalai K, Schmidt M, Grigorieff N and Fandrich M (2016) Cryo-EM reveals the steric zipper structure of a light chain-derived amyloid fibril. *Proceedings of the National Academy of Sciences of the United States of America* **113**, 6200–6205.

Schneider JP, Pochan DJ, Ozbas B, Rajagopal K, Pakstis L and Kretsinger J (2002) Responsive hydrogels from the intramolecular folding and self-assembly of a designed peptide. *Journal of the American Chemical Society* **124**, 15030–15037.

Selinger RL, Selinger JV, Malanoski AP and Schnur JM (2004) Shape selection in chiral self-assembly. *Physical Review Letters* **93**, 158103.

Sharp TH, Bruning M, Mantell J, Sessions RB, Thomson AR, Zaccai NR, Brady RL, Verkade P and Woolfson DN (2012) Cryo-transmission electron microscopy structure of a gigadalton peptide fiber of *de novo* design. *Proceedings of the National Academy of Sciences of the United States of America* **109**, 13266–13271.

Sheldrick G (1990) Phase annealing in SHELX-90: direct methods for larger structures. *Acta Crystallographica Section A* **46**, 467–473.

Shen H, Fallas JA, Lynch E, Sheffler W, Parry B, Jannetty N, Decarreau J, Wagenbach M, Vicente JJ, Chen J, Wang L, Dowling Q, Oberdorfer G, Stewart L, Wordeman L, De Yoreo J, Jacobs-Wagner C, Kollman J and Baker D (2018) *De novo* design of self-assembling helical protein filaments. *Science (New York, N.Y.)* **362**, 705–709.

Siemer AB, Ritter C, Ernst M, Riek R and Meier BH (2005) High-resolution solid-state NMR spectroscopy of the prion protein HET-s in its amyloid conformation. *Angewandte Chemie International Edition* **44**, 2441–2444.

Smith AM, Banwell EF, Edwards WR, Pandya MJ and Woolfson DN (2006) Engineering increased stability into self-assembled protein fibers. *Advanced Functional Materials* **16**, 1022–1030.

Song B, Lenhart J, Flegler VJ, Makbul C, Rasmussen T and Böttcher B (2019) Capabilities of the Falcon III detector for single-particle structure determination. *Ultramicroscopy* **203**, 145–154.

Song Q, Cheng Z, Kariuki M, Hall SCL, Hill SK, Rho JY and Perrier S (2021) Molecular self-assembly and supramolecular chemistry of cyclic peptides. *Chemical Reviews* **121**, 13936–13995.

Spaulding CN, Schreiber HLIV, Zheng W, Dodson KW, Hazen JE, Conover MS, Wang F, Svenmarker P, Luna-Rico A, Francetic O, Andersson M, Hultgren S and Egelman EH (2018) Functional role of the type 1 pilus rod structure in mediating host-pathogen interactions. *Elife* **7**, e31662.

Spencer R, Chen KH, Manuel G and Nowick JS (2013) Recipe for β-sheets: foldamers containing amyloidogenic peptide sequences. *European Journal of Organic Chemistry* **2013**, 3523–3528.

Spillantini MG, Schmidt ML, Lee VMY, Trojanowski JQ, Jakes R and Goedert M (1997) α-Synuclein in Lewy bodies. *Nature* **388**, 839–840.

Stubbs G and Kendall A (2012) Helical viruses. *Advances in Experimental Medicine and Biology* **726**, 631–658.

Subramaniam S, Earl LA, Falconieri V, Milne JLS and Egelman EH (2016) Resolution advances in cryo-EM enable application to drug discovery. *Current Opinion in Structural Biology* **41**, 194–202.

Sun J and Zuckermann RN (2013) Peptoid polymers: a highly designable bioinspired material. *ACS Nano* **7**, 4715–4732.

Sun L, Young LN, Zhang X, Boudko SP, Fokine A, Zbornik E, Roznowski AP, Molineux IJ, Rossmann MG and Fane BA (2014) Icosahedral bacteriophage PhiX174 forms a tail for DNA transport during infection. *Nature* **505**, 432–435.

Sun J, Jiang X, Lund R, Downing KH, Balsara NP and Zuckermann RN (2016) Self-assembly of crystalline nanotubes from monodisperse amphiphilic diblock copolypeptoid tiles. *Proceedings of the National Academy of Sciences of the United States of America* **113**, 3954–3959.

Sunde M, Serpell LC, Bartlam M, Fraser PE, Pepys MB and Blake CC (1997) Common core structure of amyloid fibrils by synchrotron X-ray diffraction. *Journal of Molecular Biology* **273**, 729–739.

Tarabout C, Roux S, Gobeaux F, Fay N, Pouget E, Meriadec C, Ligeti M, Thomas D, IJsselstijn M, Besselievre F, Buisson DA, Verbavatz JM, Petitjean M, Valery C, Perrin L, Rousseau B, Artzner F, Paternostre M and Cintrat JC (2011) Control of peptide nanotube diameter by chemical modifications of an aromatic residue involved in a single close contact. *Proceedings of the National Academy of Sciences of the United States of America* **108**, 7679–7684.

Tarafder AK, Von Kügelgen A, Mellul AJ, Schulze U, Aarts DGAL and Bharat TAM (2020) Phage liquid crystalline droplets form occlusive sheaths that encapsulate and protect infectious rod-shaped bacteria. *Proceedings of the National Academy of Sciences* **117**, 4724–4731.

Tayeb-Fligelman E, Tabachnikov O, Moshe A, Goldshmidt-Tran O, Sawaya MR, Coquelle N, Colletier JP and Landau M (2017) The cytotoxic *Staphylococcus aureus* PSMα3 reveals a cross-α amyloid-like fibril. *Science (New York, N.Y.)* **355**, 831–833.

Thomas F, Dawson WM, Lang EJM, Burton AJ, Bartlett GJ, Rhys GG, Mulholland AJ and Woolfson DN (2018) *De novo*-designed α-helical barrels as receptors for small molecules. *ACS Synthetic Biology* **7**, 1808–1816.

Thomson AR, Wood CW, Burton AJ, Bartlett GJ, Sessions RB, Brady RL and Woolfson DN (2014) Computational design of water-soluble α-helical barrels. *Science (New York, N.Y.)* **346**, 485–488.

Tian Y, Polzer FB, Zhang HV, Kiick KL, Saven JG and Pochan DJ (2018) Nanotubes, plates, and needles: pathway-dependent self-assembly of computationally designed peptides. *Biomacromolecules* **19**, 4286–4298.

Urvoas A, Guellouz A, Valerio-Lepiniec M, Graille M, Durand D, Desravines DC, Van Tilbeurgh H, Desmadril M and Minard P (2010) Design, production and molecular structure of a new family of artificial alpha-helicoidal repeat proteins (αRep) based on thermostable HEAT-like repeats. *Journal of Molecular Biology* **404**, 307–327.

Usov I, Adamcik J and Mezzenga R (2013) Polymorphism complexity and handedness inversion in serum albumin amyloid fibrils. *ACS Nano* **7**, 10465–10474.

Valéry C, Paternostre M, Robert B, Gulik-Krzywicki T, Narayanan T, Dedieu J-C, Keller G, Torres M-L, Cherif-Cheikh R, Calvo P and Artzner F (2003) Biomimetic organization: octapeptide self-assembly into nanotubes of viral capsid-like dimension. *Proceedings of the National Academy of Sciences of the United States of America* **100**, 10258–10262.

Valéry C, Artzner F, Robert B, Gulick T, Keller G, Grabielle-Madelmont C, Torres ML, Cherif-Cheikh R and Paternostre M (2004) Self-association process of a peptide in solution: from β-sheet filaments to large embedded nanotubes. *Biophysical Journal* **86**, 2484–2501.

Valery C, Deville-Foillard S, Lefebvre C, Taberner N, Legrand P, Meneau F, Meriadec C, Delvaux C, Bizien T, Kasotakis E, Lopez-Iglesias C, Gall A, Bressanelli S, Le Du MH, Paternostre M and Artzner F (2015) Atomic view of the histidine environment stabilizing higher-pH conformations of pH-dependent proteins. *Nature Communications* **6**, 7771.

Van Rijt MMJ, Ciaffoni A, Ianiro A, Moradi MA, Boyle AL, Kros A, Friedrich H, Sommerdijk N and Patterson JP (2019) Designing stable, hierarchical peptide fibers from block co-polypeptide sequences. *Chemical Science* **10**, 9001–9008.

Vauthey S, Santoso S, Gong H, Watson N and Zhang S (2002) Molecular self-assembly of surfactant-like peptides to form nanotubes and nanovesicles. *Proceedings of the National Academy of Sciences of the United States of America* **99**, 5355–5360.

Violette A, Averlant-Petit MC, Semetey V, Hemmerlin C, Casimir R, Graff R, Marraud M, Briand JP, Rognan D and Guichard G (2005) *N,N′*-linked oligoureas as foldamers: chain length requirements for helix formation in protic solvent investigated by circular dichroism, NMR spectroscopy, and molecular dynamics. *Journal of the American Chemical Society* **127**, 2156–2164.

Walshaw J and Woolfson DN (2001) Open-and-shut cases in coiled-coil assembly: alpha-sheets and alpha-cylinders. *Protein Science* **10**, 668–673.

Wang YA, Yu X, Yip C, Strynadka NC and Egelman EH (2006) Structural polymorphism in bacterial EspA filaments revealed by cryo-EM and an improved approach to helical reconstruction. *Structure (London, England: 1993)* **14**, 1189–1196.

Wang F, Burrage AM, Postel S, Clark RE, Orlova A, Sundberg EJ, Kearns DB and Egelman EH (2017) A structural model of flagellar filament switching across multiple bacterial species. *Nature Communications* **8**, 960.

Wang F, Gu Y, O'Brien JP, Yi SM, Yalcin SE, Srikanth V, Shen C, Vu D, Ing NL, Hochbaum AI, Egelman EH and Malvankar NS (2019) Structure of microbial nanowires reveals stacked hemes that transport electrons over micrometers. *Cell* **177**, 361–369.e310.

Wang F, Gnewou O, Modlin C, Beltran LC, Xu C, Su Z, Juneja P, Grigoryan G, Egelman EH and Conticello VP (2021*a*) Structural analysis of cross α-helical nanotubes provides insight into the designability of filamentous peptide nanomaterials. *Nature Communications* **12**, 407.

Wang F, Gnewou O, Wang S, Osinski T, Zuo X, Egelman EH and Conticello VP (2021*b*) Deterministic chaos in the self-assembly of beta sheet nanotubes from an amphipathic oligopeptide. *Matter* **4**, 3217–3231.

Wang F, Gnewou O, Solemanifar A, Conticello VP and Egelman EH (2022) Cryo-EM of helical polymers. *Chemical Reviews*. doi: 10.1021/acs.chemrev.1c00753.

Warmack RA, Boyer DR, Zee C-T, Richards LS, Sawaya MR, Cascio D, Gonen T, Eisenberg DS and Clarke SG (2019) Structure of amyloid-β (20–34) with Alzheimer's-associated isomerization at Asp23 reveals a distinct protofilament interface. *Nature Communications* **10**, 3357.

Wlodawer A and Dauter Z (2017) 'Atomic resolution': a badly abused term in structural biology. *Acta Crystallographica Section D: Structural Biology* **73** (Pt 4), 379–380.

Wlodawer A, Li M and Dauter Z (2017) High-resolution cryo-EM maps and models: a crystallographer's perspective. *Structure (London, England: 1993)* **25**, 1589–1597 e1581.

Woolfson DN (2017) Coiled-coil design: updated and upgraded. *Subcellular Biochemistry* **82**, 35–61.

Wu Y, Norberg PK, Reap EA, Congdon KL, Fries CN, Kelly SH, Sampson JH, Conticello VP and Collier JH (2017) A supramolecular vaccine platform based on alpha-helical peptide nanofibers. *ACS Biomaterials Science & Engineering* **3**, 3128–3132.

Wu X, Ma Y, Zhao K, Zhang J, Sun Y, Li Y, Dong X, Hu H, Liu J, Wang J, Zhang X, Li B, Wang H, Li D, Sun B, Lu J and Liu C (2021) The structure of a minimum amyloid fibril core formed by necroptosis-mediating RHIM of human RIPK3. *Proceedings of the National Academy of Sciences of the United States of America* **118**, 14.

Xu C, Liu R, Mehta AK, Guerrero-Ferreira RC, Wright ER, Dunin-Horkawicz S, Morris K, Serpell LC, Zuo X, Wall JS and Conticello VP (2013) Rational design of helical nanotubes from self-assembly of coiled-coil lock washers. *Journal of the American Chemical Society* **135**, 15565–15578.

Xu J, Dayan N, Goldbourt A and Xiang Y (2019) Cryo-electron microscopy structure of the filamentous bacteriophage IKe. *Proceedings of the National Academy of Sciences* **116**, 5493–5498.

Xuan S and Zuckermann RN (2020) Diblock copolypeptoids: a review of phase separation, crystallization, self-assembly and biological applications. *Journal of Materials Chemistry B* **8**, 5380–5394.

Yan H, Nykanen A, Ruokolainen J, Farrar D, Gough JE, Saiani A and Miller AF (2008) Thermo-reversible protein fibrillar hydrogels as cell scaffolds. *Faraday Discussions* **139**, 71–84; discussion 105–128, 419–120.

Yoo SH, Collie GW, Mauran L and Guichard G (2020) Formation and modulation of nanotubular assemblies of oligourea foldamers in aqueous conditions using alcohol additives. *ChemPlusChem* **85**, 2243–2250.

Zaccai NR, Chi B, Thomson AR, Boyle AL, Bartlett GJ, Bruning M, Linden N, Sessions RB, Booth PJ, Brady RL and Woolfson DN (2011) A *de novo* peptide hexamer with a mutable channel. *Nature Chemical Biology* **7**, 935–941.

Zhang S, Holmes T, Lockshin C and Rich A (1993) Spontaneous assembly of a self-complementary oligopeptide to form a stable macroscopic membrane. *Proceedings of the National Academy of Sciences* **90**, 3334–3338.

Zhang S, Lockshin C, Cook R and Rich A (1994) Unusually stable β-sheet formation in an ionic self-complementary oligopeptide. *Biopolymers* **34**, 663–672.

Zhang HV, Polzer F, Haider MJ, Tian Y, Villegas JA, Kiick KL, Pochan DJ and Saven JG (2016) Computationally designed peptides for self-assembly of nanostructured lattices. *Science Advances* **2**, e1600307.

Zhang SQ, Huang H, Yang J, Kratochvil HT, Lolicato M, Liu Y, Shu X, Liu L and Degrado WF (2018) Designed peptides that assemble into cross-α amyloid-like structures. *Nature Chemical Biology* **14**, 870–875.

Zhang W, Falcon B, Murzin AG, Fan J, Crowther RA, Goedert M and Scheres SHW (2019) Heparin-induced tau filaments are polymorphic and differ from those in Alzheimer's and Pick's diseases. *Elife* **8**, e43584.

Zhao Y, Wang J, Deng L, Zhou P, Wang S, Wang Y, Xu H and Lu JR (2013) Tuning the self-assembly of short peptides via sequence variations. *Langmuir* **29**, 13457–13464.

Zhao Y, Deng L, Wang J, Xu H and Lu JR (2015) Solvent controlled structural transition of KI4K self-assemblies: from nanotubes to nanofibrils. *Langmuir* **31**, 12975–12983.

Zhao Y, Yang W, Wang D, Wang J, Li Z, Hu X, King S, Rogers S, Lu JR and Xu H (2018) Controlling the diameters of nanotubes self-assembled from designed peptide bolaphiles. *Small* **14**, 1703216.

Zimenkov Y, Conticello VP, Guo L and Thiyagarajan P (2004) Rational design of a nanoscale helical scaffold derived from self-assembly of a dimeric coiled coil motif. *Tetrahedron* **60**, 7237–7246.

Zimenkov Y, Dublin SN, Ni R, Tu RS, Breedveld V, Apkarian RP and Conticello VP (2006) Rational design of a reversible pH-responsive switch for peptide self-assembly. *Journal of the American Chemical Society* **128**, 6770–6771.

Ziserman L, Lee HY, Raghavan SR, Mor A and Danino D (2011) Unraveling the mechanism of nanotube formation by chiral self-assembly of amphiphiles. *Journal of the American Chemical Society* **133**, 2511–2517.